Unraveling the biological role of two putative polysaccharide deacetylases from *Bacillus anthracis*

Department of Biology

University of Crete

2019

Table of Contents

Ευχαριστίες 3

List of Figures 5

List of Tables 7

Περίληψη 9

Abstract 12

Introduction 14

History of anthrax 14

Life cycle of anthrax 15

Toxins and pathogenesis of anthrax 17

Treatment and Epidemiology of anthrax 19

Biology of *B. anthracis* 21

-Sporulation 21

-Germination 26

Cell wall components of *B. anthracis* vegetative cells 29

Cell wall components of *B. anthracis* spores 34

Polysaccharide deacetylases (PDAs) 37

Structural analysis of PDAs 40

Proline hydroxylation in the active site of PDAs 44

Pseudoenzymes 45

Materials 49

Methods 52

Cloning and expression of *ba3943* gene into pET26b expression vector and *ba1836* gene into pET26b, pET16b-TEV and pET16b-MBP-TEV expression vectors 52

Site-directed mutagenesis of *ba3943* and *ba1836* genes 53

Purification of recombinant BA3943 and BA3943 mutant proteins 53

Purification of recombinant MBP-BA1836 fusion protein 54

Preparation of radiolabeled H^3-glycol chitin 54

Enzyme Assays 54

Analysis of reaction products 54

2-Hydroxyproline identification and quantitation 55

Metal identification 55

Construction of *B. anthracis* Δ*ba1836* and Δ*ba3943* knockout strains, Δ*ba3943* complemented strain, GFP fusions and *lacZ* transcriptional fusions 56

Preparation of sporulating cell cultures 57

β-galactosidase activity assay 58

Competition experiments ... 58
***In vitro* determination of lysozyme sensitivity** ... 59
Autolysis Assay ... 59
Fluorescence Microscopy, Scanning and Transmission Electron Microscopy ... 59
Western Blotting analysis ... 60
Purification of peptidoglycan and neutral polysaccharide from *B. anthracis* ... 60
Spore preparation and purification ... 61
Spore viability ... 61
Spore germination ... 61
Results ... 62
BA1836 ... 62
BA1836 is a putative PDA ... 62
***ba1836* is expressed in stationary phase cells and further induced during sporulation** ... 64
BA1836-GFP localizes to the cell periphery and septa ... 66
Cells lacking *ba1836* suffer reduced sporulation fitness ... 67
Δ*ba1836* cells display severe delay in spore development ... 72
Δ*ba1836* knockout strain lowers the spore germination rate ... 74
BA3943 ... 75
BA3943 is a pseudoPDA ... 75
The crystal structure of BA3943 reveals a unique *N*-terminal domain ... 77
Restoration of deacetylase activity and levels of hydroxylation and the effect of mutations on active-site residues on deacetylase activity ... 78
***ba3943* is expressed at the engulfment stage of sporulation** ... 87
BA3943-GFP localizes to the forespore membrane ... 89
Cells lacking *ba3943* suffer reduced sporulation fitness ... 90
BA3943 affects autolysis of vegetative cells ... 93
Discussion ... 95
References ... 104
Curriculum Vitae ... 116

Ευχαριστίες

Καθώς ο κύκλος αυτός κλείνει θα ήθελα να ευχαριστήσω από καρδιάς όλους αυτούς που συνέβαλλαν στην ολοκλήρωση της διδακτορικής μου διατριβής.

Αρχικά θα ήθελα να ευχαριστήσω τον επίβλεποντα καθηγητή κ. Μπουριώτη για την καθοδήγηση και τη βοήθεια που μου προσέφερε ώστε να ολοκληρώσω επιτυχώς την διδακτορική μου διατριβή.

Θα ήθελα να ευχαριστήσω θερμά τον κ. Κοκκινίδη, καθώς και τα μέλη του εργαστηρίου του, για την άψογη συνεργασία. Πιο συγκεκριμένα ευχαριστώ τους Αλέξη Μολφέτα, Βίκυ Φαδούλογλου και Ντίνα Κοτσιφάκη για τη συνεργασία και τη βοήθειά τους.

I would also like to heartily thank Prof. Waldemar Vollmer for his priceless contribution to the completion of my thesis. Thank you for spending time and effort to share your ideas on my project and for contributing to the writing of our paper.

Επίσης, θα ήθελα να ευχαριστήσω τον κ. Τζαμαρία για τις συμβουλές του και τη βοήθειά του καθώς και για τη συμβολή του στη συγγραφή της δημοσίευσής μας.

Ακόμη, ευχαριστώ τον κ. Πετράτο που πάντα έβρισκα την πόρτα του ανοιχτή όταν τον χρειάστηκα καθώς και την Μαρία Παπαδοβασιλάκη για τη βοήθειά της.

Ευχαριστώ πολύ και τα υπόλοιπα μέλη της επταμελούς επιτροπής την κ. Αθανασάκη και τον κ.Καλαντίδη που δέχτηκαν να συμμετάσχουν στην αξιολόγηση της διδακτορικής μου διατριβής.

Πολλά ευχαριστώ και στον κ. Περγαντή, καθώς και στους φοιτητές του Λεωνίδα Μαυρουδάκη και Λευκοθέα Τρανσανίδου, για τις αναλύσεις ICP-MS και ESI-MS που πραγματοποίησαν ώστε να συμπεριληφθούν στη διατριβή αυτή.

Ένα ευχαριστώ και στα μέλη του εργαστηρίου Ηλεκτρονικής Μικροσκοπίας για τη βοήθεια και το χρόνο τους.

Δεν θα μπορούσα να παραλείψω τα μέλη του εργαστηρίου Ενζυμικής Βιοτεχνολογίας που τα τελευταία έξι χρόνια ήταν το δεύτερό μου σπίτι. Ευχαριστώ πολύ τους Εύη Μπαλωμένου, Σοφία Αρναουτέλη, Δημήτρη Κουτσιούλη, Μαίρη Τζανοδασκαλάκη και Σπυριδούλα Χαρόβα που ήταν δίπλα μου σε αυτή τη διαδικασία, κάποιοι για μεγαλύτερο και κάποιοι για μικρότερο διάστημα, συμβάλλοντας ο καθένας με τον

τρόπο του στην ολοκλήρωση της διατριβής μου. Ευχαριστώ και τον, μεταπτυχιακό φοιτητή πλέον, Δημήτρη Μανιά για την συμβολή του στη διατριβή μου. Νιώθω πολύ τυχερή που στο χώρο αυτό απόκτησα πραγματικούς φίλους.

Ένα μεγάλο ευχαριστώ στην αδερφική μου φίλη Νικολέτα που είναι πάντα δίπλα μου να μοιράζεται τη χαρά μου και την αγωνία μου καθώς και στον σύντροφό μου Γιάννη για τη στήριξη, την ενθάρρυνση και την αγάπη του. Ευχαριστώ πολύ και τις αγαπημένες μου φίλες Άννα- Μαρία και Θάνια καθώς και όλους τους ανθρώπους που είχα την τύχη να συναναστραφώ τα τελευταία χρόνια, εντός και εκτός πανεπιστημιακού χώρου.

Τέλος, ένα τεράστιο ευχαριστώ στην οικογένειά μου που είναι πάντα δίπλα μου και στηρίζει κάθε μου βήμα με ενθουσιασμό. Νιώθω πολύ τυχερή που σας έχω και δεν θα σας άλλαζα με τίποτα στον κόσμο. Μαμά είσαι η ηρωίδα μου!

Η συγκεκριμένη διδακτορική διατριβή χρηματοδοτήθηκε από το πρόγραμμα ΙΚΥ-Siemens 2013-2016.

List of Figures

Figure 1. Life cycle of *B. anthracis* 16
Figure 2. Cellular model of anthrax toxins 18
Figure 3. Types of anthrax infection 19
Figure 4. Stages of sporulation of *B. anthracis* and other *Bacillus* species 26
Figure 5. Stages of germination of *B. anthracis* and other *Bacillus* species 28
Figure 6. Transmission electron microscopy image of a *B. anthracis* vegetative cell 29
Figure 7. Structure of the repeating unit of peptidoglycan in gram-positive bacteria 30
Figure 8. Biosynthetic pathway of peptidoglycan 31
Figure 9. Transmission electron microscopy image of a *B. anthracis* spore 34
Figure 10. Structure of cortex 35
Figure 11. Modifications of the glycan strands of peptidoglycan 38
Figure 12. Structure-based sequence alignment of the NodB domains of PDAs 41
Figure 13. Proposed catalytic mechanism of PDAs 42
Figure 14. Crystal structures of PDAs from *B. anthracis/B.cereus* 43
Figure 15. Proposed interwining of deacetylation with the Pro → 2-Hyp conversion in PDAs 44
Figure 16. Examples of pseudoenzymes of different enzyme families and their function 45
Figure 17. Evolution of an inactive enzyme from its active homologue 47
Figure 18. Sequence alignment of the NodB domain of BA1836 with PDAs 63
Figure 19. Overexpression of BA1836 (A) SDS-PAGE analysis of *E. coli* lysates 64
(B) Western blot analysis of *E. coli* lysates
Figure 20. Expression of *ba1836* gene (A) During *B. anthracis* 7702 growth conditions 65
(B) Following induction of sporulation of *B. anthracis* 7702 stationary phase cells
Figure 21. Expression of *ba1836* gene following induction of sporulation of exponentially phase cells 66
Figure 22. (A) Localization of BA1836-GFP 67
(B) Western blot analysis of lysates of 7702 cells expressing BA1836-GFP
Figure 23. Growth curves of *B. anthracis* parental and Δ*ba1836* mutant strains in (A) BHI and (B) SPY 68
Figure 24. (A) Lysozyme sensitivity 68
(B) Autolysis rate and
(C) Morphology of 7702 and Δ*ba1836* strains
Figure 25. HPLC analysis of (A) Peptidoglycan isolated from 7702 and Δ*ba1836* cells 69
(B) Neutral Polysaccharide isolated from 7702 and Δ*ba1836* cells
Figure 26. (A) Examination of morphology and structure of 7702 and Δ*ba1836* spores 69
(B) Spore viability of 7702 and Δ*ba1836* spores
Figure 27. Competition experiment under sporulation-inducing conditions using 71
(A) 1:1 ratio 7702 wild type to Δ*ba1836* mutant strain
(B) 1:3 ratio 7702 wild type to Δ*ba1836* mutant strain
(C) Competition experiment under growth conditions
(D) Competition experiment under sporulation-inducing conditions using 1:1 ratio 7702 wild type to Δ*ba1836* mutant strain heat-treated at a lower temperature
Figure 28. Phenotypic analysis of parental and mutant sporulating cells 73

Figure 29. HPLC analysis of spore PG from 7702 and Δ*ba1836* strains 73
Figure 30. Germination of 7702 and Δ*ba1836* spores 74
Figure 31. Sequence alignment of BA3943 with YlxY from *B. subtilis* using BLASTp 76
Figure 32. Sequence alignment of the NodB domain of BA3943 with PDAs 76
Figure 33. SDS-PAGE of the purified BA3943 77
Figure 34. Crystal structure and active site of BA3943 78
Figure 35. HPLC analysis of (A) $GlcNAc_6$ 80
(B) $GlcNAc_7$ after treatment with BA3943 N94D V95D A183R
Figure 36. ESI-MS of $GlcNAc_7$ resulting from incubation of $GlcNAc_7$ with BA3943 N94D V95D A183R 82
(A) Chemical structure, mass and m/z ratio of $GlcNAc_7$
(B) ESI-MS analysis of the first peak collected after HPLC analysis of $GlcNAc_7$ reaction products
(C) ESI-MS analysis of the second peak collected after HPLC analysis of $GlcNAc_7$ reaction products
(D) Deacetylation of $GlcNAc_7$ is performed on the third and/or the fourth unit
Figure 37. HPLC analysis of PG isolated from 83
(A) *B. subtilis* following incubation with BA3943 N94D V95D A183R
(B) *E. coli* following incubation with BA3943 N94D V95D A183R
Figure 38. (A) Superposition of the active sites of BA3943 N94D V95D A183R and BA3943 84
(B) Superposition of the active sites of BA3943 N94D V95D A183R and PGDA BC1960
Figure 39. HPLC analysis of $GlcNAc_7$ following incubation with BA3943 N94D A183R 86
Figure 40. HPLC analysis of MDP following incubation with 87
(A) BA3943 N94D A183R
(B) BA3943 N94D V95N A183R
Figure 41. Expression of *ba3943* gene 88
(A) Following induction of sporulation of exponential phase *B. anthracis* 7702 cells
(B) During *B. anthracis* 7702 growth conditions
Figure 42. (A) Localization of BA3943-GFP 89
(B) Western blot analysis of lysates of 7702 cells expressing BA3943-GFP
Figure 43. (A) Examination of morphology and structure of 7702 and Δ*ba3943* spores 90
(B) Spore viability of 7702 and Δ*ba3943* spores
(C) Germination assay of 7702 and Δ*ba3943* spores
(D) HPLC analysis of spore PG from 7702 and Δ*ba3943* spores
Figure 44. Competition experiment under sporulation-inducing conditions using 92
(A) 1:1 ratio 7702 wild type to Δ*ba3943* mutant strain
(B) 1:3 ratio 7702 wild type to Δ*ba3943* mutant strain
(C) Competition experiment under growth conditions
Figure 45. (A) Lysozyme sensitivity 94
(B) Autolysis rate and
(C) Morphology of 7702 and Δ*ba3943* strains
Figure 46. HPLC analysis of 94
(A) Peptidoglycan isolated from 7702 and Δ*ba3943* cells
(B) Neutral Polysaccharide isolated from 7702 and Δ*ba3943* cells

List of Tables

Table 1. Putative polysaccharide deacetylases from *B. anthracis* and *B. cereus* 40
Table 2. List of oligonucleotides used in the present study 50
Table 3. List of strains and plasmids used in the present study 51
Table 4. List of mutant *ba3943* genes and corresponding recombinant BA3943 mutant proteins 53
Table 5. Deacetylase activity against H^3-glycol chitin and mass spectrometric characterization of 2-Hyp level in BA3943 and BA3943 mutant proteins 79

List of Abbreviations

PA	Protective Antigen
EF	Edema Factor
LF	Lethal Factor
PG	Peptidoglycan
PBPs	Penicillin Binding Proteins
GR	Germinant Receptor
CaDPA	Calcium Dipicolinate
CLEs	Cortex Lytic Enzymes
SASPs	Small Acid-Soluble proteins
GlcNAc	*N*-acetylglucosamine
MurNAc	*N*-acetylmuramic acid
D-Glu	D-Glutamic Acid
D-Ala	D-Alanine
meso-DAP	Meso-Diaminopimelic Acid
PS	Neutral Polysaccharide
SCWP	Secondary Cell Wall Polysaccharides
S-layer	Surface Layer
PDAs	Polysaccharide Deacetylases
CE4	Carbohydrate Esterase family 4
Asp	Aspartic Acid
His	Histidine
Pro	Proline
Arg	Arginine
2-Hyp	2-Hydroxyproline
BHI	Brain Heart Infusion
SPY	Spizizen Yeast
LB	Luria-Bertani
IPTG	Isopropyl-β-D-thiogalactoside
Ni-NTA	Nickel-Nitrilotriacetic acid
MBP	Maltose Binding Protein
GFP	Green Fluorescent Protein
HPLC	High Pressure Liquid Chromatography
MDP	*N*-acetylmuramyl-L-alanyl-D-isoglutamine hydrate
ESI	Electrospray Ionization
MS	Mass Spectrometry
ONPG	2-Nitrophenyl-β-D-galactopyranoside
PGDA	Peptidoglycan *N*-acetylglucosamine deacetylase
MU	Miller Units
SEM	Scanning Electron Microscopy
TEM	Transmission Electron Microscopy
CFU	Colony Forming Units

Περίληψη

Ο *Bacillus anthracis,* ένα θετικό κατά Gram βακτήριο που έχει την ικανότητα να σχηματίζει σπόρια, χρησιμοποιείται ως βιολογικό όπλο σε τρομοκρατικές ενέργειες. Η κατάποση ή η εισπνοή των σπορίων του *B. anthracis* προκαλεί την ασθένεια του άνθρακα, η οποία, τις περισσότερες φορές, οδηγεί στο θάνατο του ξενιστή.

Τα αντιβιοτικά που χρησιμοποιούνται για την καταπολέμηση της ασθένειας του άνθρακα, παρουσιάζουν μειωμένη δραστικότητα σε ανθεκτικά στελέχη *B. anthracis*, καθιστώντας απαραίτητη την ανάγκη για την ταυτοποίηση νέων στόχων και την ανάπτυξη νέων αντιμικροβιακών φαρμάκων για το συγκεκριμένο παθογόνο.

Οι απακετυλάσες πολυσακχαριτών του *B. anthracis* αποτελούν στόχους αντιβιοτικών λόγω των σημαντικών τους ρόλων στη φυσιολογία του συγκεκριμένου παθογόνου. Οι απακετυλάσες πολυσακχαριτών εμπλέκονται στην ανθεκτικότητα του *B. anthracis* στη λυσοζύμη του ξενιστή καθώς και σε άλλες κυτταρικές λειτουργίες όπως στη βιογένεση της πεπτιδογλυκάνης κατά την επιμήκυνση και την κυτταρική διαίρεση, στη διατήρηση του κυτταρικού σχήματος και στην διατήρηση της κυτταρικής σταθερότητας παρουσία υψηλής οσμωτικής πίεσης, στο σχηματισμό βιοφίλμ αλλά και στην προσκόλληση και εισβολή στα κύτταρα του ξενιστή. Οι απακετυλάσες πολυσακχαριτών είναι μέλη της οικογένειας 4 των εστερασών υδατανθράκων (CE4) στην οποία ανήκουν οι εστεράσες ακετυλ-ξυλάνης, οι απακετυλάσες χιτίνης, οι απακετυλάσες χιτοολιγοσακχαριτών και οι απακετυλάσες πεπτιδογλυκάνης.

Εξαιρετικό ενδιαφέρον παρουσιάζει το γεγονός ότι το γονιδίωμα του *B. anthracis* περιέχει έντεκα γονίδια τα οποία κωδικοποιούν για πιθανές απακετυλάσες πολυσακχαριτών. Εκτός από τις ενεργές απακετυλάσες, ο *B. anthracis* διαθέτει και ψευδο-απακετυλάσες πολυσακχαριτών. Τα ψευδο-ένζυμα αποτελούν ομόλογα ενζύμων τα οποία διατηρούν την γονιδιακή έκφραση, τον κυτταρικό εντοπισμό και την χαρακτηριστική πρωτεϊνική αναδίπλωση των ενεργών τους ομόλογων ενζύμων όμως έχουν χάσει την καταλυτική τους δράση. Τα ψευδο-ένζυμα εμπλέκονται σε διαφορετικές κυτταρικές διεργασίες όπως στη ρύθμιση των ενεργών ομόλογών τους

ή στην αλληλεπίδραση με τα υποστρώματα αυτών ή στην πρόσδεση και στόχευση πρωτεϊνών σε συγκερκιμένα υποκυτταρικά διαμερίσματα ή στην ρύθμιση της ουβικουιτινιλίωσης πρωτεϊνών ή στη μεταγωγή σήματος.

Στην παρούσα διδακτορική διατριβή μελετήθηκε ο ρόλος των πιθανών απακετυλασών πολυσακχαριτών BA1836 και BA3943 στη φυσιολογία του *B. anthracis* πραγματοποιώντας βιοχημική και γενετική ανάλυση.

Το γονίδιο *ba1836* εκφράζεται κατά την είσοδο των κυττάρων στη στατική φάση ανάπτυξης και επάγεται κατά τα πρώτα στάδια της σπορίωσης. Το στέλεχος *B. anthracis* στο οποίο είχαμε διαγράψει το γονίδιο *ba1836* (Δ*ba1836*) εμφάνισε φυσιολογικό ρυθμό ανάπτυξης, δεν παρουσίασε σημαντικές διαφορές στην σύσταση της πεπτιδογλυκάνης κυττάρων στατικής φάσης ανάπτυξης και δεν ήταν ευαίσθητο στη λυσοζύμη, όμως έδειξε αδυναμία διαχωρισμού των κυτταρικών αλυσίδων σε σύγκριση με το στέλεχος αγρίου τύπου. Μεγάλο ενδιαφέρον παρουσίασε το γεγονός ότι το μεταλλαγμένο στέλεχος Δ*ba1836* παρουσίασε σημαντική καθυστέρηση στη δημιουργία των σπορίων, παρότι τα ώριμα σπόρια εμφάνισαν φυσιολογική μορφολογία. Τέλος, η υδρόλυση της πεπτιδογλυκάνης των ώριμων μεταλλαγμένων σπορίων με μουραμιδάση παρήγαγε παρόμοια αλλά ποσοτικά μειωμένα μουροπεπτίδια σε σύγκριση με την πεπτιδογλυκάνη των σπορίων του αγρίου τύπου ενώ τα μεταλλαγμένα σπόρια παρουσίασαν χαμηλότερο ρυθμό εκβλάστησης.

Τα αποτελέσματα της παρούσας μελέτης αποδεικνύουν ότι η BA3943 είναι μία ψευδο-απακετυλάση πολυσακχαριτών. Τρία συντηρημένα και απαραίτητα για την κατάλυση αμινοξέα απουσιάζουν από το ενεργό της κέντρο με αποτέλεσμα να μην εμφανίζει δράση απακετυλάσης. Επιπλέον, απουσιάζει η υδροξυλίωση στον Cα της συντηρημένης προλίνης του ενεργού της κέντρου η οποία πρόσφατα βρέθηκε ότι ενισχύει την ενζυμική δράση των απακετυλασών πολυσακχαριτών του *B. anthracis*. Επίσης, η κρυσταλλική δομή της BA3943 αποκάλυψε την παρουσία μίας περιοχής πλούσιας σε λυσίνες στο άμινο-τελικό της άκρο. Η περιοχή αυτή είναι μοναδική καθώς δεν έχει βρεθεί σε καμία άλλη οικογένεια ενζύμων εώς τώρα. Κατευθυνόμενη μεταλλαξιγένεση στις τρεις συντηρημένες αμινοξικές θέσεις του ενεργού κέντρου της BA3943 οδήγησε σε επαναφορά των δράσεων της απακετυλίωσης και των επιπέδων της υδροξυλίωσης.

Το γονίδιο της *ba3943* εκφράζεται στη σπορίωση, κατά την είσοδο των κυττάρων στο στάδιο της εγκόλπωσης. Μεγάλο ενδιαφέρον παρουσίασε το γεγονός ότι το στέλεχος *B. anthracis* στο οποίο είχαμε διαγράψει το γονίδιο της *ba3943* (Δ*ba3943*) εμφάνισε σημαντικό μειονέκτημα κατά τον συναγωνισμό με κύτταρα αγρίου τύπου σε συνθήκες σπορίωσης, υποδεικνύοντας ότι η BA3943 εμπλέκεται ενεργά στη διαδικασία αυτή. Εντούτοις, τα ώριμα σπόρια εμφάνισαν φυσιολογική μορφολογία και ήταν ικανά να εκβλαστήσουν. Τέλος, το μεταλλαγμένο Δ*ba3943* στέλεχος είχε φυσιολογικό ρυθμό ανάπτυξης, δεν παρουσίασε σημαντικές διαφορές στην σύσταση της πεπτιδογλυκάνης κυττάρων στατικής φάσης ανάπτυξης αλλά και ώριμων σπορίων και δεν ήταν ευαίσθητο στη λυσοζύμη, όμως έδειξε αδυναμία διαχωρισμού των κυτταρικών αλυσίδων σε σύγκριση με το στέλεχος αγρίου τύπου

Ο ρόλος της BA1836 στη σπορίωση και στην εκβλάστηση είναι μοναδικός ανάμεσα στις λειτουργίες των υπόλοιπων απακετυλασών πολυσακχαριτών ενώ η BA3943 αποτελεί μία ψευδο-απακετυλάση, η οποία επηρεάζει τη σπορίωση του *B. anthracis*. Η παρούσα διδακτορική διατριβή παρέχει πληροφορίες οι οποίες θα συνεισφέρουν στην κατανόηση των πολύπλοκων διαδικασιών της σπορίωσης και εκβλάστησης του συγκεκριμένου παθογόνου.

Abstract

Bacillus anthracis, a Gram-positive, spore-forming bacterium, is a potential bioterrorism weapon. Ingestion or inhalation of *B. anthracis* spores can lead to anthrax disease in mammalian hosts which, in most cases, proves to be fatal.

Presently used antibiotics to combat *B. anthracis* infections exhibit low potency against *B. anthracis* strains that show antimicrobial resistance, necessitating the need to identify new targets and to develop novel antibacterial drugs against this pathogen.

Putative and known polysaccharide deacetylases (PDAs) from *B. anthracis* are validated drug targets due to their key roles in bacterial physiology. PDAs have been implicated in lysozyme resistance and also participate in distinct cellular functions including cell division/elongation, cell shape maintenance and osmotic stability, biofilm formation and adhesion/invasion to host cells. PDAs are members of the carbohydrate esterase family 4 (CE4) which includes acetylxylan esterases, chitin deacetylases, chitooligosaccharide deacetylases and peptidoglycan (PG) deacetylases.

There is an unusual occurrence of eleven putative PDAs in *B. anthracis.* Except from the characterized active PDAs, *B. anthracis* also possesses putative pseudoPDAs. Pseudoenzymes are defined as enzyme homologues that are predicted to retain protein expression, subcellular localization and typical protein folding but lack catalytic activity. Different roles of pseudoenzymes have been reported including regulation of their active homologues, interaction with the substrates of their enzyme homologues, binding and targeting of other proteins to specific cellular locations, modulation of protein ubiquitination and signal transduction.

Here we elucidated the physiological role of the putative PDAs BA1836 and BA3943 from *B. anthracis* by employing biochemical and genetic (knockout) analysis.

The *ba1836* gene is expressed upon entrance into the stationary phase of growth and enhanced during the early stages of sporulation. Δ*ba1836* knockout strain had normal growth rate, did not exhibit any significant alterations in PG composition of stationary phase cells and was not sensitive to lysozyme, but showed a defect in cell separation. Strikingly, the Δ*ba1836* mutant strain exhibited a severe delay in spore

development although mature spores were ultimately developed and exhibited normal morphology. Finally, digestion of mutant spore PG with muramidase produced similar but less muropeptides compared to PG from wild type spores, and mutant spores exhibited a lower germination rate.

Our *in vitro* data demonstrated that BA3943 is a pseudoenzyme consistent with the absence of three conserved, essential, catalytic residues. In addition, BA3943 lacks hydroxylation at the Cα of a highly conserved Pro residue of the active site, which has been recently shown to enhance the enzymatic activity of PDAs from *B. anthracis*. The crystal structure revealed the presence of a lysine-rich domain at the *N*-terminus of the pseudoPDA. The lysine-rich domain is unique and to our knowledge it has not been identified in any other enzyme family. Site-directed mutagenesis at the three residues of the active site of BA3943 resulted in restoration of both deacetylase activity and hydroxylation levels.

The *ba3943* gene is expressed upon entrance into the engulfment stage of sporulation. Interestingly, the Δ*ba3943* mutant strain exhibited a significant competition deficit under sporulation-inducing conditions, suggesting that BA3943 is actively involved in sporulation. Nevertheless, Δ*ba3943* mature spores were ultimately developed, exhibited normal morphology and could efficiently sporulate and germinate. Finally, a Δ*ba3943* knockout strain had normal growth rate, did not exhibit any significant alterations in PG composition of stationary phase cells or spores and was not sensitive to lysozyme, but showed a defect in cell separation.

To our knowledge BA1836 has a unique, sporulation/germination-specific role among the functions of other PDAs, while BA3943 is the first characterized pseudoPDA which affects the sporulation process in *B. anthracis*. Our data provide information towards a more complete understanding of the complex processes of sporulation and germination in this bacterial pathogen.

Introduction

History of anthrax

Anthrax is a contagious and fatal disease caused by the bacterium *Bacillus anthracis*. The name "anthrax" comes from the Greek word for coal because of the black color of the skin lesions developed by patients after cutaneous anthrax infection. The first recorded appearance of anthrax was in 1491 B.C. in Exodus of the Bible, where it was described as the 5th plague of Egypt. It was also described in the early Greek, Roman and Hindi literature (1).

Until the end of the 19th century, anthrax had caused the massive death of animals around the globe. In 1613, the "Black Bane" caused over 60.000 deaths in humans and cattle and became the first European pandemic (1, 2).

It was not until 1850, when Pierre Rayer and Casimir-Joseph Davaine identified filamentous formations in the blood of anthrax infected sheep. They suggested that these formations were the etiology of anthrax but their hypothesis was not verified at that time. Later, in 1876, Robert Koch started searching the cause of anthrax after an epidemic in a farm. He discovered the presence of a rod-shaped microorganism, which could transform to spores under poor nutrient conditions, in the blood and tissues of deceased animals (3). Koch's observations were further confirmed in 1881, when Louis Pasteur verified that the microorganism is the sole cause of anthrax (4). In 1875, Ferdinand Cohn named this microorganism *Bacillus anthracis* (5).

The first successful anthrax live spore vaccine for animals was created by Max Sterne in 1937. Most countries still vaccinate their animals using Sterne's vaccine. The first cutaneous anthrax vaccine for humans was created in 1950s, after being tested in a group of goat hair mill workers in the United States. Twenty years later an updated version of this human anthrax vaccine was created, which is still used today (6).

Anthrax has been used as a weapon since World War I, when the German army used it to infect livestock and animal feed traded to the Allied Nations. In 1932, Japan conducted research with biological weapons and attacked several Chinese cities by spraying anthrax from aircrafts. Bioweapon research programs were also performed in the United States and Great Britain in 1942. The U.S. filled more than 50.000 bombs

with anthrax in order to be prepared for any possible attack from Germany. Great Britain did the same but released the bombs over the Gruinard Island in order to test the widespread release of anthrax. Bioweapon programs were expanded in the U.S. during the Korean War (1950) (7).

In 2001, a little after the September 11 attacks, two U.S. Senators' offices and news media agencies along the East Coast received letters containing a white powder of anthrax spores. Twenty two confirmed cases of anthrax were reported, 11 diagnosed with inhalation and 11 with cutaneous anthrax. In total, 43 people were tested positive while more than 100.000 people were considered at risk of anthrax exposure. This act led to an extreme increase of the U.S. research budget for studies aiming to prevent and combat bioterrorism (8, 9).

Life cycle of anthrax

Bacillus anthracis belongs to the *Bacillus cereus sensu lato* group which includes *Bacillus cereus, Bacillus mycoides, Bacillus pseudomycoides, Bacillus thuringiensis, Bacillus weihenstephanensis* and *Bacillus cytoxicus* (10). It is a gram-positive, non-motile, aerobic, facultative anaerobic, rod-shaped, spore-forming and capsulated bacterium (11). Bacterial spores are extremely resistant to harsh environmental conditions including ultraviolet and ionizing radiation, high temperature, pressure, pH, chemical agents and deprivation of nutrients. They are metabolically inactive and can survive for years in soil, air and water (12, 13). Sporulation is triggered when vegetative cells come across adverse environmental conditions. Discrimination of the members of the *Bacillus cereus* group is possible when it is based on species-specific characteristics related to pathogenicity.

B. anthracis fully virulent strains harbor two plasmids, pXO1 and pXO2. pXO1 plasmid carries the genes *pagA* (encoding for protective antigen, PA), *lef* (encoding for lethal factor, LF) and *cya* (encoding for edema factor, EF) which comprise a tripartite toxin (13). pXO1 plasmid also carries *atxA,* a virulence factor which regulates the expression of pXO1 and pXO2 genes, and *gerX*, a three-gene germination operon (14, 15). pXO2 plasmid carries the genes for capsule production (*capB*, *capC*, *capA, capD* and *capE*), degradation (*dep*) and regulation (*acpA*) (13, 16). The two regulatory genes

acpA and *atxA* have been reported to control expression of the *B. anthracis* capsule biosynthesis operon *capBCAD*. The capsule is composed of γ-linked poly-D-glutamic acid which gives mucoid appearance to the colony. Even though the capsule is non-toxic and it does not provoke host immune system reaction, its formation is important for virulence. More specifically, the capsule plays a vital role in establishing the infection by helping the bacterium to escape phagocytic action, while the later phase of the disease is controlled by the anthrax toxin (6).

B. anthracis is a severe zoonotic pathogen of ruminants whose dormant spores are usually found in the soil of agricultural areas. Its infection occurs upon uptake of the spores, which inside the mammalian host, come across favorable conditions like aqueous environment and sufficient nutrients, leading to their germination. The germination process of spores into vegetative cells is vital for pathogenesis since the main virulence factors-the capsule and the tripartite toxin-are produced by vegetative cells. The capsule evades the host immune system while lethal and edema toxins are produced in the capillaries of invaded organs causing the fatal effects of the infection. Upon death of the host, the capsulated bacteria are released through blood, back into the environment. Vegetative cells are converted to spores, after being exposed to oxygen, infecting the agricultural fields and subsequently the grazing animals (17) (Fig. 1).

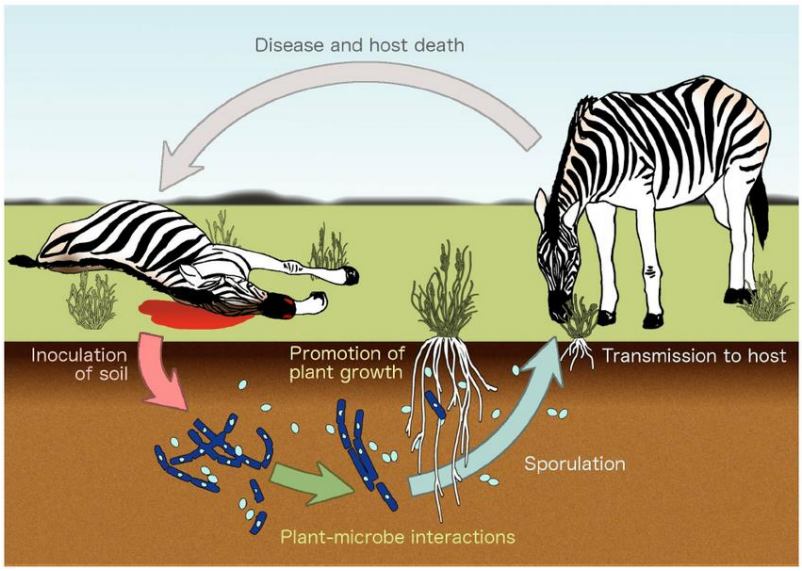

Figure 1. Life cycle of *B. anthracis* (18).

Toxins and pathogenesis of anthrax

The tripartite anthrax toxin is comprised of three non-toxic proteins which act in binary combinations: the protective antigen (PA), which is able to elicit a protective immune response against *B. anthracis*, the edema factor (EF), which causes tissue edema, and the lethal factor (LF), which provokes cell death. EF and LF are enzymes acting on substrates within the cytosolic compartment of host cells (19) while PA binds on the receptors of host cells and forms a pore to mediate the transportation of EF and LF to the cytosol (20).

During infection, circulating PA specifically binds to one of at least two host cellular receptors, anthrax toxin receptor (ATR) or capillary morphogenesis gene 2 (CMG2), which are present on many tissues. The bound PA is cleaved by furin, releasing a 20kDa fragment (21). The remaining 63kDa bound PA fragment self-assembles in order to form a ring-shaped heptamer. There is evidence that up to three copies of EF and/or LF can competitively bind to a heptameric ring (22). A decreased amount of PA forms octamers (20%-30% of oligomers) which can bind up to 4 molecules of EF and/or LF (23). This complex is internalized and the toxic factors are then released into the cytoplasm where they disrupt the cell via their catalytic action (24). EF is an adenylate cyclase which converts intracellular ATP into cAMP, thus inducing a significant increase in intracellular cAMP levels. This conversion is dependent on the eukaryotic protein calmodulin (19). LF is a zinc protease which cleaves the *N*-terminus of mitogen-activated protein kinases (MAPKs), Mek1 and Mek2 (25). The MAPK pathway relays environmental signals to the transcriptional machinery in the nucleus and therefore modulates gene expression via a burst of protein phosphorylation (26, 27) (Fig. 2). In anthrax infection, these two toxins, EF and LF, are responsible for immune system failure and consequent death of the host.

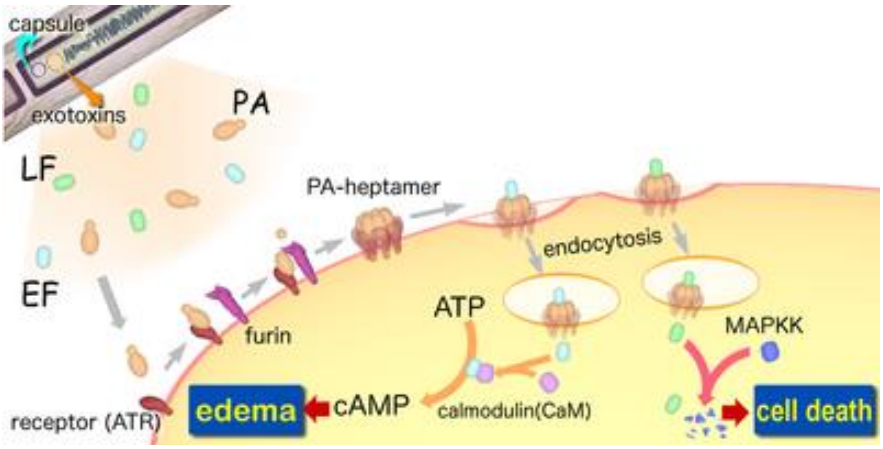

Figure 2. Cellular model of anthrax toxins (28).

Different types of *B. anthracis* infection include cutaneous, gastrointestinal and pulmonary anthrax (29). Recently, a new type of anthrax was identified, namely injectional anthrax (Fig. 3). All the patients who carried this infection were drug users who injected spore-infected heroin into their bodies (30). Cutaneous anthrax is caused after exposure to *B. anthracis* spores when handling sick animals or contaminated wool, hair or animal hides. Gastrointestinal anthrax is caused after ingestion of spore-contaminated meat while pulmonary anthrax is caused after spore inhalation. During cutaneous and gastrointestinal anthrax infection, spores germinate and grow at a low-level at the primary site of infection, inducing local edema and necrosis. Whatever the route of infection, spores are taken up by professional phagocytes, such as macrophages, where they germinate to become vegetative bacteria. Macrophage-containing bacilli detach and migrate to the regional lymph node. Subsequently, vegetative anthrax bacilli grow and therefore create regional hemorrhagic lymphadenitis. Bacteria spread through the blood and lymph and proliferate, leading to massive septicemia. In the case of pulmonary anthrax, pulmonary lymphatic drainage is blocked by peribronchial hemorrhagic lymphadenitis, causing pulmonary edema. Septicemia, toxemia or pulmonary complications lead to death and can occur one to seven days after exposure (13). In injectional anthrax the bacterium spreads throughout the body very fast, affecting the function of vital organs (liver, kidney, heart and brain), leading to septic shock and death within 1-2 days (31).

A. Cutaneous
B. Pulmonary
C. Gastrointestinal
D. Injectional

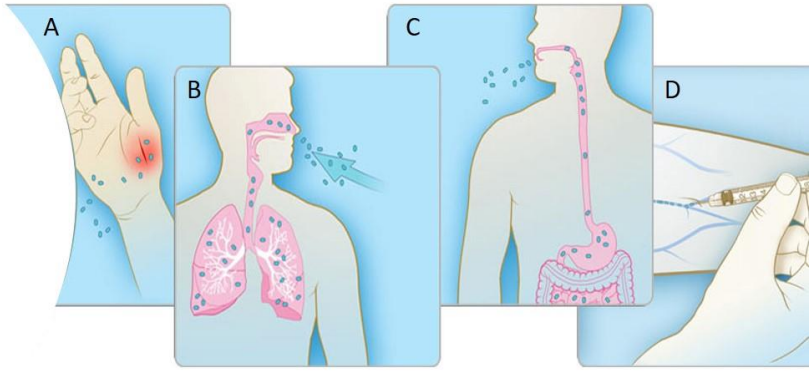

Figure 3. Types of anthrax infection (adapted from (32)).

Treatment and Epidemiology of anthrax

Treatment of anthrax infection can be successful depending on the type of infection, the rapidness of the diagnosis and the advance of the infection. At the moment, there are three types of therapeutics for *B. anthracis* infection: antibiotics, vaccines and antitoxins (21).

FDA has approved three antibiotics for the treatment of anthrax namely, penicillin, doxycycline and ciprofloxacin. A 60-day course of multiple antibiotics, which includes at least one of the three antibiotics approved, is the recommended treatment for pulmonary anthrax. This treatment is based on the long incubation time of anthrax in the organism of the host and it responds to combination therapy if detected early. Other members of the β-lactam family, such as tetracycline and fluoroquinolone, might be effective, but this has not been validated yet. Recently, it has been shown that antibiotics such as daptomycin, dalbavancin and faropenem are effective in mouse models, giving promising data for further clinical evaluation (33).

The Sterne live spore vaccine, created in 1937, is still successfully used in livestock and even in humans in certain countries. Western countries, such as the United States and the United Kingdom, use an acellular vaccine containing the PA toxin of *B. anthracis* in order to induce immunity. There have been reports of reactogenicity

of this vaccine because of the variation in the content of PA and other cellular components, including EF and LF. Presently, the vaccine is administered to people who are at a repeated occupational exposure risk, in six doses: 0, 4, 6, 12 and 18 months, followed by yearly boosters. The vaccine has been approved for pre-exposure administration but recent studies have shown that it is also effective when administered post-exposure. It has also been demonstrated that post-exposure vaccination can shorten the duration of antibiotic treatment (34).

Protective immunity is demonstrated by antibodies to the anthrax toxins, isolated from serum. Obiltoxaximab (commercially known as Anthim) is an injectable drug for the treatment and prophylaxis of pulmonary anthrax. Obiltoxaximab was FDA approved on March 2016 for the treatment for pulmonary anthrax in adults and children in combination with antibacterial drugs. It is a high-affinity humanized and deimmunised monoclonal antibody that binds to the free PA anthrax toxin thus preventing the entry of EF and LF into the cells of the host and ultimately their spreading throughout the body (35).

The largest known anthrax outbreak was reported in Zimbabwe from 1979 to 1985 when 10.000 cases of cutaneous infection were identified. An accidental release of *B. anthracis* spores from a military research facility resulted in the death of 66 people in Sverdlovsk, in 1979. Fortunately, only 18 cases of pulmonary anthrax were reported in the U.S. from 1900 to 2000. As of 2001, after the attacks through U.S. post, the potential of anthrax as a biological weapon was highlighted. A total of 11 pulmonary anthrax cases were identified, 5 of which were fatal. In 2010, 47 intravenous drug users were infected by injectional anthrax in the U.K. The outbreak resulted in 13 deaths. Smaller outbreaks were reported in Germany and Norway (17, 36).

Biology of *B. anthracis*

-Sporulation

As already mentioned, *B. anthracis* has the ability to form spores. The relatively simple developmental process of sporulation has been mostly studied in the model organism *Bacillus subtilis*. During sporulation, a single rod-shaped cell divides assymetrically resulting in two genetically identical daughter cells that undergo different cell fates. The genes necessary for sporulation are often non-essential for normal growth facilitating the identification of novel factors that participate in this developmental process. The purpose of sporulation is to produce a largely metabolically inactive dormant cell type called endospore or spore which is able to survive harsh environmental conditions until favorable growth conditions are restored. When the spore senses that environmental conditions are favorable to growth, it is able to germinate and continue its vegetative cell cycle (37).

The sporulation process involves several "stages", which are reported as "0" to "VII", according to classical nomenclature, based on various morphological landmarks as viewed by electron microscopy (Fig. 4). However, as techniques have advanced, it has become clear that sporulation is not composed of distinct stages that occur sequentially but rather in a continuum in which there might be significant overlap (38).

Stage 0: The decision to sporulate

The entry into sporulation is regulated and dependent, as many other developmental processes, on feedback and feedforward loops. Sporulation occurs in subpopulations rather than homogenously, in the entire bacterial population. It is a highly energy-consuming process and the cells have to confirm the need to sporulate before engaging to it. It is an irreversible process, after cells' commitment. The entry into sporulation can be delayed by the employment of a "cannibalistic" behavior of the subpopulation of cells which have detected the onset of starvation conditions. During the cannibalism, this subpopulation kills surrounding cells, by secreting kill factors, which have not yet detected such conditions and thus are considered unbeneficial. The death of the surrounding cells releases nutrients which are necessary to support the growth of the cannibal subpopulation. Spo0A is the transcriptional master regulator which governs the transition from vegetative growth

to sporulation. A phosphorelay system, which is governed by five autophosphorylating histidine kinases (KinA-KinE), is responsible for the transcriptional activity of Spo0A. The extent of Spo0A phosphorylation determines whether the cells will develop biofilms and cannibalism (low level of phosphorylation) or spores (high level of phosphorylation) (39). Even though the broadly defined signal for the entry into sporulation is "limited nutrient availability", there are specific molecular signals that activate histidine kinases which remain unidentified. Upon activation and autophosphorylation, the phosphoryl group from the histidine kinases is transferred to Spo0A which then becomes active (Spo0A-P) (40). The activated Spo0A-P directly regulates the expression of approximately 120 genes (41). While high levels of Spo0A-P are required for entry into sporulation, the dynamics through which this is achieved are also important. According to previous studies, a threshold level of, not only Spo0A-P, but also phosphorelay components has to be crossed in order for sporulation initiation to occur (42-44). Recent studies suggest that there is a significant overlap in Spo0A-P levels in sporulating and non-sporulating cells (45), indicating that there may also be other downstream events responsible for the decision to enter sporulation. Consistent with this idea, is the observation that entry into sporulation may still be reversible after activation of several *spo* genes by Spo0A and only becomes irreversible upon activation of sporulation-specific sigma factors (46).

Stage I: Axial filamentation

Two chromosomes are harbored by each cell upon entry to sporulation: one for the mother cell and one for the forespore. The so-called axial filament is an elongated serpentine-like structure formed by the duplicated chromosomes that stretches from one cell pole to the other. The anchoring of the axial filament to the cell poles, in order to promote proper chromosome segregation, is performed by RacA. RacA binds to GC-rich inverted repeats located near the origin of replication, making sure that each daughter cell receives one chromosome (47). Robust sporulation is also dependent on proper chromosome number, which is regulated by SirA, Sda and Spo0A-P. Spo0A-P activates *sirA* transcription upon entry to sporulation. SirA interacts with DnaA thus inhibiting DNA replication during sporulation (48). Sda binds to KinA during DNA replication and therefore inhibits the initiation of

sporulation (49). Taken together, initiation of sporulation is limited between rounds of DNA replication (38).

Stage II: Assymetric division

The shift from a medial septum to a polar septum divides the cell into two compartments: the mother cell and the forespore. Assymetric division of the cell induces a cascade of sporulation sigma factors which are compartment-specific. Two effects are essential for the switch to an assymetric septum and these are the accumulation of increased levels of the cell division protein FtsZ and the synthesis of the DNA translocase SpoIIIE. These two effects lead to the repositioning of FtsZ into two separate rings, one near each of the cell poles. The switch in position occurs by helical redistribution of the FtsZ from the mid-cell to subpolar positions. The Z-rings near the two poles are usually unequal and one of them is chosen for the formation of the polar septum (50). The assymetric septum is almost completed before chromosome segregation is finished resulting in the forespore initially containing only 30% of the chromosome. In order for sporulation to proceed, 70% of the remaining chromosome is pumped into the forespore by SpoIIIE. The first sporulation-specific sigma factors are activated after assymetric septation: the forespore-specific σ^F and the mother cell-specific σ^E. Both sigma factors are synthesized before the polar septum is formed but they are held in an inactive state. The activation of σ^E activates the transcription of genes essential for engulfment (51).

Stage III: Engulfment

Assymetric cell division is followed by a second unusual morphological event, the forespore engulfment, a phagocytosis-like process. The mother cell surrounds the forespore while the assymetric septum curves and bends around it. The engulfment process results in a double-membrane forespore located in the cytosol of the mother cell. Three partially redundant molecular mechanisms are responsible for the membrane movement that occurs during engulfment. 1) The DMP machine, which is composed of SpoIID, SpoIIM and SpoIIP, is responsible for membrane migration by hydrolyzing the peptidoglycan (PG) between the two membranes thereby moving the mother cell-derived outer forespore membrane around the forespore (52). According to a recent study, a thin layer of PG remains during the engulfment process, possibly to serve as a template for subsequent remodeling events or cortex assembly (53). 2)

The SpoIIQ-SpoIIIAH zipper, which spreads across the intermembrane space that separates the mother and the forespore, may function as a ratchet to irreversibly drive engulfment (54, 55). 3) The PG synthesis of the germ cell wall could provide a motive force for membrane movement during early engulfment as well as the final step of forespore detachment (39). The final step of the engulfment is the fusion of the engulfing membranes in order for the forespore to be released in the mother cell cytosol. After that, the metabolic capacity of the forespore is diminished. For that reason a channel called "feeding tube" is formed between the mother cell and the forespore (56). SpoIIIAA-SpoIIIAH and SpoIIQ comprise this channel through which small molecules that enable the forespore to continue expressing sporulation genes, are transferred (57). Sporulation-specific σ^F and σ^E factors from Stage II, activate the transcription of σ^G (forespore-specific) and σ^K (mother cell-specific) respectively. The completion of the engulfment process is linked to the completion of the chromosome translocation into the forespore (38).

Stage IV-V: Cortex and coat assembly

The mature *B. anthracis* spore is surrounded by a cell wall which is comprised of (from outside to inside) the exosporium, mostly composed of proteins, the coat, also comprised of around 70 proteins and the cortex, made of specialized PG. The cell wall protects the spore from harsh environmental conditions.

The coat has three distinct layers: the basement layer, the inner coat and the outer coat. The proper assembly of each layer is dependent on one or two major morphogenetic proteins. For example, SpoIVA is the structural component of the basement layer, SafA of the inner coat and CotE of the outer coat. Coat assembly occurs mainly in the mother cell, where the coat is assembled on the surface of the outer forespore membrane. SpoVM is one of the first coat proteins, exclusively produced in the mother cell, that were found to be localized in the outer forespore surface (58, 59). Even though the coat and the cortex are separated by the outer forespore membrane, their assembly is somehow linked. For example, deletion of *spoVM* from *B. subtilis* abolishes the initiation of coat as well as cortex assembly (60). Unfortunately, the mechanism that coordinates the assembly of both structures remains unidentified.

Spore PG is located between two membrane layers and consists of the inner germ cell wall and the outer cortex (61). The germ cell wall is a thin layer adjacent to the inner forespore membrane and has a structure similar to that of the vegetative PG (62). It normally serves as a template for organized synthesis of the cortex (63). The cortex differs in structure due to the decreased degree of crosslinking of the glycan strands and the presence of the muramic-delta-lactam ring (64, 65). Cross-linking increases progressively toward the outermost region of the cortex (66). The decreased degree of cortex crosslinking might allow the spore to expand and contract during maturation or in response to environmental changes, without germinating (67). The mechanism of cortex synthesis is similar to that of vegetative PG synthesis. The enzymes and precursors utilized for cortex synthesis are produced in the mother cell while those involved in germ cell wall synthesis are produced in the forespore (68). The Mur proteins, also present in vegetative cells, produce and modify PG precursors in the cytosol of the mother cell. PG precursors are then tethered to the outer forespore membrane through the formation of the lipid intermediates Lipid I and Lipid II. The lipid-linked precursors are then flipped across the membrane into the intermembrane space between the outer and inner forespore membranes via a Lipid II flippase. Even though there are homologues of putative Lipid II flippases that are expressed specifically during sporulation, their identity is currently unknown. The lipid-linked precursors, now present into the intermembrane space, are assembled into glycan strands via transglycosylation and peptide cross-links between the glycan strands are formed via transpeptidation, both performed by high-molecular-weight Penicillin Binding Proteins (PBPs) (38). Some vegetative PBPs are upregulated (PBP2B and PBP3) while others are downregulated (PBP1, PBP2A, PBP4 and PBP5) during sporulation (69). The production of the muramic-delta-lactam in *B. subtilis* is catalyzed by CwlD and PdaA. First, the muramoyl-L-alanine amidase, CwlD, removes the pentapeptide from *N*-acetylmuramic acid residues and then the PG *N*-acetylmuramic acid deacetylase, PdaA, releases the acetyl group so that lactam cyclization can occur (70). Both of these proteins possess signal peptides that direct them to the intermembrane space where the cortex is polymerized. Formation of the lactam ring likely occurs during and not after polymerization of the glycan strands (68).

Stage VI-VII: Spore maturation and mother cell lysis

During spore maturation, the chromosome gets tightly condensed and forms a characteristic toroidal structure.

When spore maturation is complete, mother cell undergoes autolysis, releasing the dormant spore into the environment.

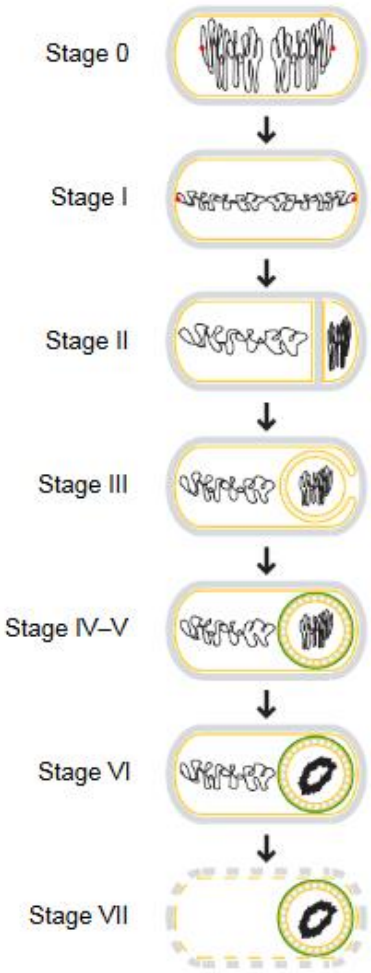

Figure 4. Stages of sporulation of *B. anthracis* and other *Bacillus* species (38).

-Germination

Dormant spores monitor the environment, and when appropriate molecules and/or conditions are sensed, spore germination is initiated. The germination process is divided into five stages: activation, commitment, stage I of germination, stage II of germination and outgrowth (Fig. 5) (71).

Spore activation

Activated spores respond more rapidly to germination. Activation of spores can be achieved by exposure to sublethal heating or extended storage at 4^{o}C. Heat activation solely affects germinant receptors (GRs)-dependent germination, proposing that heat makes GRs more accessible to nutrient germinants. Spore activation is a reversible process, probably because of reversible conformational changes to proteins (72). The need for spore activation can be limited after stimulation of spore germination by multiple germinants that target different GRs. Germinants are the molecules that trigger spore germination and are generally low molecular weight compounds. Small molecule germinants are divided into nutrients, such as amino acids, sugars and purine nucleosides, and non-nutrients, such as CaDPA, cationic surfactants, PG fragments, lysozyme and other PG hydrolases and pressure. GRs are located in the inner forespore membrane and are able to specifically recognize and bind nutrient germinants. GRs, in most cases, are not involved in non-nutrient germination (71).

Spore commitment

Nutrient germinants are added to the spores following activation and the first measurable event is commitment to germinate, even if the germinant is removed. Two germination events happen during commitment: the release of monovalent cations including Na^{+}, K^{+} and H^{+}, most probably from the spore core, and the rise of the spore core pH to 8 (73).

Stage I of germination

A little after commitment, the large depot of CaDPA in the spore core is released and is replaced by water. The influx of water, raises the core water content, thus partially rehydrating the spore core. This event results in the reduction of the wet-heat resistance of the spore (74). CaDPA release during germination as well as CaDPA uptake from the mother cell compartment during sporulation is mediated via channels in the spore's inner forespore membrane formed by proteins of the spoVA operon (75, 76). Spore metabolism is still undetectable after the early events of germination (77).

Stage II of germination

The end of Stage I events, triggers the initiation of the last part of spore germination, Stage II. In Stage II of germination, two, partially redundant cortex lytic enzymes (CLEs), namely CwlJ and SleB, are activated and cleave the cortex leaving the germ cell wall intact. SleB is a lytic transglycosylase and CwlJ may also have this mode of action (78). The two CLEs localize differently in the spore: CwlJ is produced in the mother cell and is localized in the spore by the coat protein YwdL, while SleB is produced in the forespore and is localized in the inner membrane and the outer layers of the mature spore in association with the YpeB protein (79, 80). Cortex hydrolysis leads to the expansion and rehydration of the spore core. The inner membrane surface increases, without new membrane synthesis, while the germ cell wall is remodeled. These events mark the end of spore dormancy (71). The spore core now contains approximately 80% wet weight as water and enzymes in the core are activated (81). This leads to the degradation of small acid-soluble proteins (SASPs), which are DNA associated, releasing the DNA for transcription and providing a source of amino acids for biosynthesis during outgrowth (82). The end of Stage II of germination also leads to partial breakdown of the spore coat and exosporium probably by proteolysis (77).

Outgrowth

The resumption of metabolism and *de novo* synthesis of macromolecules in the cell results in outgrowth of the germinated spore into vegetative cell. Lipid synthesis starts early, followed by bulk protein and DNA synthesis. Generally, genes required during outgrowth are also required for vegetative growth (77).

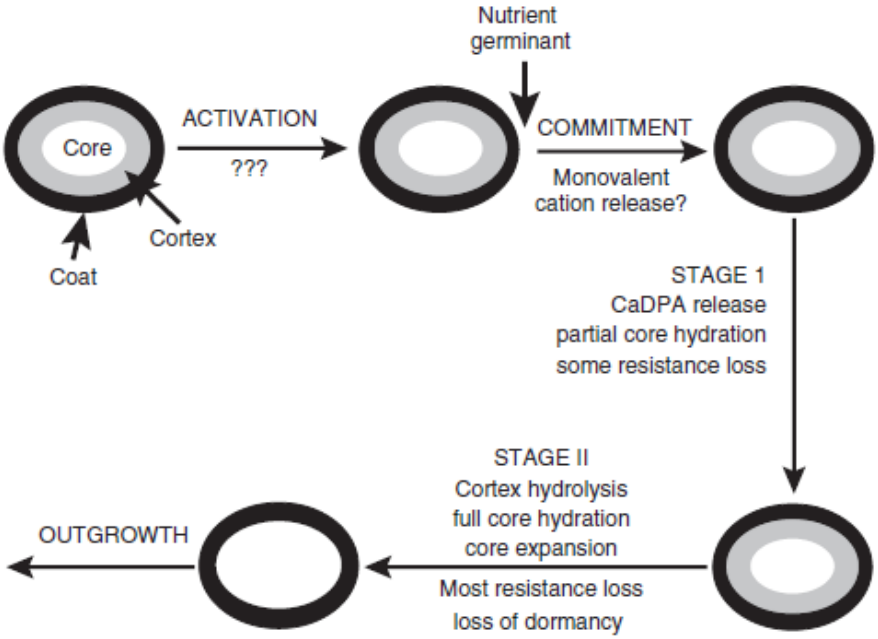

Figure 5. Stages of germination of *B. anthracis* and other *Bacillus* species (71).

Cell wall components of *B. anthracis* vegetative cells

The cell wall of *B. anthracis* has a multilayered structure whose main components are described below (Fig. 6).

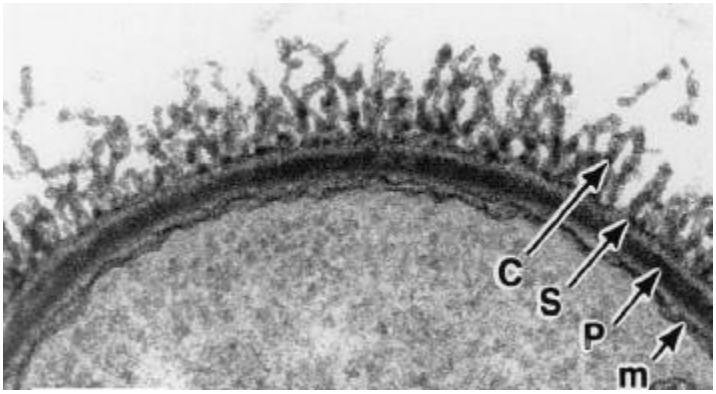

Figure 6. Transmission electron microscopy image of a *B. anthracis* vegetative cell. m: membrane, p: peptidoglycan, s: S-layer, c: capsule (83).

Peptidoglycan

PG is the fundamental component of the cell wall. It is a complex macromolecule which is essential for cell integrity, since it enables the bacterium to resist osmotic pressure. It is also a dynamic macromolecule with tight regulation. PG

remodeling allows cell growth and division. *B. anthracis* PG consists of alternating units of *N*-acetylglucosamine (GlcNAc) and *N*-acetylmuramic acid (MurNAc) held together by β-(1-4) glycosidic bonds and the stem peptides, attached to the MurNAc residue, which are composed by L-Ala, D-Glu, meso-DAP, D-Ala, D-Ala. 32% of the stem peptides are cross-linked between meso-DAP and D-Ala (84) (Fig. 7). A variety of different enzymes, including glycosyltransferases, transpeptidases, D,D-carboxypeptidases and hydrolases shape the three-dimensional structure of PG, increasing the complexity of this macromolecule (85).

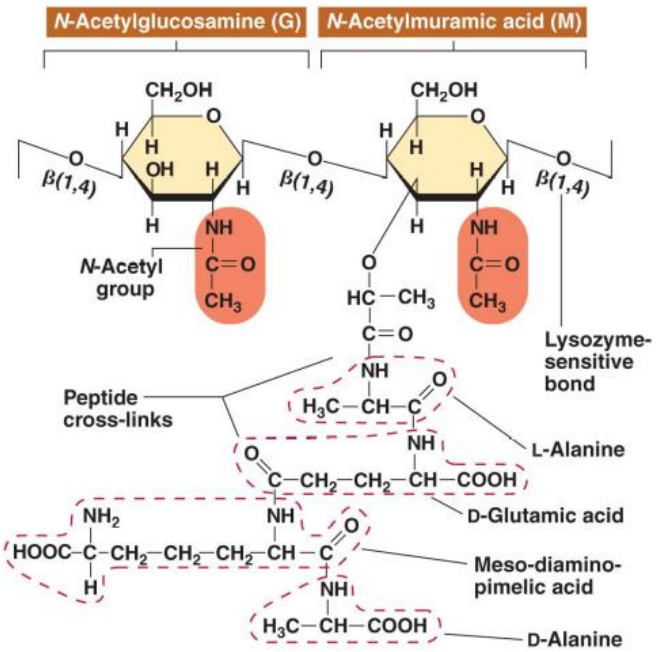

Figure 7. Structure of the repeating unit of peptidoglycan in gram-positive bacteria (86).

PG biosynthesis is a three step process depending on the compartment in which each step takes place (Fig. 8).

1) Cytoplasmic reactions (synthesis of nucleotide precursors)

Fructose-6-phosphate is converted to UDP-GlcNAc via a series of enzymatic reactions in the cytoplasm. UDP-GlcNAc is then converted to UDP-MurNAc by two enzymatic reactions involving MurA and MurB. The transfer of the enolpyruvate moiety of phosphoenolpyruvate (PEP) to the 3-hydroxyl of UDP-GlcNAc is mediated by MurA while the reduction of the UDP-GlcNAc-enolpyruvate product by using one equivalent NADPH and a solvent-derived protein is mediated by MurB. This two-

electron reduction creates the lactyl ether of UDP-MurNAc. The stem peptide of UDP-MurNAc-pentapeptide is assembled by MurC, D, E and F enzymes (87).

2) Reactions at the inner side of the cytoplasmic membrane (synthesis of lipid-linked intermediates)

The transfer of the phospho-MurNAc-pentapeptide moiety of UDP-MurNAc-pentapeptide to the membrane acceptor undecaprenyl phosphate in order to form Lipid I is catalyzed by MraY transferase. The addition of GlcNAc to the MurNAc residue of Lipid I, producing Lipid II, is catalyzed by MurG transferase (88).

3) Reaction at the outer side of the cytoplasmic membrane (polymerization reactions)

The first steps of PG formation initiate upon transfer of Lipid II to the outer side of the membrane. Lipid II translocation might be mediated by the integral membrane protein FtsW (89). Subsequently, Lipid II is polymerized by transglycosylation in order to form the immature PG. Transglycosylation reaction is followed by a transpeptidation reaction for maturation of PG and formation of cross-bridges (90).

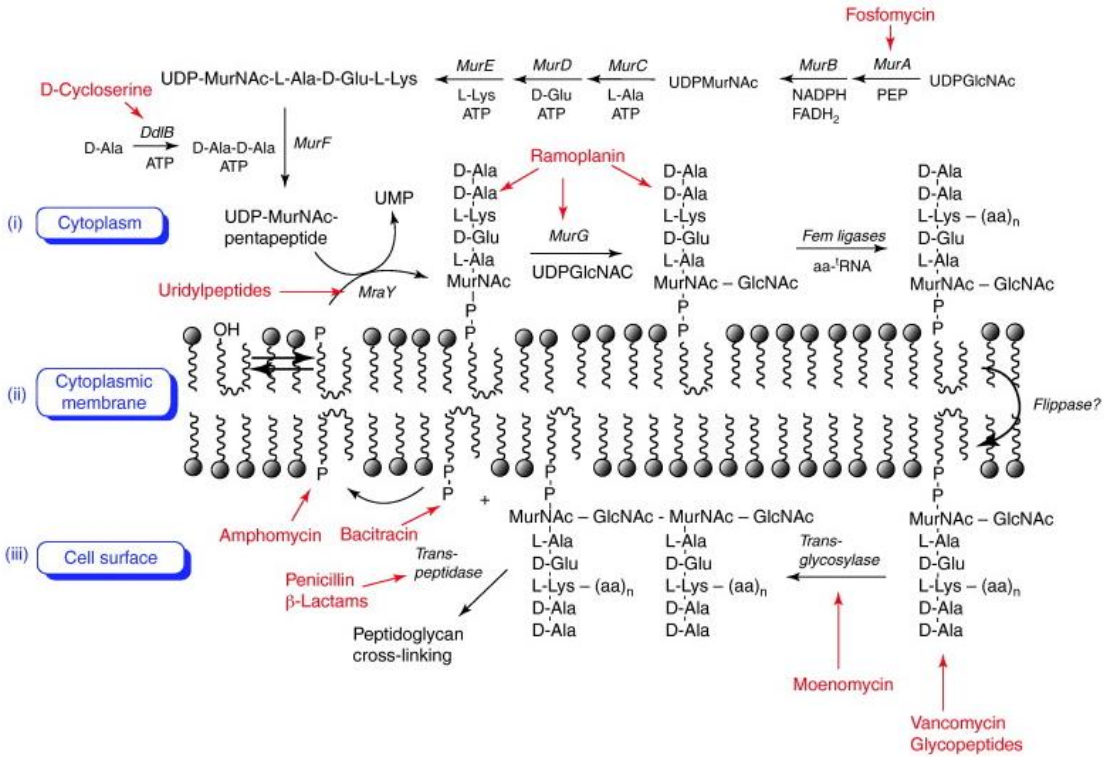

Figure 8. Biosynthetic pathway of peptidoglycan (91).

Neutral polysaccharide (PS)

Except from PG, Gram-positive bacteria synthesize secondary cell wall polysaccharides (SCWPs) which usually have anionic nature and are covalently linked to PG. SCWPs are categorized into: teichoic or teichuronic acids, lipoteichoic acids and other neutral or acidic polysaccharides. Teichoic acids have not yet identified in the surface of *B. anthracis* and they might even be absent, since the phosphate concentration in the cell wall is very low (92). SCWPs are involved in a variety of biological functions including binding of divalent cations and proteins, interaction with cell wall lytic enzymes and formation of a barrier to prevent diffusion of nutrients and metabolites (93).

B. anthracis cell wall contains a non-classical SCWP, called neutral polysaccharide, which is extracted from PG by hydrofluoric acid treatment. Neutral polysaccharide has a molecular mass of 12 kDa and consists of galactose, *N*-acetylglucosamine and *N*-acetylmannosamine (94, 95). Its backbone is composed of multiple trisaccharide repeats of: →6)-alpha-GlcNAc-(1→4)-beta-ManNAc-(1→4)-beta-GlcNAc-(1→ and is highly substituted at alpha-GlcNAc residues with alpha- and beta-Gal residues at O-3 and O-4 respectively and at beta-GlcNAc residues with alpha-Gal at O-3 (96). Neutral polysaccharide is linked to PG through murein linkage units via a phosphodiester bond (97). This polymer has been identified in both vegetative and spore cell wall (98). Neutral polysaccharide has been found to be pyruvylated exclusively at the terminal beta-ManNAc residue of the distal non-reducing end, opposite the end linked to PG. Pyruvylation of the neutral polysaccharide is essential for the interaction of the SLH domain-containing proteins to the cell wall, including autolysins that are required for the bacterium correct septation (99). It has been reported that the neutral polysaccharide of *B. anthracis* is also O-acetylated and *N*-deacetylated at specific HexNAc residues, adjacent to the pyruvylated residue (100).

Surface layer (S-layer)

The S-layer is a paracrystalline layer which is comprised of two proteins, namely the surface array protein (Sap) and the extractable antigen 1 (EA1), encoded by the chromosomal genes *sap* and *eag* (101). Sap and EA1 are expressed during different developmental stages in *B. anthracis*: Sap during exponential while EA1 during stationary growth (102). The two proteins self-assemble in order to form the

paracrystalline layer. Both Sap and EA1 proteins are composed of an anchoring domain made of three structurally conserved surface layer homology (SLH) motifs and a second motif, which possibly plays a role in their crystallization (103). As mentioned above, SLH domain-containing proteins are attached to the neutral polysaccharide via electrostatic interactions with its pyruvylated moieties (99, 104). S-layer proteins represent up to 15% of the total protein in the bacterium and they can function as protective coats, molecular or ion traps and structures involved in cell adhesion (84).

Capsule

The capsule of *B. anthracis* is the outermost layer of the cell envelope. Although most bacterial capsules are composed of polysaccharides, *B. anthracis* capsule is a polymer of D-glutamic acid, linked by peptide bonds between c-carboxyl and a-amino groups. The genes required for capsule synthesis are located in the pXO2 plasmid (105). Capsule formation involves a two-step procedure, including polymerization and transport through the membrane. First, CapB and CapC regulate capsule synthesis and then CapA and CapE facilitate its transport (106). Finally, CapD catalyzes the covalent anchoring of the poly-γ-glutamate molecule to PG (107). More specifically, CapD either catalyzes the amide bond formation between the capsule and the meso-DAP residues of the stem peptides (108) or the *N*-deacetylated GlcNAc residues of PG (109). According to the second hypothesis, the deacetylation reaction is performed by the PG deacetylases BA1961 and BA3679 (109). *B. anthracis* capsule is currently considered to be one of its major virulence factors. The capsule does not provoke host immune response since it is a weak immunogen (110). In addition, the polymer enables the bacterium to evade the host immune responses and cause septicemia once it has infected the host (111).

Cell wall components of *B. anthracis* spores

B. anthracis spore is a series of concentric shells. Spore structure is depicted in Fig. 9.

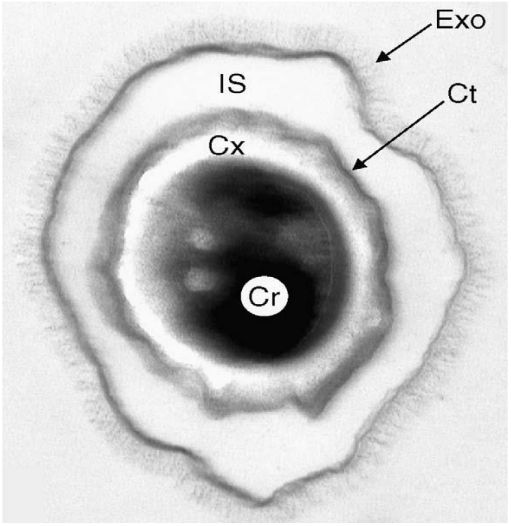

Figure 9. Transmission electron microscopy image of a *B. anthracis* spore. Cr: core, Cx: cortex, Ct: coat, IS: interspace, Exo: exosporium (112).

Core

The core is the inner compartment of the spore where the chromosome is located, tightly complexed with SASPs. The core also contains high levels of calcium dipicolinic acid and other ions which together with the interactions between the DNA and the SASPs, provide spore protection against heat and UV radiation. The membrane surrounding the core is also crucial for spore resistance (113).

Germ cell wall

The germ cell wall is the thin inner PG layer of the spore. It is structurally similar to the PG of vegetative cells since it contains more tripeptide side chains and higher level of cross-linking compared to the cortex. The germ cell wall is not degraded during germination and functions as the initial wall of the outgrowing spore (67).

Cortex

The cortex is the thick outer PG layer of the spore. It has a distinctive structure as the peptide chain from half of the MurNAc residues are removed and replaced by muramic-delta-lactam (Fig. 10). These residues are spaced in every second MurNAc along the glycan strands. In most species, the peptide chains of an additional 15-25% of MurNAc residues are removed or are shortened to a single L-Ala residue. The cortex

appears to have a relatively loose cross-linking. More specifically, only 3% of MurNAc residues carry peptides which are cross-linked. As mentioned earlier, cortex synthesis is performed at Stage IV-V of sporulation and is similar to that of vegetative PG. In all species in which the spore PG structure has been directly examined, the peptide side chains contain meso-DAP. The cortex is a predominant factor in maintaining spore dehydration and by extension spore dormancy, heat and chemical resistance (68, 70, 114, 115).

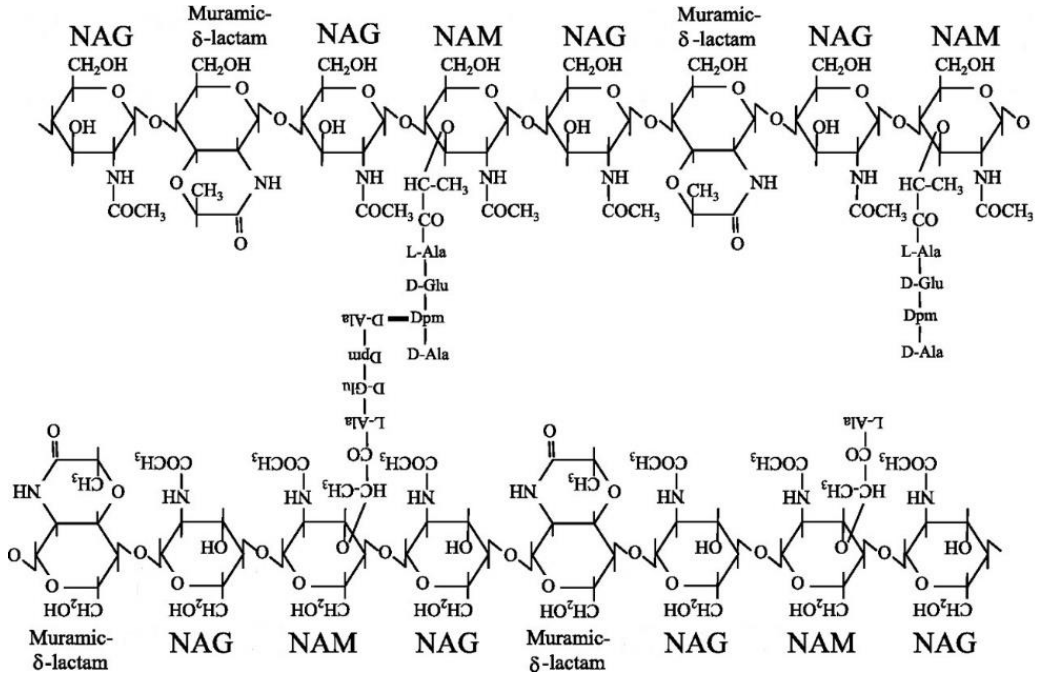

Figure 10. Structure of cortex. NAG: GlcNAc, NAM: MurNAc (116).

Coat

The coat is a protein shell that surrounds the cortex. It is a multilayered organization which consists of the basement layer, the inner coat and the outer coat. Its layers appear to be in close contact with the spore suggesting that they are connected with chemical bonds. Coat's surface is not that of a smooth sphere but it appears to possess ridges that look like folds around the entire circumference. When these ridges unfold, they accommodate expansion in the volume of the spore core that occurs when the relative humidity changes. The ability of the coat to respond to changes in interior volume might be important in natural environments. The coat has a number of roles. It acts as a permeability barrier preventing the entry of large

molecules such as enzymes (e.g. lysozyme) as well as small reactive molecules (e.g. glutaraldehyde) or predation by bacterivores to the inner spore layers (117-119).

Exosporium

The exosporium is the outermost layer of *B. anthracis* mature spore. It is a loose-fitting, balloon-like structure which is composed of two layers: the outer-layer nap and the basal layer. The inner layer consists of a paracrystalline basal layer with a hexagonal lattice structure. The outermost layer is formed by either type II or type III crystals, depending on the strain. The arrays formed by type II crystals would presumably form a semipermeable barrier with pores around the spore. The composition of the exosporium was determined to be approximately 50% protein, 20% lipid, 20% neutral polysaccharides and 10% other components (120). To date, several exosporium proteins have been identified in *B. anthracis* including BclA, BclB, BxpA and BxpB (121-124). The exosporium may function as a barrier that does not allow the access of antibodies to antigens present in the spore coat. There is no evidence that it is involved in spore resistance in any other way (119).

Taken together, the protective functions of *B. anthracis* spore structure components allow the spores to remain dormant for years.

Recently, a novel exopolysaccharide, called pzX, has been identified in *B. cereus sensu lato* group, including *B. anthracis*. The XNAc operon contains the genes involved in the formation of pzX. pzX is produced during late stationary phase of growth under defined nutrient medium. It is believed to co-form during sporulation and surround the mature spores upon release from the mother cells. Production of pzX can be regulated by the addition of specific nutrients in the medium and rich medium appears to suppress its formation. The structure of pzX is distinctive since it is composed of an unusual three amino-sugar sequence repeat of [-3)XylNAc4OAc(α1-3)GlcNAcA4OAc(α1-3)XylNAc(α1-]$_n$. Except from its unique structure, pzX has unique properties including surfactant, adherence and antiaggregant (125).

Polysaccharide deacetylases (PDAs)

Polysaccharide deacetylases (PDAs) are members of the Carbohydrate Esterase 4 (CE4) family which includes acetylxylan esterases, chitin deacetylases, chitooligosaccharide deacetylases and PG deacetylases. CE4 family enzymes catalyze the hydrolysis of either *N*-linked acetyl group from GlcNAc and/or MurNAc residues (chitooligosaccharide, chitin and PG deacetylase), or *O*-linked acetyl groups from *O*-acetylxylose residues (acetylxylan esterase). CE4 esterases are metal dependent enzymes that contain a conserved catalytic core termed NodB homology domain (126).

The biological role of PG deacetylases was for many years strongly connected to conferring lysozyme resistance. Lysozyme belongs to the first line of defense of the innate immune system of the host. It is a 14.5 kDa cationic protein present in tears, gastric juice and milk. The antibacterial properties of lysozyme result from an enzymatic and a non-enzymatic activity. Lysozyme is a muramidase which hydrolyzes the β-(1-4) glycosidic bonds between C1 of MurNAc and C4 of GlcNAc residues of PG. The generation of PG fragments that are recognized by different immune receptors result in triggering of an immune reaction to the host. In addition, lysozyme functions as a cationic antimicrobial peptide which is capable of disrupting bacterial membranes (127).

Many pathogenic bacteria have developed sophisticated strategies to avoid recognition and/or lysis by the innate immune system of the host, including the modification of the glycan strands of their PG. Three well-known modifications conferring resistance to lysozyme are *N*-glycolylation of MurNAc, *O*-acetylation of MurNAc and *N*-deacetylation of GlcNAc (Fig. 11) (128). The first enzyme responsible for the deacetylation of GlcNAc residues in PG, PgdA, was identified in the naturally lysozyme resistant *Streptococcus pneumoniae* (129). Functional homologues of PdgA have been identified in various microorganisms: BA1977 from *B. anthracis* (130), BC1974 from *B. cereus* (130), PdgA from *L. monocytogenes* (131), PgdA from *L. lactis* (132), PgdA from *S. suis* (133), SfPgdA from *S. flexneri* (134) and PgdA from *E. faecalis* (135). In the case of *S. suis* and *E. faecalis*, expression of PgdA is induced after exposure of bacterial cells to neutrophils or lysozyme respectively (133, 135). Deacetylation has

also been identified in spore cortex in several species, including *B. anthracis*, but no physiological significance has been associated with this modification. The level of deacetylation of the cortex is generally lower than that observed in PG since the mature spore has permeability barriers which function as lysozyme resistance mechanisms (68).

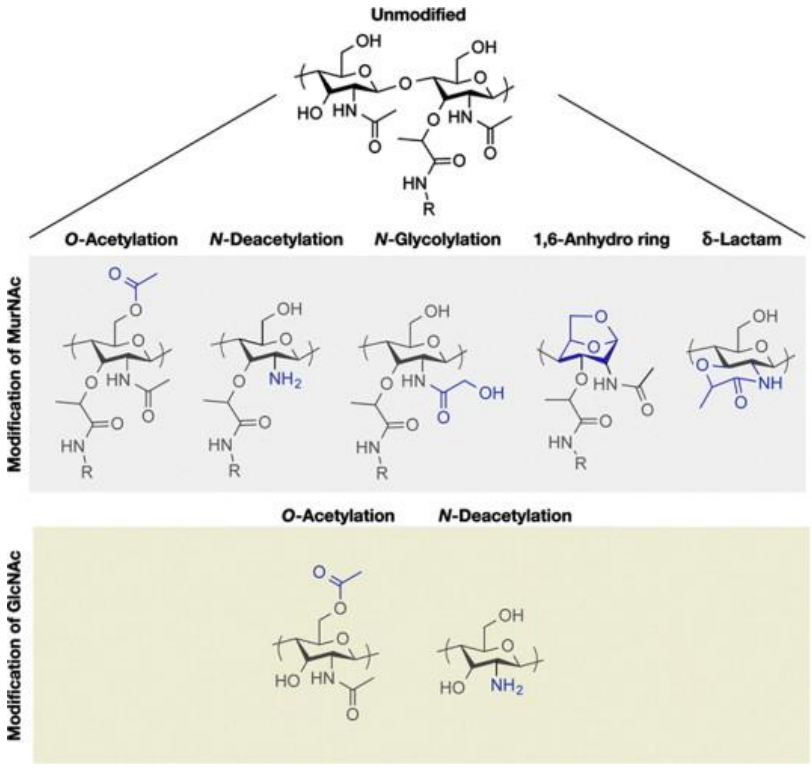

Figure 11. Modifications of the glycan strands of peptidoglycan (136).

Even though the role of PG deacetylases in conferring lysozyme-resistance has been extensively studied, very little information is available for their roles in bacterial physiology. One of these roles is the indirect regulation of autolysin activity. Autolysins are hydrolytic enzymes that digest the PG of the bacteria in which they are produced and are involved in PG remodeling during cell division and cell elongation, as well as in PG maturation and turnover (137). PgdA from *L. lactis*, except from conferring lysozyme resistance, also regulates the major autolysin AcmA (132). Likewise, two recently studied PG GlcNAc deacetylases (PGDAs) from *B. anthracis*, BA1961 and BA3679, seem to impair the substrate recognition of PG hydrolases that are crucial for autolysis and cell division respectively. Δ*ba1961* and Δ*ba3679* knockout strains do not

exhibit a lysozyme sensitivity phenotype but show a defect in daughter cell separation and local cell wall thickenings, suggesting their participation in PG biogenesis during cell elongation and division (130). PG deacetylases are also involved in sporulation. The MurNAc PG deacetylase PdaA from *B. subtilis* participates in the formation of the muramic-delta-lactam of cortex. *pdaA*-deficient spores are unable to germinate since the lactamized *N*-acetyl-muramic acid residues are essential for the activity of CLEs during germination (138). PdaA has homologues in other Gram-positive bacteria such as BA0424 from *B. anthracis* (139). Another polysaccharide deacetylase associated to sporulation, PdaB, has been identified and characterized in *B. subtilis*. *pdaB*-deficient spores are empty or cortex-less implying its importance in cortex formation and in further maintenance of spores after the late stage of sporulation (140). Besides PG, deacetylases act on other polysaccharides which are either secreted or decorate their cell envelope. PelA from *P. aeruginosa* for example, deacetylates the Pel exopolysaccharide, which is implicated in biofilm formation. PelA is also considered to be essential for the formation and secretion of the Pel polymer (141). Likewise, IcaB from *S. epidermidis* (142) and PgaB from *E. coli* (143) have been reported to modify and export the poly-β-1,6-*N*-acetyl-D-glucosamine (PNAG) exopolysaccharide.

Interestingly, Bacillus sp. genomes, especially those of *B. cereus* and *B. anthracis,* contain multiple putative PDA genes (11 open reading frames) (Table 1), including those encoding for the three above-mentioned PG deacetylases (BA1977, BA1961 and BA3679). Two of these enzymes, BA5436 and BA2944, are active on common deacetylase substrates and participate in neutral polysaccharide attachment to PG (BA5436) or in polysaccharide modification (BA2944) (130). Two additional putative polysaccharide deacetylases, BA0330 and BA0331, which are predicted lipoproteins, were demonstrated to be required for osmotic stability and cell shape maintenance respectively, functions which do not involve enzymatic activities (144).

Table 1. Putative polysaccharide deacetylases from *B. anthracis* and *B. cereus*

***B. anthracis* Ames**	***B. cereus* ATCC14579**	**Biological role**	**Identity %**	**PDB code**
BA1977	BC1974	Lateral PG synthesis, Lysozyme resistance	98	5N1J
BA1961	BC1960	PG biogenesis (elongation, cell division)	94	4L1G
BA2944	BC2929	PS modification	94	-
BA3679	BC3618	PG biogenesis (elongation, cell division)	97	-
BA5436	BC5204	Anchoring of S-layer to PS	93	-
BA0330	BC0361	Structural interactions with PG	87	4V33, 4HD5
BA0331	-	Cell shape maintenance	-	-
BA0424	BC0467	ND	98	2J13
BA0150	BC0171	ND	95	4M1B
BA1836	BC1768	ND	92	-
BA3943	BC3804	ND	95	-

Structural analysis of PDAs

Except from functional analysis, structural studies have also been performed for several PDAs from different bacteria, either Gram-positive or Gram-negative, and fungi (127).

The first two PDAs of the CE4 family enzymes, whose crystal structures were determined were the PG GlcNAc deacetylase PgdA from *S. pneumoniae* (145) and the PG MurNAc deacetylase PdaA from *B. subtilis* (146). All CE4 family members share the conserved catalytic NodB domain. In addition, a highly flexible *N*-terminus domain, with an average length of 40-50 amino acids, is common in most of the CE4 structures. Remarkably, in some cases, one or more additional domains are also present but their functions have not yet been clarified (127).

The NodB domain adopts a distorted beta/alpha barrel fold, formed by 6 or 7 parallel beta-strands, with the active site lying in a groove. Since CE4 members are metal-dependent enzymes, most of the structures contain a divalent cation, usually Zn^{+2}, in their active sites, which is essential for enzymatic activity. The NodB domain consists of five conserved sequence motifs, each of which contains residues important

for catalysis and metal binding (145) (Fig. 12). It has been proposed that catalysis follows a general acid-base mechanism (Fig. 13). Motif 1 (TFDD) contains two Asp residues: the first Asp residue of the motif acts as the catalytic base which activates the catalytic water, while the second one coordinates the metal ion. Motif 2 (H(S/T)xxH) provides the two His residues which coordinate the metal ion together with the Asp of Motif 1. Motif 3 (RpPxG) contributes a conserved Arg residue which coordinates the catalytic base (Asp) and a strictly conserved Pro residue. The catalytic acid is a His residue which lies in Motif 5 (LxH) (Fig. 12, 13). This His residue is coordinated by an Asp residue provided by Motif 4. It has been proposed that the interaction of His residue (Motif 5) with Asp residue (Motif 4) increases the pKa of His which is then protonated at physiological pH. The His residue could therefore contribute this hydrogen to the amine leaving group of substrate to facilitate the breakdown of the tetrahedral intermediate. The active site is completed with the presence of a water molecule which coordinates the metal and is located in a position suitable to perform nucleophilic attack (Fig. 13) (145).

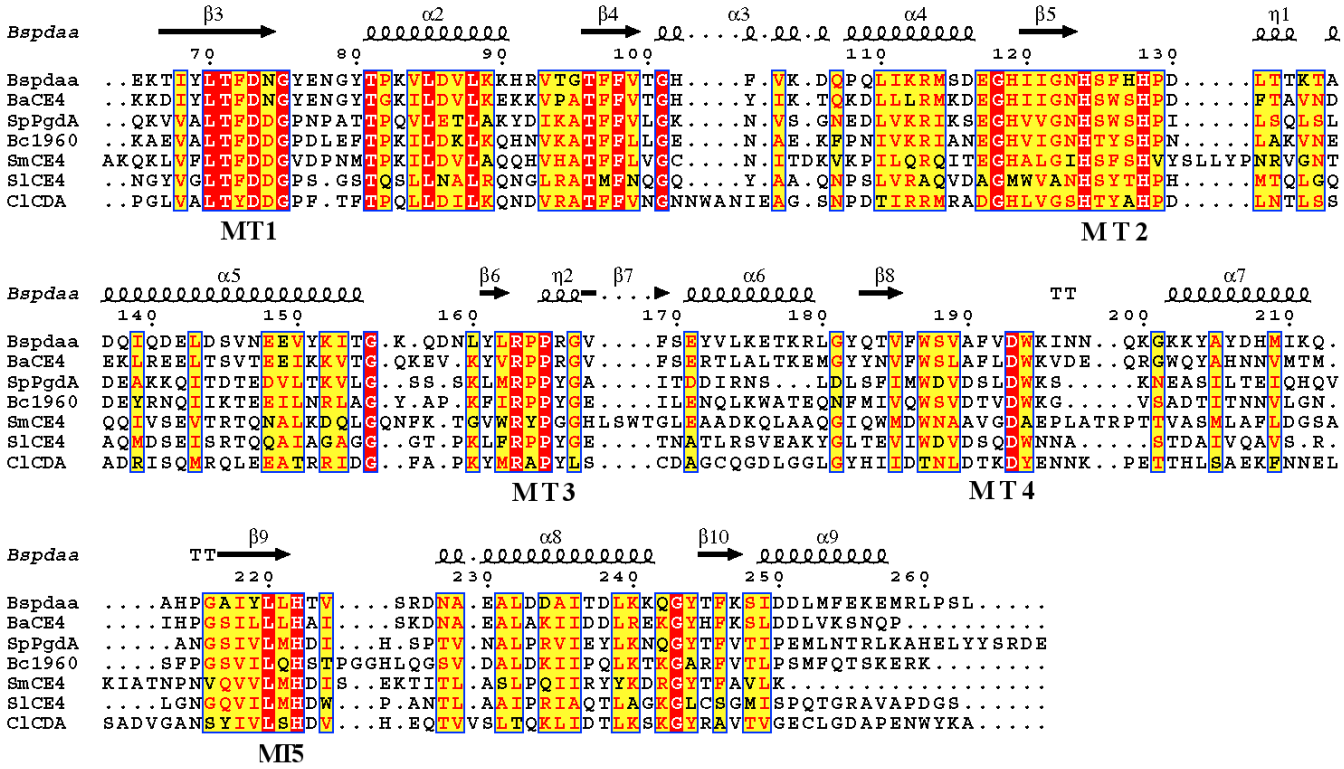

Figure 12. Structure-based sequence alignment of the NodB domains of representative members of the CE4 family including the peptidoglycan deacetylases SpPdgA, BaCE4, BC1960 and BsPdaA, the chitin deacetylase ClCDA, the acetylxylan esterase SlCE4 and the putative polysaccharide deacetylase SmCE4. The secondary structure elements shown at the top of the

alignment are those of the BsPdaA structure. Alignment was performed with T-coffee and plotted with the ESPRIPT (147) programs. Strictly conserved residues are colored white in dark background and similar residues are red and boxed. The five CE4 active-site motifs (MT1 to MT5) are indicated below the alignment (127).

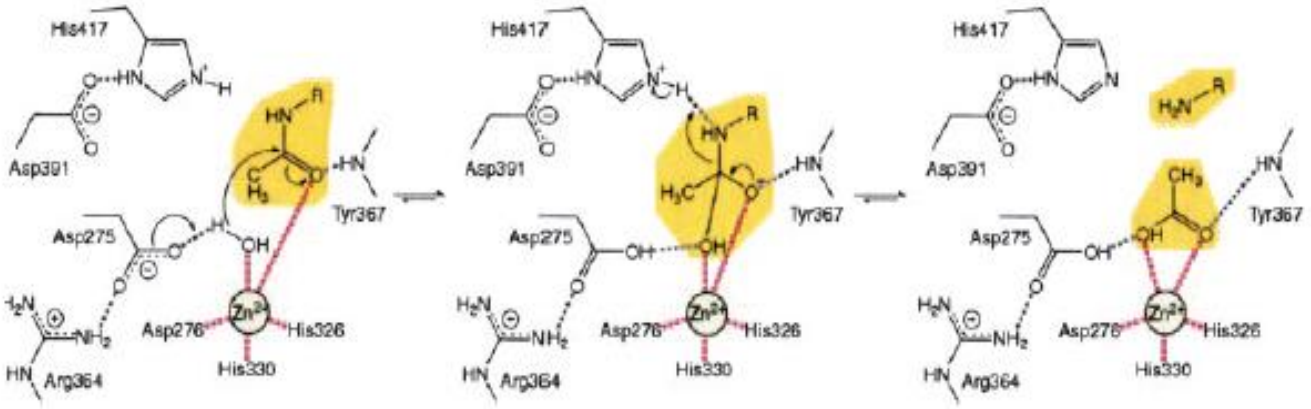

Figure 13. Proposed catalytic mechanism of PDAs. View of a deacetylation reaction in the active site of SpPgdA (145).

The crystal structures of six PDAs from *B. anthracis*/*B. cereus* have been determined so far, while the biological roles of most of them have been elucidated (Fig. 14). BC1960 and BC1974 from *B. cereus* have been identified and further characterized as PG GlcNAc deacetylases (130, 148). BC1960 and BC1974 exhibit 94% and 98% sequence identity to BA1961 and BA1977 from *B. anthracis* respectively (130). Both enzymes are representative members of the CE4 family since they retain the metal-binding triad and all the essential for catalysis amino acids. In addition, both enzymes contain Zn^{+2} in the active site (149, 150). In contrast, BA0424 from *B. anthracis* is proposed to be a PG MurNAc deacetylase, based on similarities with PdaA from *B. subtilis*, even though this function awaits confirmation. BA0424, similarly to PdaA, lacks the otherwise conserved Asp residue, which coordinates the metal ion. In its place it possesses an Asn residue which points away from the active site. The crystal structure also revealed the presence of a metal ion in the active site which is believed to be coordinated by an acetate ion (139). It becomes apparent that modification in the five motifs of the NodB domain can affect enzyme activity, substrate specificity and metal preference. *B. anthracis* BA0150 is a distinct PDA case since it completely lacks the Asp-His-His metal-binding triad. Instead, it contains Ile, Met and Tyr residues

respectively, none of which have strong affinity for metal ions. Consequently, it was proposed to be a pseudoPDA (151). The *B. cereus* BC0361 and its *B. anthracis* homologue BA0330 also deviate from the characteristic members of the CE4 family. They are both inactive on a wide range of substrates usually employed for PDAs. The structures of these proteins revealed an *N*-terminal, typical fibronectin type 3-like fold (Fn3), in addition to the NodB domain (144, 152). BC0361/BA0330 are the first reported PDAs which incorporate an Fn3 module. Even though both proteins contain most of the NodB motifs, the Arg typically provided by motif 3 is given here from a different part of the structure. In addition, the His residue, which acts as a catalytic acid, typically provided by motif 5 is given from a position of the sequence which does not belong to the NodB domain. Furthermore, the Asp residue which is usually provided by motif 4 and it is responsible for tuning the pK_a of the catalytic base (His of motif 5) is absent from the sequence. Instead, BC0361/BA0330 provide an Arg residue which may act as a charge distribution modulator to the catalytic His (127).

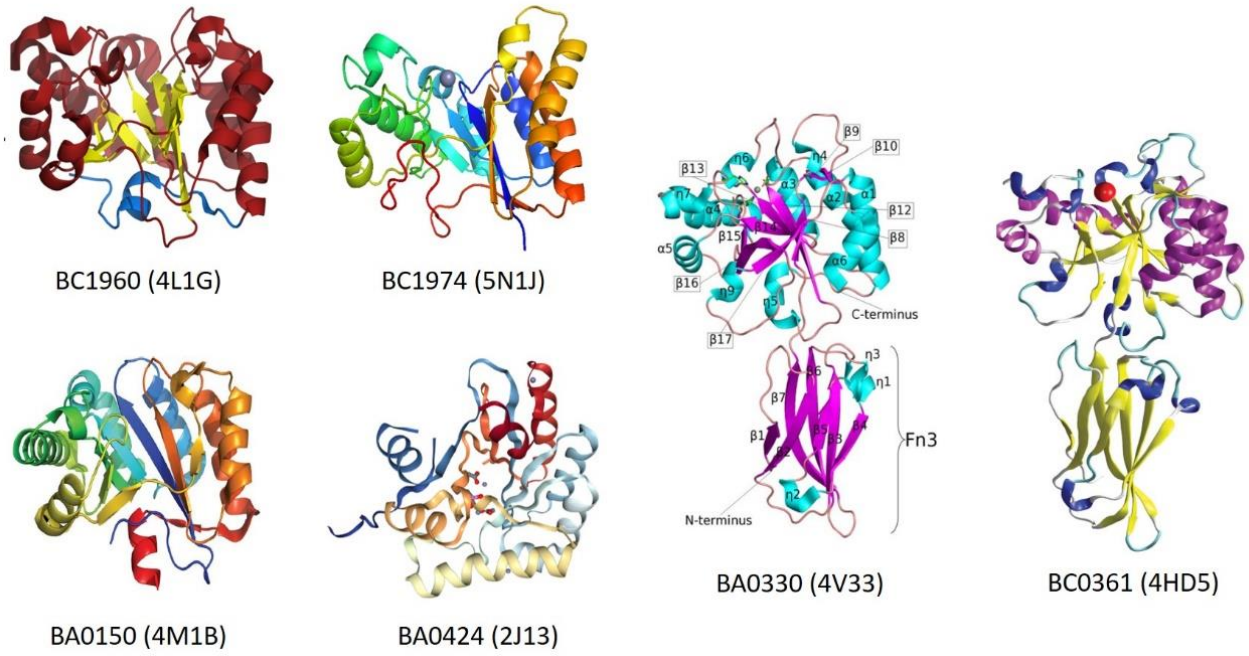

Figure 14. Crystal structures of PDAs from *B. anthracis/B. cereus.*

Proline hydroxylation in the active site of PDAs

Interestingly, the BC0361/BA0330 structures revealed that the strictly conserved Pro of motif 3 is a modified 2-hydroxyproline (2-Hyp). This unusual post-translational modification represents a new type of protein hydroxylation which targets the main chain of protein molecules modifying the Cα atom of Pro residues to produce 2-Hyp. Due to its occurrence in the active sites of PDAs, 2-Hyp could be potentially linked to various aspects of bacterial pathogenicity. The Pro→2-Hyp conversion is a widespread occurrence in PDAs of the CE4 family affecting a highly conserved proline residue of the active site. The origin of the hydroxyl group is molecular oxygen and the Pro hydroxylation mechanism is probably autocatalytic, sharing at least one catalytic residue (Asp) with the deacetylation reaction. In addition, the new post-translational modification represents a maturation process of the active site which establishes an intertwining between hydroxylation and deacetylation, thereby significantly enhancing deacetylase activity.

It is proposed that during catalysis, the 2-Hyp residue gives rise to a hydrogen bond and provides additional stabilization at the transition state of the deacetylation reaction, complementing its interactions with the divalent metal and with the backbone –NH group (from the residue following 2-Hyp) (Fig. 15) (149).

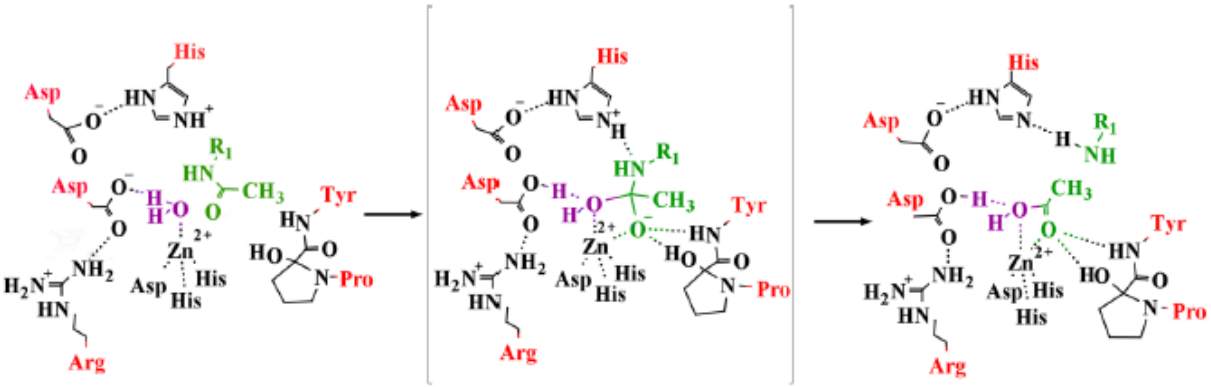

Figure 15. Proposed interwining of deacetylation with the Pro → 2-Hyp conversion in PDAs. All residues shown are conserved in PDAs with the exception of the residue following 2-Hyp (Tyr in the case of BC1960) (149).

Pseudoenzymes

Inactive enzymes, pseudoenzymes or dead enzymes can be defined as enzyme homologues which are predicted to retain protein expression, subcellular localization and typical protein folding but lack catalytic activity (153). Ever since the original identification of dead enzymes, there have been examples of enzymes which have lost their catalytic activity but still exerted biological functions. However, these examples were assumed to be relatively rare. This assumption was dramatically altered when large-scale sequencing of whole genomes was employed (154).

It has been estimated that at least 10% of mammalian enzymes are predicted to be pseudoenzymes and the estimate for worms and flies increases to 15%. The best studied dead enzymes belong to the kinase, phosphatase and protease families (Fig. 16). 10% of mammalian kinases are predicted to be inactive and this ratio rises to 16% for human proteases and for *D. melanogaster* serine proteases the percentage may be as high as 30% (155). It is now understood that dead enzymes are present in a wide variety of enzyme families and play diverse roles in physiology and pathophysiology. In addition, they are well-conserved, implying a selective pressure to keep them during evolution and to maintain their function (156).

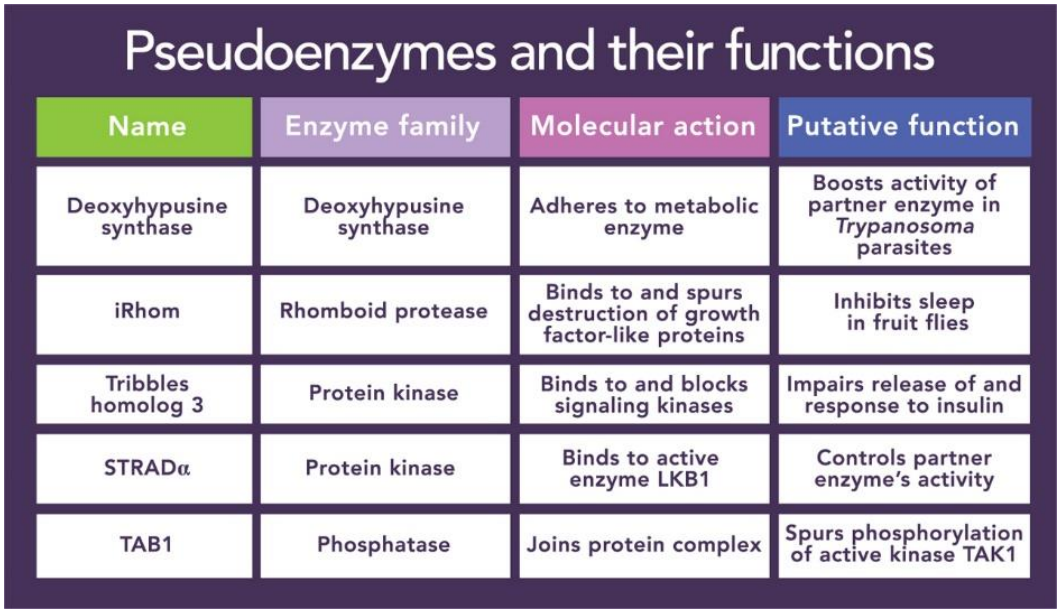

Figure 16. Examples of pseudoenzymes of different enzyme families and their function (153).

The first example of a non-catalytic enzyme relative was reported in 1967, when the partial sequence of bovine α-lactalbumin was found to share approximately 35% sequence identity with chicken lysozyme. Lysozyme hydrolyzes β-1,4-sugar linkages in bacterial cell walls, while α-lactalbumin is a non-catalytic, regulatory subunit of the unrelated enzyme β-1,4-galactosyltransferase, found in mammalian milk. Remarkably, both proteins are involved in processing β-1,4-sugar linkages but with different outcomes and in different contexts. It was suggested that this similarity could be a result of either convergent or divergent evolution. However, it was argued that in this case divergence had occurred which means that an ancestral lysozyme-like gene had duplicated and one of its descendants had then mutated to the non-enzymatic form of α-lactalbumin (157).

The dominating theory on the evolution of inactive enzyme homologues proposes that they are generated after a gene duplication event of the catalytically active ancestor. One of the gene copies maintains the original enzymatic function while the other copy is mutated to an inactive version. Such mutations usually target the catalytic key residues leading to loss of enzyme activity. However, conformational alterations can also occur leading to steric blocking of the active site or disruption of substrate-binding sites. The resulting "dead" enzyme maintains some of the functional characteristics of its ancestor but can subsequently acquire new function (Fig. 17) (158).

Over 20 years ago it was shown that the serum protein haptoglobin, which binds and helps remove the free haemoglobin in the blood, has a common ancestor with the chymotrypsinogen family of serine proteases. In this case, similarly to lysozyme and α-lactalbumin, an ancestral gene duplication event occurred, followed by diversification and loss of essential catalytic residues. This duplication event was not recent, since haptoglobin is conserved in primitive vertebrates, implying that there was selective pressure to retain its new function. Haptoglobin's new function requires much of the serine protease structure as the sequence similarity with serine proteases extends throughout its length. Indeed, structural modelling confirmed that the three-dimensional structure of haptoglobin strongly resembles serine proteases (159, 160).

There is also the possibility that enzymes may actually have evolved from pseudoenzymes and there are some interesting examples of likely

pseudoenzyme:active enzyme switches among the protein kinase family (161). The catalytically inactive pseudo-kinase vaccinia-related kinase 3 (VRK3) folds into a potentially active conformation *in vitro*, but catalysis is confounded by its inability to bind ATP, thus dooming it to a non-catalytic function (162).

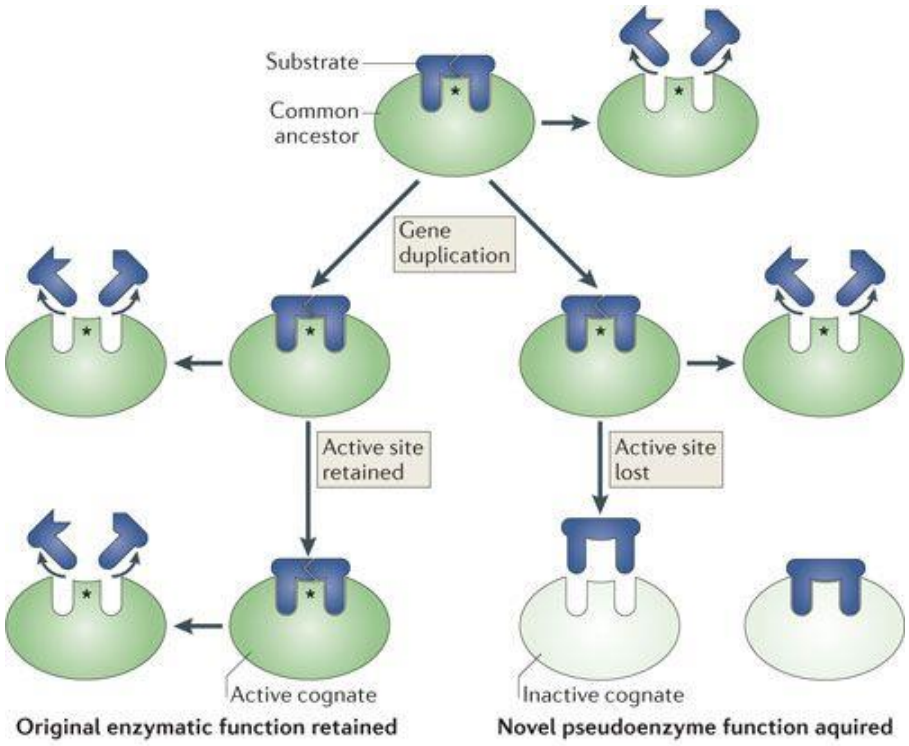

Figure 17. Evolution of an inactive enzyme from its active homologue (158).

Structural and biochemical studies have provided input on the various mechanisms by which pseudoenzymes can adopt the conventional enzyme fold to mediate new functions. Pseudophosphatases for example, adapt a tight-binding "phosphate trap" fold, which prevents substrates from being dephosphorylated and/or shields this phosphorylated epitope from the cellular machinery (163). This might prolong a signaling event or change the subcellular distribution of the target protein, including networks of proteins normally regulated by the pseudosubstrate (162). In the case of pseudokinases, conserved deviations of key residues within the active site appear to relieve selective pressures on active site geometry allowing for evolution of conformational changes and additional allosteric functions (164, 165).

The functions of pseudoenzymes include major regulatory roles in the cellular processes of prokaryotic and eukaryotic organisms. Their regulatory function typically involves protein-protein interactions (154). Different modes of action of a pseudoenzyme include the regulation of their enzyme homologues or the interaction with a separate protein by acting as an allosteric modulator. CASPS18, for example, is a caspase homologue found in the mosquito *A. aegypti*. CASPS18 is a caspase-like protease that lacks two critical for catalysis residues and is a positive regulator of its active paralogue CASPS19. *In vitro* experiments showed that co-expression of CASPS18 and CASPS19 results in an increase in CASPS19 activity and a reduction in apoptosis of cells expressing CASPS19. Several kinases and phosphatases regulate the activity of their active counterparts by serving as dimerization partners. Myotubularin-related (MTMR) phosphatases are PTP family members that dephosphorylate different phosphatidylinositol species. MTMR5, MTMR9, MTMR11, MTMR12 and MTMR13 are currently thought to be catalytically inactive since they lack specific catalytic residues. A common feature of all MTMR proteins is that they form homo and heterodimers. MTMR9 was shown to dimerize with at least two catalytically active MTMRs and to positively regulate their catalytic activity (166).

Pseudoenzymes can also interact with their natural substrates directly, sequestering them and preventing their processing by other enzymes or anchoring them in a particular subcellular space. Integrin-linked kinase (ILK) is a pseudokinase which is able to adopt an active conformation with an organized active site containing bound metal and nucleotide. However, in this active conformation ILK binds tightly to the putative pseudosubstrate α-parvin, in order to localize it to focal adhesions via distinct integrin cytosolic regions, suggesting that the pseudokinase has evolved to favor regulation through binding, rather than phosphorylation (167). However, it is not clear in these cases whether binding to the substrate also shields the substrate and makes it inaccessible for catalytically active kinases or phosphatases (162).

Materials

Primers were synthesized by the Microchemistry Facility of the Institute of Molecular Biology and Biotechnology and are listed in Table 2. The strains and plasmids used in this study are listed in Table 3. Restriction enzymes and polymerases were purchased from MINOTECH Biotechnology and New England Biolabs. PCR, gel extraction and plasmid purification kits were from MACHEREY-NAGEL GmbH. Ni-NTA agarose was from Qiagen. Chitooligomers were from OligoTech and PG from InvivoGen. All chromatographic materials were from Sigma. Common reagents were purchased from Sigma, PanReac AppliChem and Merck. Brain-heart infusion (BHI) was from Biolife. Anti-GFP rabbit IgG (polyclonal antibody) was purchased from MINOTECH Biotechnology, Anti-rabbit IgG (γ-chain specific), Anti-His mouse IgG (monoclonal) and Anti-mouse IgG peroxidase (polyclonal) from Sigma.

Table 2. List of oligonucleotides used in the present study (mutated codons are underlined)

oligonucleotides	Sequence (5'→3')
ba3943-FW-NdeI	CCCATATGCAGGATAACTTATATGAAGAA
ba3943-REV-XhoI	CCGCTCGAGATCCACACGTTTTTCATCCAGTAA
ba3943mut1-FW	TAACAATAGATGTGGCATGGGG
ba3943mut1-REV	CCCCATGCCACATCTATTGTTA
ba3943mut2-FW	TAACAATAGATGACGCATGGGG
ba3943mut2-REV	CCCCATGCGTCATCTATTGTTA
ba3943mut3-FW	AGATGGTTTAGACCGCCGAGT
ba3943mut3-REV	CTCGGCGGTCTAAACCATC
ba3943mut4-FW	AGATGGTTTAAACCGCCGAGT
ba3943mut4-REV	CTCGGCGGTTTAAACCATC
ba3943mut5-FW	GGTTTAGACCGGGCAGTGGAAGTTT
ba3943mut5-REV	AAACTTCCACTGCCCGGTCTAAAC
ba3943mut6-FW	GGTTTAGACCGGGCAGTTTTCGAGA
ba3943mut6-REV	TCTCGAAAACTGCCCGGTCTAAAC
ba3943mut7-FW	TAACAATAGATAATGCATGGGGAA
ba3943mut7-REV	TTCCCCATGCATTATCTATTGTTA
ba3943w/oK-FW	TTTGCAATGGTGGGATTAACAATAAAT
ba3943w/oK-REV	CACCATTGCAAAAACGGAATAAGAGC
ba3943-BamHI-FW	CGGGATCCATGAAAGCTCGTATATTGGCA
ba3943-NruI-REV	TCGCGACGGGCCCGGGCCATCCACACGTTTTTCATCCAG
GFPmut1-NruI-FW	TCGCGAATGAGTAAAGGAGAAGAACTTT
GFPmut1-BglII-REV	GAAGATCTCTATTTGTATAGTTCATCCATGC
Up3943-pHT304-18Z-HindIII-FW	CCCAAGCTTCAGGTATTGCAATGGGGC
Up3943-pHT304-18Z-BamHI-REV	CGGGATCCATAAACCCTCCCATTAACTAT
Upstream3943-FW	CGAGCTCCAGGTATTGCAATGGGGC
Upstream3943-REV	TCCCCCGGGGGATTGAATTTCTTCATATAAGTTATC
Downstream3943-FW	TCCCCCGGGGGATCAACAACAGAAGCTTTAG
Downstream3943-REV	GGGGTACCCTTGGAATAAACGGCTACTCA
ba3943-KpnI-REV	GGGGTACCTTAATCCACACGTTTTTCATC
Peag-FW	CCCAAGCTTTTTAGGTGATGAAGCGGAAAT
Peag-REV	CGGGATCCTTTATAAATTTCCTCCTTCAG
ba1834-FW-NdeI	CCCATATGTTTCAATTGTTTGGAGATTTAACAAACC
ba1836-REV-XhoI	CCCTCGAGTTTTGCACTTTTTTGTAATTCATTTACTGTTA
ba1836-REV-BamHI	CGGGATCCTTATTTTGCACTTTTTTGTAATTCATTTACTGTTAC
ba1836-FW-BamHI	CGGGATCCATGTTTCAATTGTTTGGAGATTTAAC
ba1836-REV-HindIII	CCCAAGCTTTTATTTTGCACTTTTTTGTAATTC
Up1836-pHT304-18Z-HindIII-FW	CCCAAGCTTCGTTATTTGCCCAAGATG
Up1836-pHT304-18Z-BamHI-REV	CGGGATCCAAAGCAACCTCACTATATTTT
ba1836-FW-BamHI-pWH1520	CGGGATCCATGAAAAAGAAAATAATCATTACAATC
ba1836-REV-NruI	TCGCGACGGGCCCGGGCCTTTTGCACTTTTTTGTAATTCATTTAC
ba1836D53A-FW	TAACTTTTGCTGATGGCCC
ba1836D53A-REV	GGGCCATCAGCAAAAGTTA
Upstram1836-FW	CCAAGCTTCCATATATCCAATACGGGCAAA
Upstream1836-REV	CCCCCGGGAACGATTGTAATGATTATTTTCTTTTTC
Downstream1836-FW	CCCCCGGGAAGAAGGGCTATCAGTTCGTAACA
Downstream1836-REV	CGCGGATCCAGTTTACCGCGTTCAGCATT

Table 3. List of strains and plasmids used in the present study

Strains, plasmids	Description	Source/Reference
Strains		
E.coli		
DH5α	F- 80dlacZ M15 (lacZYA-argF) U169 recA1 endA1hsdR17 (rk-, mk+) phoAsupE44 -thi-1 gyrA96 relA1	Novagen
BL21 DE3 C43	F– *ompT hsdSB (rB- mB-) gal dcm*	Sigma
BL21 DE3 Star pLysS	F- ompT hsdSB (rB-mB-) gal dcm rne131	Promega
GM48	*thr-1*, *araC14*, *leuB6*(Am), *fhuA31*, *lacY1*, *tsx-78*, *glnX44*(AS), *galK2*(Oc), *galT22*, λ^-, *dcm-6*, *dam-3*, *thiE1*	Coli Genetic Stock Center (CGSC)
HB101	F- hsd-20 recA13 ara-14 proA2 lacY1 gal K2 rpsL20(Str) xyl-5 mtl-1 supE44	(168)
B. anthracis		
7702	$pXO1^+$, $pXO2^-$	(169)
Plasmids		
pET26b	Cloning vector	Novagen
pET16b-TEV	Cloning vector	In house
pET16b-MBP-TEV	Cloning vector	In house
pGEM T-Easy	Cloning vector	Promega
pNF8	pAT18Ω (PdltΩgfp-mut1)	(170)
pWH1520	Cloning vector	Mobitec
pHT304-18Z	Promoterless *lacZ* vector	(171)
pRP1028	Tm^S allelic-exchange vector	(172)
pSS4332	I-SceI expression vector	(172)

Methods

Cloning and expression of *ba3943* gene into pET26b expression vector and *ba1836* gene into pET26b, pET16b-TEV and pET16b-MBP-TEV expression vectors

ba1836 and *ba3943* genes were amplified from genomic DNA of *B. anthracis* 7702 using DNA polymerase chain reaction (PCR). Primers were synthesized to exclude the signal peptides (amino acid 1-30 for BA1836 and 1-25 for BA3943) and to incorporate a NdeI at the start and a XhoI restriction site at the end of each gene (Table 2). The amplified genes were purified, digested with the corresponding enzymes and ligated into pET26b. The resulting products were in-frame C-terminal His_6 tag-fused constructs in pET26b, placing *ba1836* and *ba3943* genes under the transcriptional control of the T_7 *lac* promoter. Primers were also synthesized to incorporate a NdeI at the start and a BamHI restriction site at the end of *ba1836* gene (Table 2). The amplified *ba1836* gene was purified, digested with the corresponding enzymes and ligated into pET16b-TEV and pET16b-MBP-TEV. The resulting products were in-frame *N*-terminal His_6 tag-fused constructs in pET16b-TEV and pET16b-MBP-TEV, placing *ba1836* gene under the transcriptional control of the T_7 lac promoter. pET26b-*ba1836* construct was transformed into BL21 (DE3) C43, Star pLysS and pGKJ-E8 *E.coli* strains and a series of conditions were tested for their efficacy to overexpress BA1836. However, no overexpression of the respective protein was observed. pET26b-*ba3943* construct was transformed into BL21 (DE3) C43 *E. coli* strains. Twenty milliliters of saturated culture of the transformed expression *E. coli* strain were inoculated into 1 liter of Luria-Bertani (LB) medium containing 30 μgr ml^{-1} kanamycin as antibiotic and incubated at 30°C on a shaker incubator to an $OD_{600\ nm}$ of 0.6. After the addition of 0.5 mM isopropyl β-D-thiogalactoside (IPTG), the *E. coli* culture overexpressing *ba3943* was incubated at 30°C for 5 hours. pET16b-TEV-*ba1836* construct was transformed into BL21 (DE3) C43, Star pLysS and pGKJ-E8 *E.coli* strains and a series of conditions were tested for their efficacy to overexpress BA1836. However, no overexpression of the respective protein was observed. pET16b-MBP-TEV-*ba1836* construct was transformed into BL21 (DE3) Star pLysS *E. coli* strains. Twenty milliliters of saturated

culture of the transformed expression *E. coli* strain were inoculated into 1 liter of LB medium containing 100 μgr ml^{-1} ampicillin and 34 μgr ml^{-1} chloramphenicol as antibiotics and incubated at 30°C on a shaker incubator to an $OD_{600\ nm}$ of 0.6. After the addition of 0.5 mM isopropyl β-D-thiogalactoside (IPTG), the *E. coli* culture overexpressing the fusion *malE-ba1836* was incubated at 30°C for 3 hours.

Site-directed mutagenesis of *ba3943* and *ba1836* genes

Mutants of the *ba3943* (Table 4) and *ba1836* genes were constructed using a two-step/four-primer overlap extension PCR method (173). Primers used in this method are listed in Table 2. The amplified *ba3943* products were cloned into pET26b vector as described above (*Cloning and Expression of ba3943 Gene of B. anthracis into pET26b Expression Vector*) and the amplified *ba1836* product was cloned into pWH1520 vector as described below (*Construction of B. anthracis GFP-fusions*).

Table 4. List of mutant *ba3943* genes and corresponding recombinant BA3943 mutant proteins

Mutant *ba3943* gene	Mutant BA3943 protein
ba3943mut1	BA3943 N94D
ba3943mut2	BA3943 N94D V95D
ba3943mut3	BA3943 N94D V95D A183R
ba3943mut4	BA3943 N94D V95D A183K
ba3943mut5	BA3943 N94D V95D A183R P185G
ba3943mut6	BA3943 N94D V95D A183R/P185 S186 deletion
ba3943mut7	BA3943 N94D D95N A183R
ba3943mut8	BA3943 N94D D95V A183R

Purification of recombinant BA3943 and BA3943 mutant proteins

Cells were harvested by centrifugation and resuspended in 50 mM Tris-HCl buffer, pH 7.6, 300 mM NaCl and 1 mM phenylmethylsulfonyl fluoride (PMSF). The suspension was lysed by sonication and centrifuged. The soluble fractions were loaded onto Ni-NTA agarose equilibrated with 50 mM Tris-Cl buffer, pH 7.6, 300 mM NaCl and 10 mM imidazole. BA3943 was eluted using a gradient of imidazole (10-400 mM).

Fractions containing BA3943 were collected, dialyzed against 50 mM Tris-Cl buffer, pH 7.6 and 300 mM NaCl, concentrated and stored at 4^{o}C.

Purification of recombinant MBP-BA1836 fusion protein

Cells were harvested by centrifugation and resuspended in 50 mM Tris-Cl buffer, pH 7.6, 200 mM NaCl and 1 mM PMSF. The suspension was lysed by sonication and centrifuged. The soluble fractions were loaded onto Ni-NTA agarose equilibrated with 50 mM Tris-Cl buffer, pH 7.6, 200 mM NaCl and 50 mM imidazole. MBP-BA1836 was eluted using a gradient of imidazole (50-400 mM). Fractions containing MBP-BA1836 were collected and analyzed by SDS-PAGE, which revealed fusion proteolysis. As a result, BA1836 could not be further utilized for biochemical characterization.

Preparation of radiolabeled H^3-glycol chitin

Preparation of H^3- glycol chitin was performed according to Araki *et al*. (174).

Enzyme Assays

For the determination of deacetylase activity of BA3943 and its mutants, we employed a radiometric assay (174). Enzyme assays were performed at a wide pH range and in the presence (1mM) or absence of the divalent cations Co^{2+}, Zn^{2+}, Mn^{2+} and Ni^{2+}.

The optimum reaction conditions for BA3943 N93D V94D A183R (0.2 mg ml^{-1}) was 25 mM Tris-HCl pH=7.0, 1 mM $CoCl_2$ and 5 µl H^3-glycol chitin (1mg ml^{-1}). Incubation time was overnight at 37^{o}C. Identical reaction conditions were used for BA3943 N94D D95V A183R and BA3943 N94D D95N A183R.

Analysis of reaction products

BA3943 N94D V95D A183R (0.2 mg ml^{-1}) was incubated at optimum reaction conditions with $GlcNAc_5$, $GlcNAc_6$, $GlcNAc_7$ (1 mg ml^{-1}) and PG (0.2 mg) isolated from *E. coli* and *B. subtilis*. BA3943 N94D D95V A183R (0.2 mg ml^{-1}) was incubated with $GlcNAc_7$ and *N*-acetylmuramyl-L-alanyl-D-isoglutamine hydrate (MDP) (1 mg ml^{-1})

while BA3943 N94D D95N A183R (0.2 mg ml^{-1}) was incubated with MDP (1 mg ml^{-1}). Reaction products were separated and analyzed by HPLC as previously described (175, 176).

Following HPLC analysis, reaction products were collected and analyzed by electrospray ionization-mass spectrometry (ESI-MS) using a quadrupole ion trap mass spectrometer (LCQ Advantage, Thermo Finigan). The samples were directly infused in the mass spectrometer at a flow rate of 15 µl min^{-1} using a syringe pump (Cole Parmer). The ESI source settings were: spray voltage, 4 kV; sheath gas flow rate, 45 arbitrary units; auxiliary gas flow rate, 5 arb. units. In the mass spectrometer the following parameters were used: source induced dissociation, 15 V; capillary voltage, 6 V; ion transfer capillary temperature, 250 °C; tube lens offset, -10 V. The mass spectrometer was operated in the positive ion mode and the mass spectra were recorded in the m/z range 200-2000. For structure elucidation and confirmation of the identity of the cations, MS^n experiments were performed manually.

2-Hydroxyproline identification and quantitation

2-Hyp identification and relative quantitation by nanoscale liquid chromatography coupled online with electrospray ionization tandem mass spectrometry (nL CESI-MS/MS) was done on a high-mass resolution LTQ-Orbitrap XL (Thermo Fisher Scientific) mass spectrometer coupled to an Easy nLC instrument (Thermo Fisher Scientific) (149).

Metal identification

The metal content of BA3943 and BA3943 N94D V95D A183R was estimated using size exclusion chromatography (SEC) online with inductively coupled plasma mass spectrometry (ICP-MS) (149).

Construction of *B. anthracis* Δ*ba1836* and Δ*ba3943* knockout strains, Δ*ba3943* complemented strain, GFP fusions and *lacZ* transcriptional fusions

Two strains bearing an in-frame deletion of either *ba1836* or *ba3943* gene were created using a markerless gene replacement method (172). In brief, DNA fragments containing the sequence upstream and downstream of the gene of interest were amplified from genomic DNA of *B. anthracis* 7702 by PCR using the appropriate oligonucleotides (Table 2). Both fragments were cloned into the same pGEM vector and the upstream-downstream fragment was digested with SacI/KpnI and ligated into pRP1028 vector. *E.coli* HB101 was used as helper strain in order to primarily introduce pRP1028 construct and subsequently pSS4332 vector, which encodes the I-SceI enzyme, into *B.anthracis* 7702 strain. Finally, the knockout strain had no resistance to antibiotics and was validated for the correct construction by PCR.

For the construction of the Δ*ba3943* complemented strain, a DNA fragment containing the sequence upstream of *ba3943* gene and the *ba3943* gene were amplified from genomic DNA of *B. anthracis* 7702 by PCR using the appropriate oligonucleotides (Table 2). The amplified fragment was purified, digested with SacI/KpnI and ligated into pRP1028 vector. The construct was introduced into Δ*ba3943* strain using *E.coli* HB101 as helper strain. The resulting Δ*ba3943* complemented strain had resistance to spectinomycin and was validated for the correct construction by PCR.

To construct strains expressing GFP translational fusions, the *gfp-mut1* gene was amplified from pNF8 (170) with specific primers, digested with NruI and BglII, and ligated into the xylose-inducible plasmid pWH1520 (177). Then, *ba1836*, *ba3943* and *ba3943,* lacking the lysine-rich domain (*ba3943*K^-), (all genes lacking their stop codons) were amplified from *B. anthracis* 7702 chromosomal DNA with the appropriate primers to incorporate at the C terminus the polylinker GPGP. The genes were digested with BamHI and NruI and ligated in-frame to the 5' end of *gfp-mut1*, placing the gene fusion under a xylose-inducible promoter. 7702 *B. anthracis* cells were then transformed with the resulting constructs via electroporation, after initially being transformed to *E. coli* GM48 (*dam*$^-$) to obtain nonmethylated plasmid DNA. 10 ml of BHI medium were inoculated from overnight cultures to an $OD_{600\ nm}$ of 0.05 and

incubated at 37°C. For BA1836-GFP expressing strain, induction was achieved with 0.2% xylose (for expression from the xylose-inducible promoter) 1 hour before the culture reached stationary phase of growth ($OD_{600\ nm}$ around 3.0). For BA3943-GFP and BA3943^{-}K-GFP expressing strains, when $OD_{600\ nm}$ reached 1.2 (mid-exponential phase), the cultures were centrifuged for 20 min at 4800 rpm and the cell pellet was resuspended in an equal volume of modified G medium (178) in order to induce sporulation. The cultures were then transferred to 30°C and 1 hour before the cells entered Stage III of sporulation induction was achieved with 0.2% xylose. One hour after the addition of xylose in the culture, the cells were centrifuged and resuspended in an equal volume of modified G medium in order to remove xylose and let sporulation proceed normally.

In order to create the *lacZ*-transcriptional fusions, DNA fragments of the upstream region of *ba1836* and *ba3943* genes were amplified from *B. anthracis* 7702 chromosomal DNA. Primers were synthesized to incorporate a HindIII site at the start and a BamHI restriction site at the end of the amplified fragments (Table 2), which were digested with the corresponding enzymes, and ligated into pHT304-18Z (171). In this way, a *lacZ* reporter construct with the upstream region of each gene fused directly to the start codon of the *lacZ* gene was obtained. 7702 *B. anthracis* cells were then transformed with the resulting construct via electroporation, after initially being transformed to *E. coli* GM48 (*dam*$^{-}$) to obtain nonmethylated plasmid DNA.

Preparation of sporulating cell cultures

Ten ml of BHI medium were inoculated from overnight cultures of 7702 parental, Δ*ba1836* and Δ*ba3943* mutant strains to an $OD_{600\ nm}$ of 0.05 and incubated at 37°C. When $OD_{600\ nm}$ of the cultures reached 1.2 (mid-exponential phase) or 3.0 (early stationary phase), the cultures were centrifuged for 20 min at 4800 rpm and the cell pellet was resuspended in an equal volume of modified G medium (178) in order to induce sporulation. The cultures were then transferred to 30°C. Cells were collected at frequent time intervals and observed using microscopy.

β-galactosidase activity assay

Cell samples were collected in triplicates from shaking cultures at various time points during vegetative growth and after sporulation were induced by resuspension in modified G medium as previously described. $OD_{600\ nm}$ for each cell sample was recorded before collection. β-galactosidase activity was estimated as described by *Camp and Losick* (57) with minor changes. Cells pellets corresponding to 1 ml of the original sporulation medium were resuspended in 0.2 ml Z-buffer (60 mM Na_2HPO_4, 40 mM NaH_2PO_4, 10 mM KCl, 1 mM $MgSO_4$, 50 mM β-mercaptoethanol at pH 7.0). 50 µl of the cell suspension were added to individual wells of a 96-well plate containing 15 µl of 0.1% SDS and cell lysis was allowed to proceed for 30 min at 37^{o}C. 20 µl of 4 mg/mL 2-Nitrophenyl b-D-galactopyranoside (ONPG) in Z-buffer were then added to each well and mixed thoroughly. Absorbance at 420 nm for each reaction was read once per minute for 1 h at 37°C in a Fluostar Galaxy plate reader. β-galactosidase activity is expressed in miller units (MU) (179).

Competition experiments

In order to perform competition experiments a *lacZ* reporter construct with the *eag* promoter (P*eag*) fused directly to the start codon of the *lacZ* gene was constructed. P*eag* (180) was amplified from *B. anthracis* 7702 chromosomal DNA. Primers were synthesized to incorporate a HindIII site at the start and a BamHI restriction site at the end of the P*eag* (Table 2), which was digested with the corresponding enzymes, and ligated into pHT304-18Z (171) 7702 *B. anthracis* cells were then transformed with the resulting construct via electroporation, after initially being transformed to *E. coli* GM48 (*dam*$^{-}$) to obtain nonmethylated plasmid DNA.

Competition experiments were performed according to Traag *et al* (181) with minor modifications. Briefly, starting from overnight BHI culture, 7702 strain containing pHT304-18Z-P*eag* construct was mixed, either in 1:1 or 1:3 ratio with mutant Δ*ba1836* and Δ*ba3943* strains containing pHT304-18Z vector in 5 ml modified G medium. Cultures were grown and allowed to sporulate at 30^{o}C for 48 h. The cultures were then heat treated at either 60^{o}C or 80^{o}C for 20 min, briefly cooled at room temperature and inoculated in 5 ml fresh modified G medium. Before

inoculation, cultures were diluted and plated on agar plates containing 40 μgr ml^{-1} 5-bromo-4-chloro-3-indolyl-β-D-galactopyranoside (X-Gal) and 5 μgr ml^{-1} erythromycin. The blue and white colonies were counted. Similarly, competition experiments were performed for vegetative phase of growth. Briefly, starting from overnight BHI culture, 7702 strain containing pHT304-18Z-P*eag* construct was mixed in 1:1 ratio with mutant Δ*ba1836* and Δ*ba3943* strains containing pHT304-18Z vector in 5 ml BHI medium. Cultures were grown at 30^{o}C for 24 h and then inoculated in 5 ml fresh BHI medium (181).

In vitro determination of lysozyme sensitivity

To test the sensitivity of Δ*ba1836* and Δ*ba3943* mutant strains in the presence of exogenously added lysozyme, overnight cultures of the parental and mutant strains were diluted to an $OD_{600\ nm}$ of 0.1 into two cultures of 20 ml of fresh SPY medium for each strain. The cultures were incubated at 37 °C until an $OD_{600\ nm}$ of 1.2 and 3.0. Then each culture was divided in two equal parts of 10 ml, and 10 μg ml^{-1} hen egg lysozyme was added at one of the two subcultures. The growth of both treated and untreated subcultures was monitored.

Autolysis Assay

Autolysis assay was performed according to Balomenou *et al.* (130) with a few modifications. Cultures of 10 ml SPY and at an $OD_{600\ nm}$=1.2 for 7702 and Δ*ba3943* cells and at an $OD_{600\ nm}$=3.0 for 7702 and Δ*ba1836* cells were centrifuged for 20 min at 4800 rpm and the bacterial pellet was concentrated 10 times in SPY medium to which 10 mM NaN_3 was added. The decrease of OD_{600} of each culture was monitored every 30 min for a period of 180 min.

Fluorescence Microscopy, Scanning and Transmission Electron Microscopy

B. anthracis sporulating cell cultures of 7702 parental, Δ*ba1836* and Δ*ba3943* knockout strains were examined by optical and fluorescence microscopy. For membrane visualization the FM4-64 fluorescent dye was added to a final

concentration of 1 µg ml^{-1}. Sporulating cells in stages II and III were stained with FM4-64 in order to visualize the assymetric septum and engulfment respectively. Optical microscopy was used after stage III of sporulation when the forespore is formed. *B. anthracis* vegetative cell cultures of 7702 overexpressing BA1836-GFP fusion as well as *B. anthracis* sporulating cell cultures of 7702 overexpressing BA3943-GFP and BA3943K^--GFP fusions were examined by fluorescence microscopy. The images were obtained without fixation on an inverted epifluorescence microscope Nikon E800. Preparation of cell samples for scanning and transmission electron microscopy was performed according to Arnaouteli *et al*. (144). Samples were examined using a JEOL JSM-6390LV scanning electron microscope, operating at 20kV. Sections were observed in a JEOL, JEM 2100 transmission electron microscope, operated at 80kV.

Western Blotting analysis

Star pLysS *E.coli* cell lysates overexpressing BA1836 protein were separated by SDS-PAGE, blotted and probed with the following antibodies: monoclonal mouse anti-His primary antibody diluted 1:500 and monoclonal anti-mouse IgG peroxidase diluted 1:2500.

B. anthracis cell lysates, at the time points at which GFP fluorescence signal was obtained, were separated by SDS-PAGE, blotted, and probed with the following antibodies: polyclonal rabbit anti-GFP primary antibody diluted 1:25000 and monoclonal anti-rabbit IgG (γ-chain specific) alkaline phosphatase secondary antibody diluted 1:3125.

Purification of peptidoglycan and neutral polysaccharide from *B. anthracis*

PG from parental 7702 and mutants was purified from stationary growing bacteria (in SPY) as well as from spores as previously described by Popham *et al*. (182) and Mesnage *et al.* (183). Muropeptides from the native PG were generated using the muramidase mutanolysin M1 at 37^oC for 16 hours and separated by HPLC as previously described by Bui *et al*. (175).

PS was extracted from cell walls as described by Ekwunife *et al* (94).

Spore preparation and purification

Single colonies from 7702 and Δ*ba1836 B. anthracis* strains were streaked onto SPY agar plates supplemented with 0.2% glucose and 10 mM $MgSO_4$ and left to sporulate for 7 days at 30^{o}C. When needed, the SPY agar plates were additionally supplemented with 0.2% xylose.

Spores were harvested in water, centrifuged at 8000 rpm for 5 min, washed twice in water, heated at 65^{o}C for 20 min, washed again and stored at 4^{o}C. Microscopic examination indicated that all spore preparations were 98% free of contaminating vegetative cells, sporulating cells and germinated spores.

Spore viability

Spore viability was defined as the number of colony-forming units (cfu) formed when compared with the number of phase-bright spore particles plated. Purified parental 7702 and knockout Δ*ba1836* and Δ*ba3943* spores were tittered by visual counting via Neubauer haemocytometer, then diluted and plated onto LB agar to measure cfu (184).

Spore germination

Spore germination was performed according to Fazzini *et al.* (185) with certain modifications. Briefly, spores were suspended at an $OD_{600\ nm}$ of 1.0 in 1 ml water. Following heat activation at 65^{o}C for 20 min, the suspensions were centrifuged at 8000 rpm for 5 min and 900 µl were removed. Germination of spores was initiated by the addition of 1ml of a mixture of 25 mM L-alanine and 12.5 mM inosine. The suspensions were incubated at 37^{o}C for 120 min. Germination was monitored by the loss of optical density at 600 nm.

Results

BA1836

BA1836 is a putative PDA

The genome of *B. anthracis* Sterne 7702 sequence database reveals 11 coding sequences for putative PDAs of the CE4 family. Ten of them exhibit more than 90% sequence identity to their homologues from *B. cereus sensu stricto*. For BA1836, the TMHMM (186) program predicts the presence of an *N*-terminus transmembrane domain (residues 5-23). The TatP (187) and SignalP (188) programs do not predict a signal peptide. BA1836 shares 92% identity with its homologue BC1768 from *B. cereus* and displays an identity of 25-30% with *B. subtilis* PDAs, suggesting a similarity in overall fold. Additionally, BA1836 shares an approximately 30% identity with other putative and known PDAs from *B. anthracis*.

Importantly, sequence alignment of BA1836 (excluding residues 1-47) with representative members of the CE4 family (126) revealed that BA1836 retains the pattern of sequence motifs (MT1-MT5) which are typical for PDAs (Fig. 18). These include motif MT2, which is associated with a metal cation binding site formed in the catalytic center of the enzyme, and key catalytic residues (MT1, MT5), which occupy structurally homologous positions in CE4 esterases of known structures (145). More specifically, Asp^{53} of motif MT1 and His^{196} of motif MT5, corresponding to the catalytic base and the catalytic acid of the deacetylation reaction respectively, are conserved in the sequence of BA1836 (Fig. 18). Additionally, the highly conserved Pro^{145}, for which has been recently demonstrated that is autocatalytically hydroxylated in the presence of molecular oxygen at the Cα atom to produce 2-hydroxyproline (2-Hyp), is found in motif MT3, in agreement with other well characterized PDAs. The self-hydroxylation of proline at the Cα atom has been shown to significantly enhance deacetylase activity (149). The pattern of hydrophobic residues in motifs MT4 and MT5 agrees well with the patterns found in other PDAs (Fig. 18). In summary, BA1836 displays all sequence features of active PDAs.

In order to biochemically characterize BA1836, we attempted to overexpress and isolate it from *E. coli* cells. We initially cloned *ba1836* gene into pET26b and

subsequently into pET16b vector but no overexpression was observed (Fig. 19A, 19B) at different temperatures, IPTG concentrations, induction and incubation time (data not shown).

We next cloned *ba1836* gene into pET16b-MBP vector and the respective fusion protein was overexpressed (Fig. 19A, 19B). However, when we proceeded to MBP-BA1836 protein purification using Ni-NTA affinity chromatography, proteolysis was observed in the eluted MBP-BA1836 fractions (data not shown). We attempted to reduce proteolysis by decreasing culture temperature, IPTG concentration, incubation time and by using a cocktail of protease inhibitors during bacterial lysis, without success (data not shown).

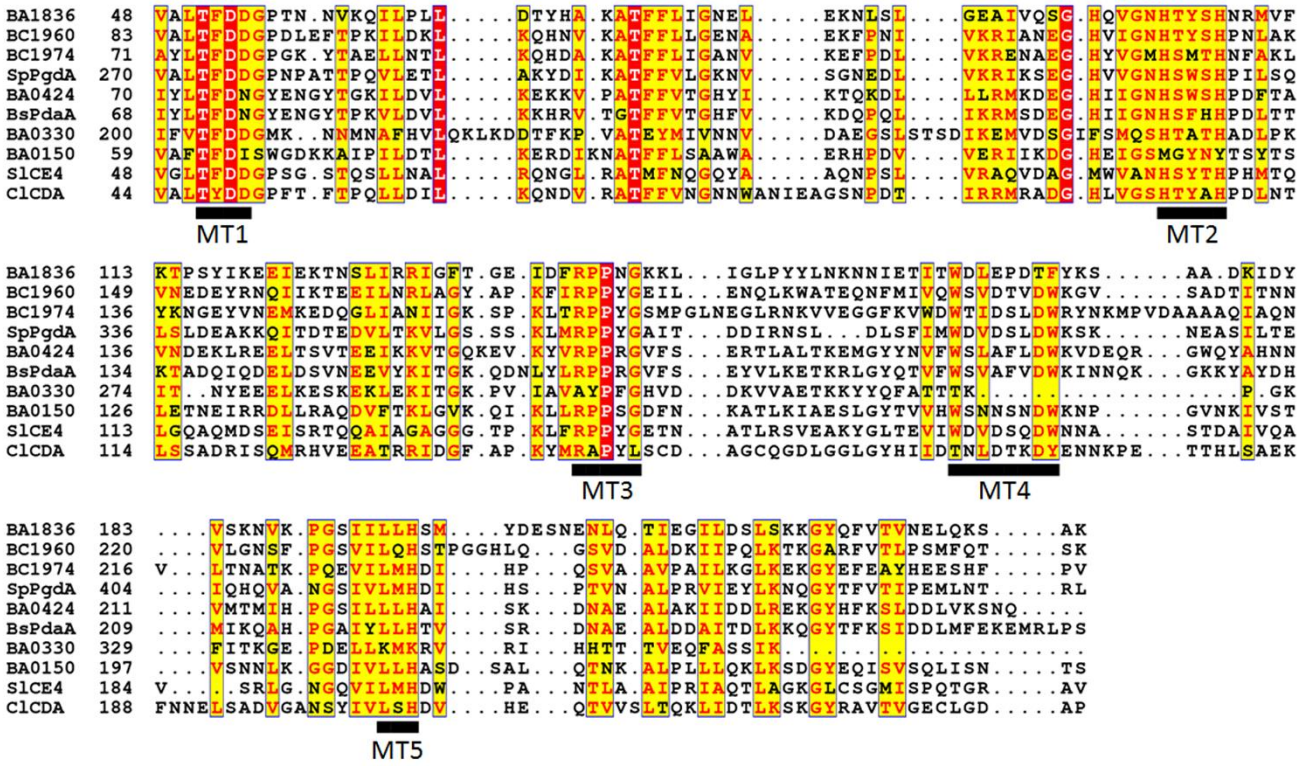

Figure 18. Sequence alignment of the NodB domain of BA1836 with representative members of the CE4 family including the peptidoglycan GlcNAc deacetylases (PGDAs) BC1960 (148, 149), BC1974 (*B. cereus*) (130, 150) and SpPgdA (*S. pneumoniae*) (129, 145), the MurNAc peptidoglycan deacetylases BA0424 (*B. anthracis*) (139) and BsPdaA (*B. subtilis*) (138, 146), the putative PDA BA0330 (*B. anthracis*) (144), the inactive PDA BA0150 (*B. anthracis*) (151), the acetylxylan esterase SlCE4 (*S. lividans*) (189) and the chitin deacetylase ClCDA (*C. lindemuthianum*) (190). The conserved sequence motifs MT1-MT5 for this class of enzymes are shown at the bottom. The alignment was performed with T-coffee and plotted with the ESPRIT (147).

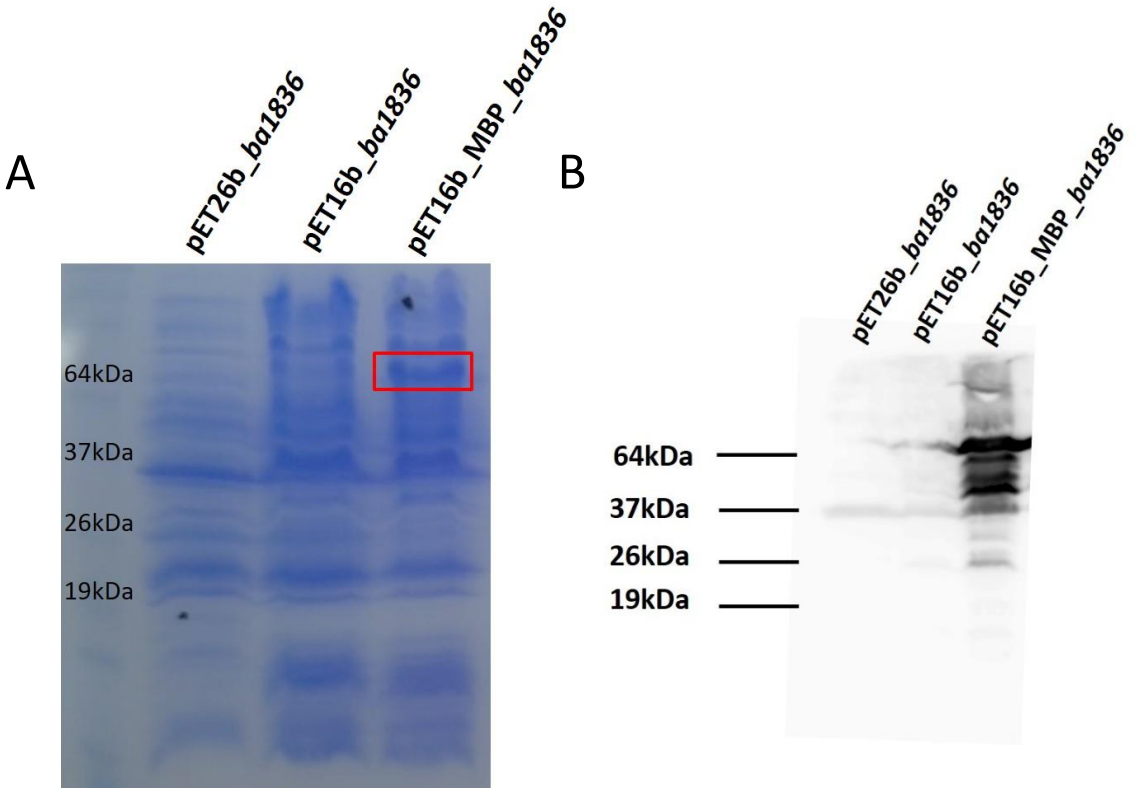

Figure 19. Overexpression of BA1836. (A) Constructs pET26b_*ba1836*, pET16b_*ba1836* and pET16b_MBP_*ba1836* were transformed into *E. coli* BL21 DE3 Star pLysS strain. 50 ml of cell cultures were grown at 30^{o}C and harvested 5 hours after induction with 0.5 mM IPTG. Cell lysates were analyzed on a 12% polyacrylamide gel under denaturing and reducing conditions. Protein bands were visualized by staining with Coomassie Brilliant Blue R (B) The lysates were also analyzed by Western blot using monoclonal anti-His antibody. Proteolysis of MBP-BA1836 was observed. MBP: 40kDa and BA1836: 26kDa.

ba1836 is expressed in stationary phase cells and further induced during sporulation

In order to monitor the expression of the *ba1836* gene we constructed a transcriptional reporter by fusing an upstream fragment of *ba1836* (containing the promoter region) with the start codon of the *E. coli lacZ* gene. 7702 *B. anthracis* cells carrying this construct were harvested at various time points during vegetative growth. As shown in Fig. 20A, *ba1836* promoter driven lacZ expression was absent during exponential growth, but was rapidly induced to high level shortly after cells entered the stationary phase of growth.

We next resuspended stationary phase 7702 *B. anthracis* cells carrying this construct into sporulation-inducing medium and collected samples at various time

points during sporulation. As we observed by optical microscopy, most cells were in stage II of sporulation (asymmetric division) about 8-12 h after transfer into sporulation medium, in stage III (engulfment) after 12-16 hours, in stage IV-V (coat and cortex assembly) after 16-20 hours and in stage VI-VII (spore maturation and mother cell lysis) about 20-24 hours. We observed that the expression of *ba1836-lacZ* further increased during the early stages of sporulation (Stage I-II) (Fig. 20B). In contrast, when exponentially growing 7702 *B. anthracis* cells, in which *ba1836-lacZ* was not expressed, were induced to sporulate, the *ba1836* promoter remained silent (Fig. 21). This suggests that sporulation conditions alone are not sufficient to induce *ba1836* expression.

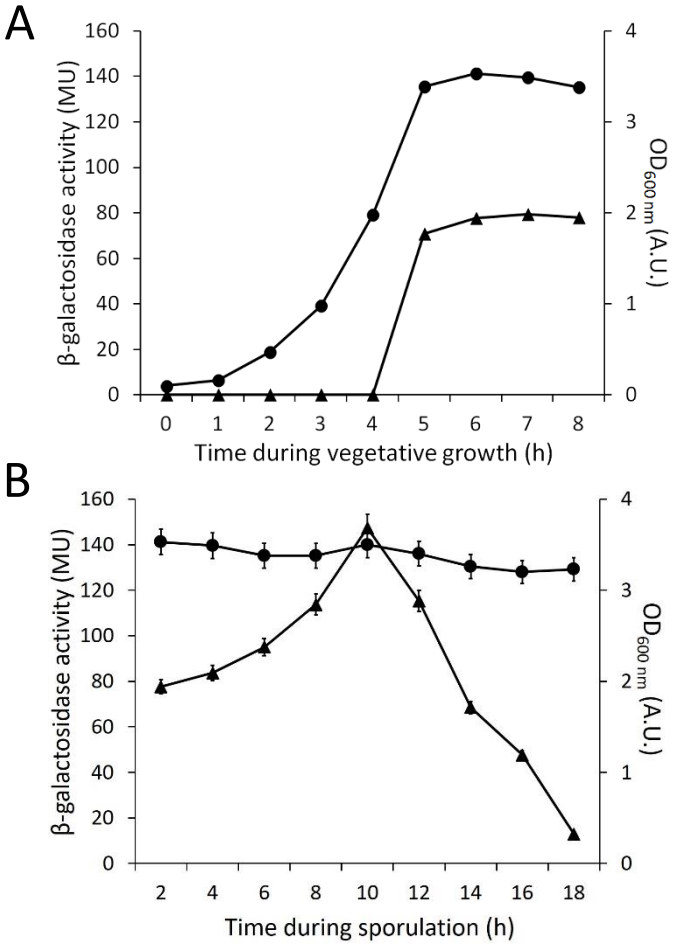

Figure 20. Expression of *ba1836* gene. (A) *B. anthracis* 7702 strain, carrying the *lacZ* transcriptional reporter for *ba1836* gene, grown in BHI (B) induction of sporulation of stationary phase cells. Samples taken at the indicated time points were assayed for β-galactosidase activity. *ba1836* is expressed after cells entered stationary phase of growth and is further induced in sporulation. (●) $OD_{600\,nm}$ (A.U.) (▲) β-galactosidase activity in Miller Units (MU).

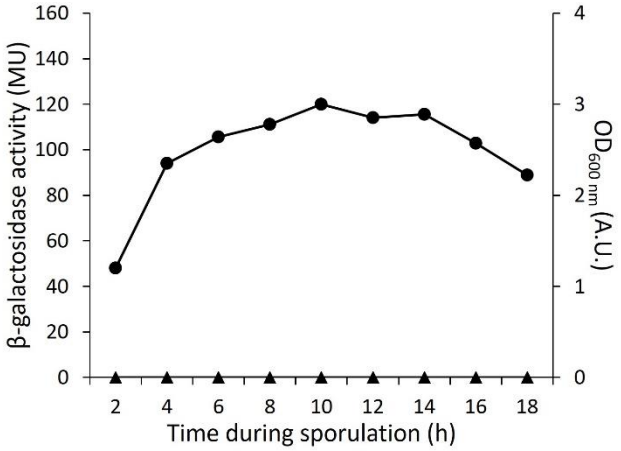

Figure 21. Expression of *ba1836* gene following induction of sporulation of exponentially phase cells into G modified medium. Samples taken at indicated time points were assayed for β-galactosidase activity. (●) $OD_{600\ nm}$ (A.U.) and (▲) β-galactosidase activity of 7702 *B. anthracis* cells in Miller Units (MU).

BA1836-GFP localizes to the cell periphery and septa

The amino acid sequence of BA1836 is predicted to include an *N*-terminal membrane spanning region that is not removed by a signal peptidase. In order to determine the subcellular localization of BA1836, a C-terminal *gfp* fusion of the *ba1836* gene was constructed and was introduced into *B. anthracis* 7702. We induced the expression of BA1836-GFP in *B. anthracis* cells that entered the stationary phase of growth, i.e., when *ba1836* is normally expressed. Expression of the GFP-fused BA1836 was confirmed by Western blot analysis (Fig. 22B). The GFP tag did not affect the function of the protein, because the mutant strain transformed with the respective BA1836-GFP protein complemented the observed phenotypes which will be presented below. BA1836-GFP localized at the cell membrane and septa in stationary phase cells (Fig. 22A).

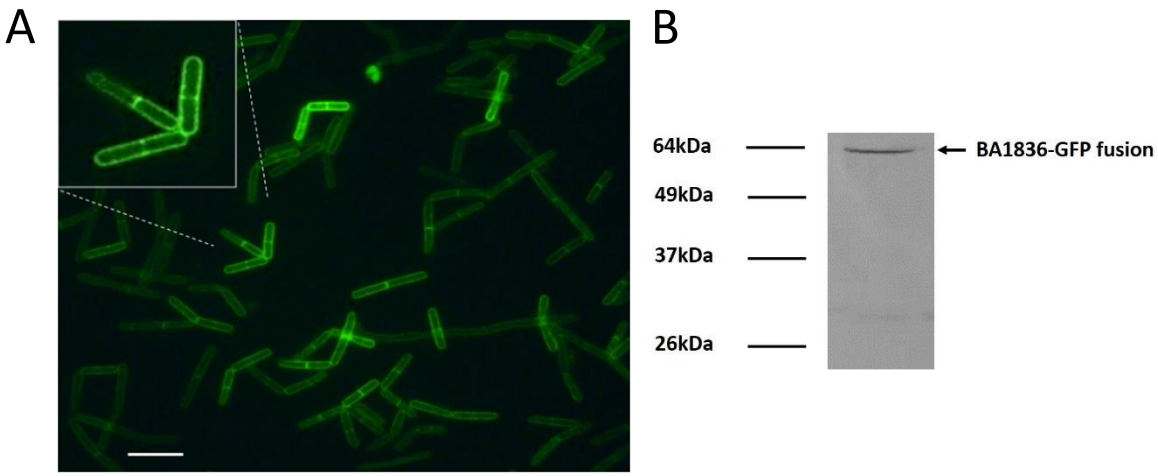

Figure 22. (A) Localization of BA1836-GFP. BA1836-GFP localizes at the cell periphery and septa in stationary phase cells. Scale bar 10 µm. (B) Western blot analysis of lysates of 7702 cells expressing BA1836-GFP during stationary phase of growth using a polyclonal anti-GFP antibody.

Cells lacking *ba1836* suffer reduced sporulation fitness

To elucidate the physiological role of BA1836, we constructed Δ*ba1836* according to the method of Janes and Stibitz (172). Mutant cells were able to grow with no obvious defect and with similar rate as wild-type cells in various liquid media (BHI and SPY broth) indicating that BA1386 is not required for growth and viability of *B. anthracis* cells (Fig. 23). Δ*ba1836* cells grown in SPY medium were not sensitive to lysozyme either in the exponential or in the stationary phase of growth (Fig. 24A) suggesting that BA1836 is not a *bona fide* PGDA involved in resistance to host lysozyme. The autolytic activity of Δ*ba1836* and 7702 strain was tested following addition of NaN_3, a known inducer of autolysis in growing cultures. Δ*ba1836* cells showed decreased autolysis at these conditions compared to the parental strain (Fig. 24B). The PG and PS composition from stationary phase cells of Δ*ba1836* mutant was similar to that of the parental strain (Fig. 25A, B).

In order to examine the morphology of Δ*ba1836* cells, we collected samples during exponential and stationary growth phase in SPY medium and visualized cells by scanning electron microscopy (SEM). Δ*ba1836* daughter cells grown exponentially displayed morphologies similar to that of the parental strain, consistent with the lack

of *ba1836* expression under these conditions (Fig. 24C). However, stationary phase Δ*ba1836* cells displayed chains of unseparated cells in contrast to the single cell morphology of the parental strain (Fig. 24C).

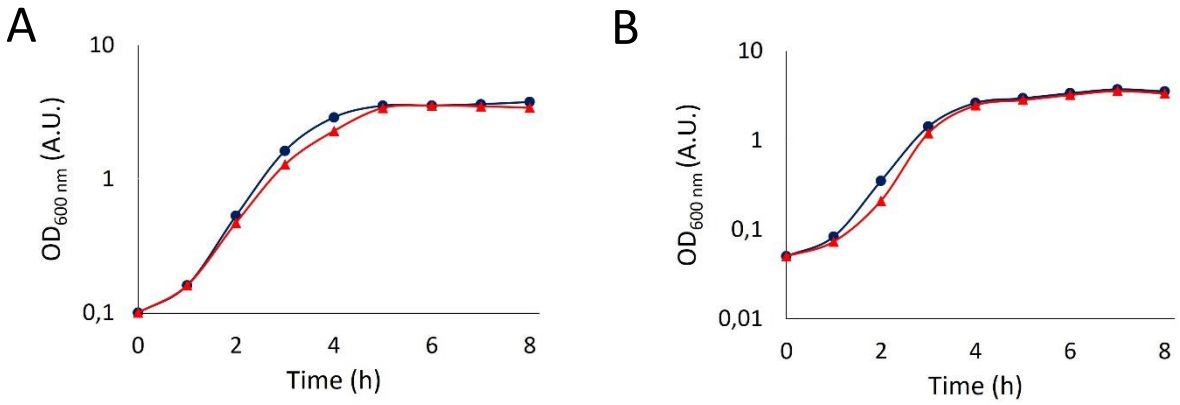

Figure 23. Growth curves of *B. anthracis* parental and mutant strains. Cultures of 7702 (●) and Δ*ba1836* mutant (▲) strains were grown in (A) BHI and (B) SPY liquid broth at 37°C. Cell growth was monitored at 600 nm.

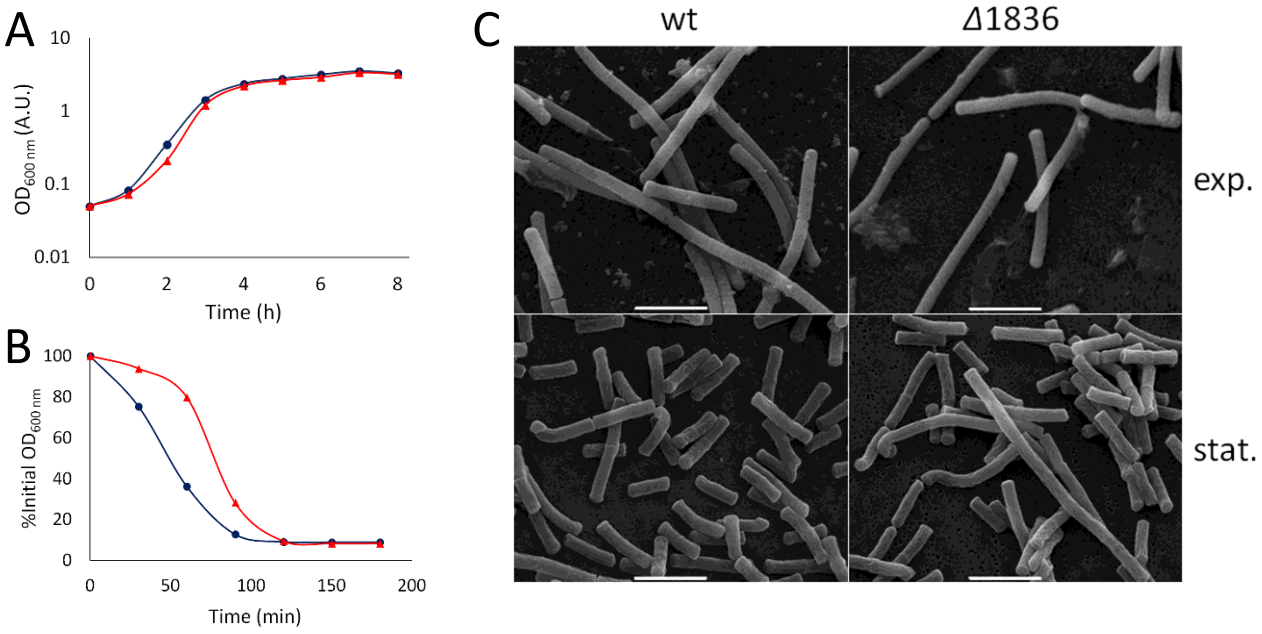

Figure 24. Lysozyme sensitivity, autolysis rate and morphology of parental and mutant strains. (A) Effect of lysozyme on 7702 (●) and Δ*ba1836* mutant (▲) strains. Strains were grown in SPY liquid broth at 37°C. Δ*ba1836* mutant is not affected by the addition of lysozyme. (B) Autolysis rate of 7702 (●) and Δ*ba1836* (▲) cells. Cell lysis was monitored by loss of absorbance at 600 nm. Δ*ba1836* strain is affected by autolysis. (C) SEM of wild type 7702 and Δ*ba1836* cells during exponential (exp.) and stationary (stat.) phase of growth. Δ*ba1836* cells exhibit longer chains of daughter cells compared to the wild type only during stationary phase of growth. Scale bar 5 µm.

Since *ba1836* gene is expressed in the stationary phase of growth and is further induced during sporulation we next examined the morphology of spores produced by Δ*ba1836* by SEM and TEM imaging. No significant differences were observed between mature spores of Δ*ba1836* and the parental strain, suggesting that Δ*ba1836* cells can produce morphologically and structurally normal spores with similar cortex thickness (Fig. 26A). The efficiency of Δ*ba1836* spore formation and their viability were similar to those of the parental strain (Fig. 26B).

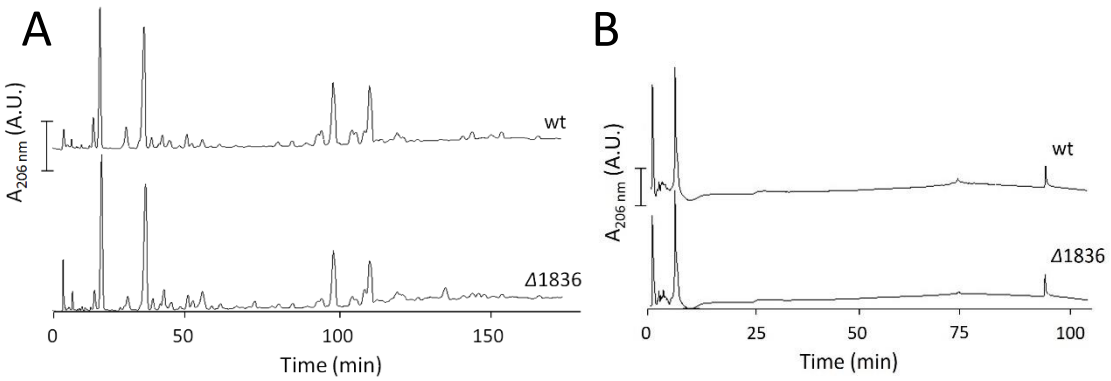

Figure 25. HPLC analysis of (A) muropeptide composition of PG and (B) PS isolated from 7702 and Δ*ba1836* cells during stationary phase of growth. Bar, 200 mAU for PG and 500 mAU for PS.

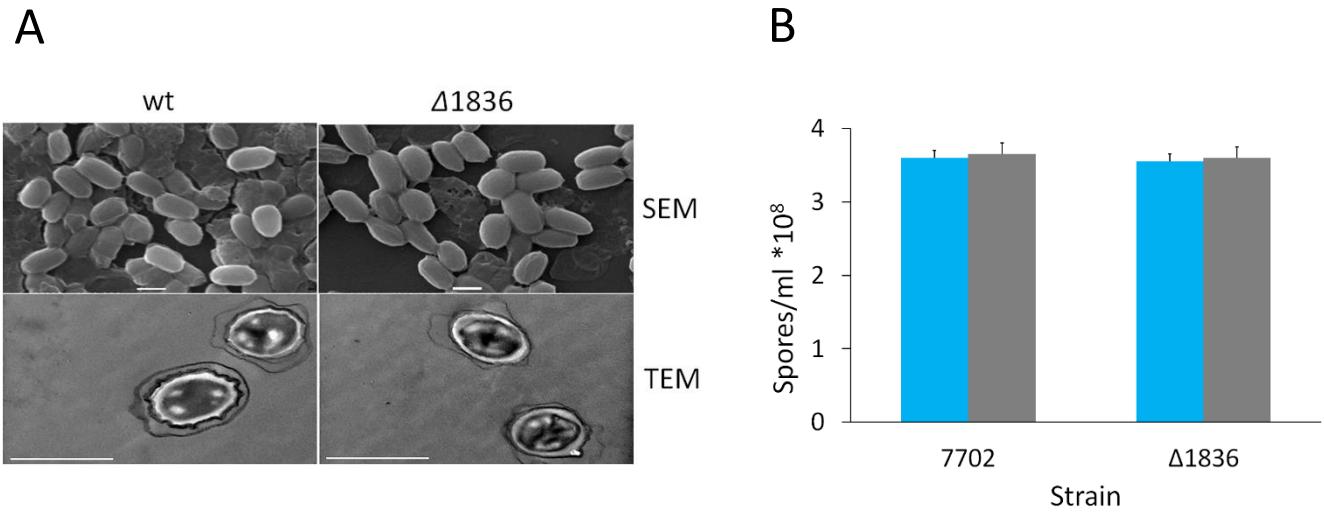

Figure 26. (A) Examination of morphology and structure of parental 7702 and mutant Δ*ba1836* mature spores using SEM and TEM. Scale bar 1 µm. (B) Spore viability of 7702 and Δ*ba1836* spores. Spore viability is defined as the number of phase bright spore particles plated (■) CFU/ml (■) spores/ml.

In order to examine for a subtle role of *ba1836* in spore formation, competition experiments were performed in which Δ*ba1836* mutant strain competed against 7702 wild type strain for several rounds of sporulation. In 7702 wild type strain, *lacZ* is under the transcriptional control of the *eag* promoter. The competition experiment was initially performed with a ratio of 1:1 (wild type to mutant cells) (Fig. 27A) but because Δ*ba1836* cells showed a severe competition deficit the mutant cells were subsequently added in threefold excess (Fig. 27B). Δ*ba1836* mutant strain had a significant competition deficit under sporulation-inducing conditions. Over the course of seven days of co-culturing the percentage of the mutant strain decreased from 75% to 1% of the population (Fig. 27B). Similar results were obtained in competition experiments involving heat treatment at 60^{o}C instead of 80^{o}C, in order to test whether mutant spores were sensitive to heat (Fig. 27C). On the contrary, the Δ*ba1836* mutant strain had no fitness defect under vegetative growth conditions (Fig. 27D). These results strongly suggest that BA1836 is actively involved in sporulation and/or germination.

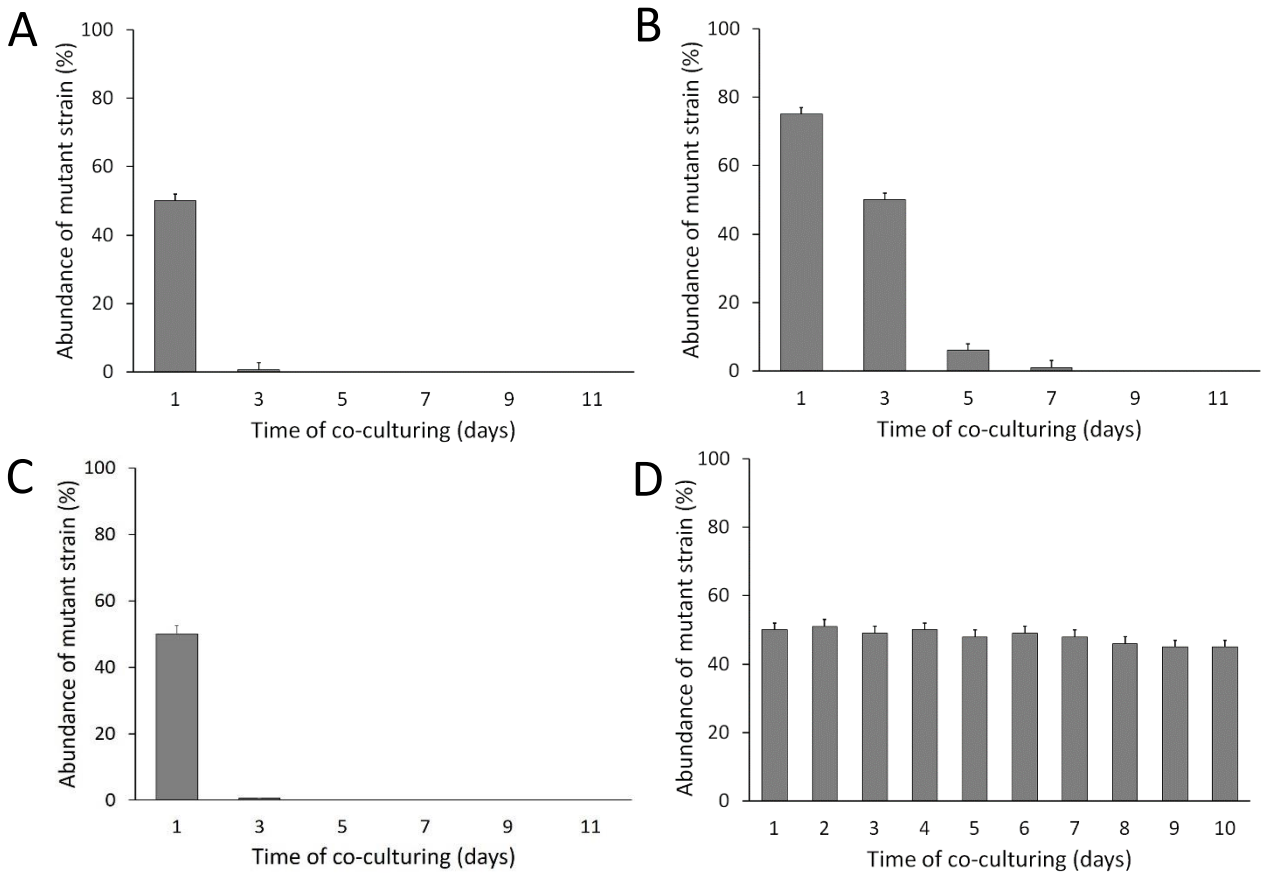

Figure 27. Competition experiment. Δ*ba1836* mutant strain exhibits reduced sporulation fitness. A wild-type reference strain carrying a *Peag-lacZ* transcriptional reporter was competed against Δ*ba1836* mutant in sporulation-inducing medium, starting with (A) 1:1 and (B) 1:3 ratio 7702 to Δ*ba1836*. (C) Δ*ba1836* mutant strain has no fitness defect under growth conditions. (D) Δ*ba1836* mutant strain exhibits reduced sporulation fitness even when spores where heat-treated at a lower temperature (60^{o}C). Mutant strain was competed against the wild type reference at 1:1 ratio.

Δ*ba1836* cells display severe delay in spore development

Since we observed a competition deficit under sporulation-inducing conditions of Δ*ba1836*, we subsequently examined every stage of sporulation by optical microscopy. Interestingly, mutant cells showed a remarkable delay in spore development (Fig. 28). At 13 hours post-resuspension into sporulation-inducing medium, the majority of 7702 mother cells have engulfed the forespore (stage III of sporulation). In contrast, at the same time point the majority of the Δ*ba1836* cells only entered assymetric septation (stage II of sporulation) (Fig. 28). Four hours later, almost every 7702 mother cell has produced a mature forespore (stage VI of sporulation), but the majority of the Δ*ba1836* mother cells have only entered stage III of sporulation (Fig. 28). Mature forespores were visible in Δ*ba1836* mother cells 21 hours post resuspension into sporulation-inducing medium (Fig. 28). These observations demonstrate that Δ*ba1836* cells display a severe delay in spore development, consistent with the expression of *ba1836* in this developmental stage.

The composition of PG from mature spores of Δ*ba1836* and of the parental 7702 strain were analyzed by HPLC (175). The digestion of PG from Δ*ba1836* spores with the muramidase mutanolysin produced a similar overall muropeptide profile compared to PG from wild type spores, although the amount of muropeptides released from the mutant was significantly reduced (Fig. 29). Expression of BA1836-GFP in Δ*ba1836* restored the wild-type spore PG profile (Fig. 29).

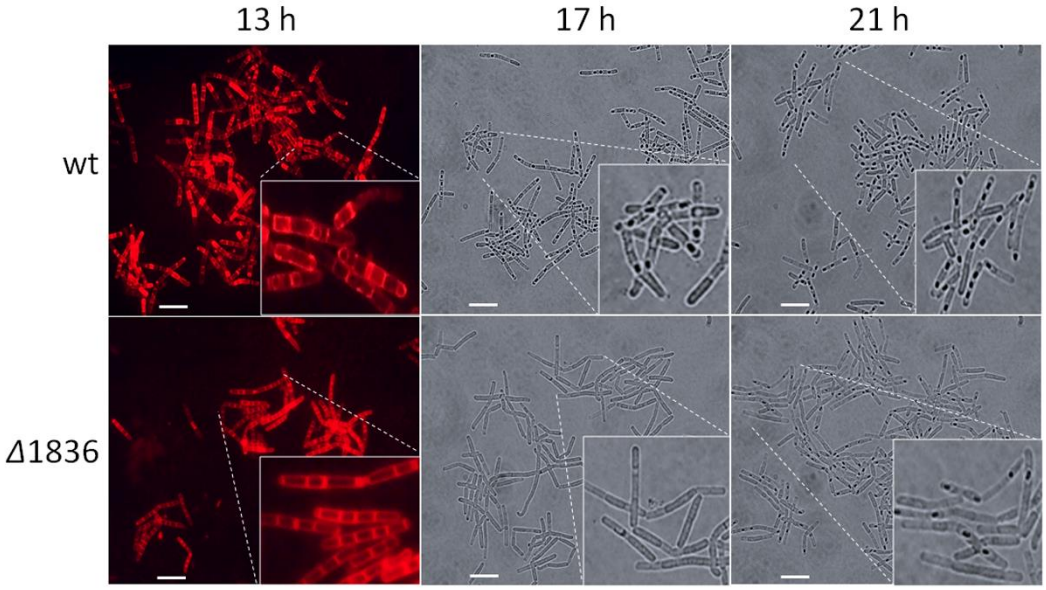

Figure 28. Phenotypic analysis of parental and Δ*ba1836* sporulating cells. Optical microscopy of 7702 and Δ*ba1836* cells, at various time points after induction of sporulation into G modified medium. According to our observation, 8-12 hours corresponded to Stage II, 12-16 hours to Stage III, 16-20 hours to Stage IV-V and 20-24 hours to Stage VI of sporulation. Δ*ba1836* shows a delay of spore development of approximately 4 hours. Scale bar 10 µm.

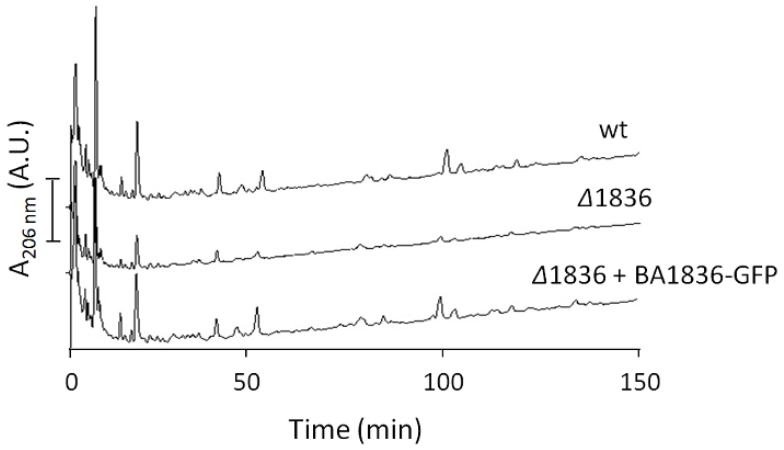

Figure 29. HPLC analysis of muropeptide composition of peptidoglycan isolated from 7702 and Δ*ba1836* mature spores. Δ*ba1836* spore PG digestion with the muramidase mutanolysin produced a similar overall muropeptide profile but reduced amount of muropeptides. Δ*ba1836* mutant strain complemented with BA1836-GFP recovers the phenotype. Bar, 200 mAU.

Δ*ba1836* knockout strain lowers the spore germination rate

We determined the rate of germination of Δ*ba1836* mutant strain as a reduction in spore-specific absorbance upon the addition of 25 mM L-alanine and 12.5 mM inosine as germinants. As shown in Fig. 30*,* Δ*ba1836* spores were capable of initiating germination but, compared to wild-type, the Δ*ba1836* spores had a lower rate of germination. Fifteen minutes after the addition of germinants there was almost 40% loss of absorbance for 7702 spores compared to a 20% loss for Δ*ba1836* spores. Δ*ba1836* spores lost a 40% of the absorbance after 90 min. These results indicate that the absence of BA1836 causes a delay in germination. The rate of germination of Δ*ba1836* mutant spores was partially complemented following expression of BA1836-GFP or the predicted catalytically inactive BA1836 (D53A)-GFP, indicating that deacetylase activity is not required to complement this phenotype (Fig. 30).

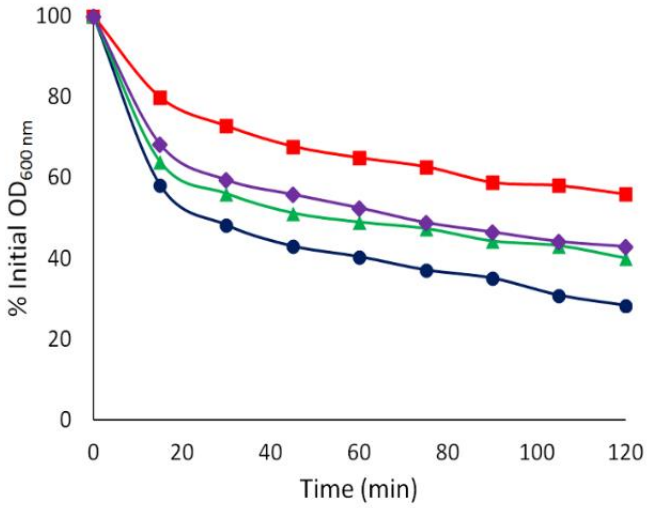

Figure 30. Germination of parental and mutant spores in response to L-ala and inosine. Spores of 7702 (●) and Δ*ba1836* (■) were induced to germinate by the addition of L-ala and inosine. Germination was monitored by loss of absorbance at 600 nm. Δ*ba1836* shows a decreased rate of germination compared to the wild type. Mutant strain complemented with BA1836-GFP (▲) and BA1836 D53A-GFP (◆) partially recovered the phenotype.

BA3943

BA3943 is a pseudoPDA

For BA3943, the TMHMM (186) program predicts the presence of an *N*-terminus transmembrane domain (residues 5-24). BA3943 shares 95% identity with its homologue BC3804 from *B. cereus* and displays 56% identity with *B. subtilis* sporulation protein YlxY (Fig. 31). Deletion of *ylxY* gene in *B. subtilis* resulted in deficits specific to sporulation-inducing conditions, however, the nature of the deficits is currently unknown (181).

Importantly, sequence alignment of BA3943 (excluding residues 1-112) with representative members of the CE4 family (126), whose crystal structures have been determined, and with its homologue YlxY from *B. subtilis*, shows that BA3943 does not retain the pattern of every sequence motif (MT1-MT5) typical for PDAs (Fig. 32). More specifically, BA3943 has a disrupted metal cation binding site, since the Asp of motif MT1 is mutated to Val^{119}. However, His^{119} and His^{123} of motif MT2, which complete the metal cation binding site, are conserved. The Asp of the metal binding triad is highly conserved in PGDAs, but MurNAc PDAs usually contain Asn at this position (139, 146). Additionally, the highly conserved Asp of motif MT1, corresponding to the catalytic base of the deacetylation reaction, is replaced by Asn^{118}, while the His^{263} of motif MT5, corresponding to the catalytic acid of the deacetylation reaction, is conserved. The conserved Arg of motif MT3 is also mutated to Ala^{207}. Furthermore, the highly conserved Pro^{209}, that is autocatalytically hydroxylated at the Cα atom (149), is present in motif MT3. The pattern of hydrophobic residues in motifs MT4 and MT5 agrees well with the patterns found in other PDAs (Fig. 32).

In summary, BA3943 does not display all the sequence features of active PDAs suggesting that it is a pseudoPDA.

Score	Expect	Method	Identities	Positives	Gaps
338 bits(868)	2e-121	Compositional matrix adjust.	154/274(56%)	203/274(74%)	0/274(0%)

```
BA3943  25   AQDNLYEEIQKHAKQYEIAPQNAMIDKIWKATPGYNGRQVDMEASYNNMKKLKKFDQKHL  84
             ++D LYEE+ + A +YE+ PQ+A +DK+WK+ PGYNG +V++E SY  MKK  +F +  L
YlxY     44  SKDPLYEELLQKAPEYEVKPQDARVDKVWKSIPGYNGLKVNIEQSYKKMKKHGEFRENDL  103

BA3943  85   EFKEVSPSVHLEDLSPAPIYRGHPNKKMVGLTINVAWGNEYLPRILEILKKHDVKATFFL  144
              + +V P+VHLE L P PIY+G+P+K MV   INVAWGNEYL ++L IL+KH VKATFFL
YlxY    104  VYSQVKPNVHLESLQPEPIYKGNPDKPMVAFLINVAWGNEYLEKMLPILQKHQVKATFFL  163

BA3943 145   EGRWVKENLRFAKMIVDANQEVGNHSYTHPNMKTLSSDEIRDQLQKTNRMIEAATNQKVR  204
             EG WV+ N + AK I +   E+GNHSY HP+M  L++  I +QL KTN  IE     K +
YlxY    164  EGNWVRNNKQLAKKIAEDGHEIGNHSYNHPDMSKLTTGRISEQLDKTNEQIEQTIGVKPK  223

BA3943 205   WFAPPSGSFRDEVVKIADDFQMGTIMWTVDTIDWKRPEPDVLLQRVMRKIHPGAIVLMHP  264
             WFAPPSGS R  VV IA + QMGTIMWTVDTIDW++P P VL  RV+ KIH GA++LMHP
YlxY    224  WFAPPSGSLRKAVVDIAAEKQMGTIMWTVDTIDWQKPAPSVLQTRVLSKIHNGAMILMHP  283

BA3943 265   TSSTTEALDTMITKLKEQGYKVGNITELLDEKRV  298
             T ST E+L+ +ITK+K++GY +G +TEL+DE R+
YlxY    284  TDSTAESLEVLITKIKDKGYALGTVTELMDETRL  317
```

Figure 31. Sequence alignment of BA3943 with YlxY from *B. subtilis* using BLASTp. The two proteins show 56% sequence identity.

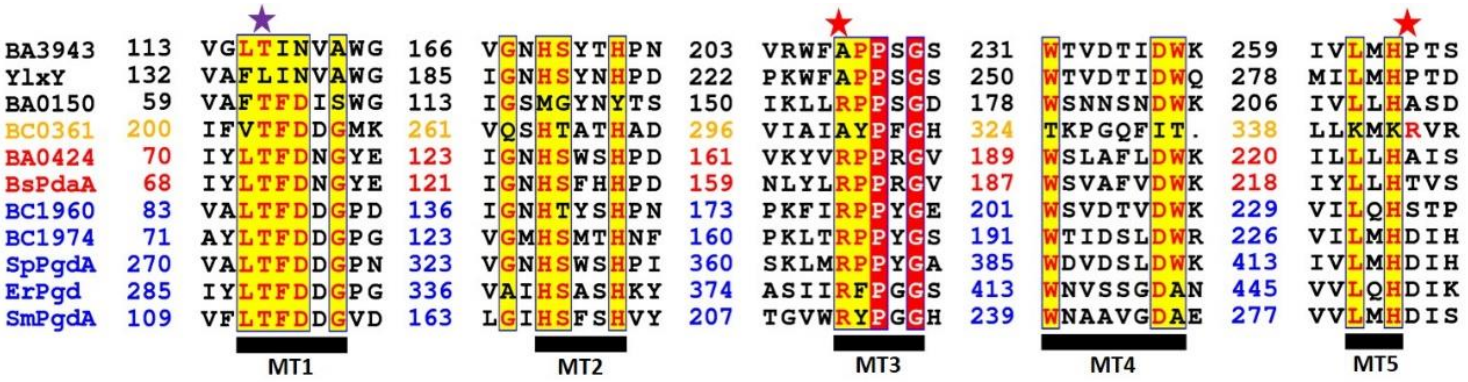

Figure 32. Sequence alignment of the NodB domain of BA3943 with representative members of the CE4 family including the PGDAs (blue color) BC1960 (148, 149), BC1974 (*B. cereus*) (130, 150), SpPgdA (*S. pneumoniae*) (129, 145), ErPgd (*E. rectale*) and SmPgdA (*S. mutans*) (191), the MurNAc peptidoglycan deacetylases (red color) BA0424 (*B. anthracis*) (139) and BsPdaA (*B. subtilis*) (138, 146), the putative PDA (orange color) BC0361 (*B. cereus)* (144, 152) and the inactive PDA (black color) BA0150 (*B. anthracis*) (151). The conserved sequence motifs MT1-MT5 for this class of enzymes are shown at the bottom. The alignment was performed with T-coffee and plotted with the ESPRIT (147). PDB codes: BA0150_4M1B, BC0361_4HD5, BA0424_2J13, BsPdaA_1W17, BC1960_4L1G, BC1974_5N1J, SpPgdA_2C1G, ErPgd_5JMU, SmPgdA_2W3Z. The purple star indicates the conserved Thr (T) residue of MT1 and the red stars indicate the conserved Arg (R) of MT3.

ba3943 lacking the transmembrane domain (residues 1-25) was expressed in *E. coli* and the recombinant protein was purified to homogeneity (Fig. 33). BA3943 was incubated with commonly used deacetylase substrates and shown to be inactive against H^3-glycol chitin, $GlcNAc_{4-7}$ and PG isolated from *E. coli,* at a wide pH range and in the presence or absence of the divalent cations Co^{+2}, Zn^{+2}, Ni^{+2} and Mn^{+2} (data not shown). In addition, no Pro^{185} hydroxylation was detected by MS/MS (149) (Table 5).

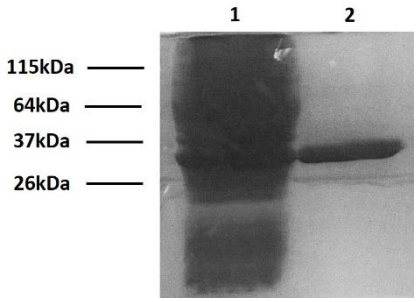

Figure 33. SDS-PAGE of the purified BA3943: lane 1, crude extract; lane 2, Ni-NTA eluate. Samples were electrophoresed on a 12% polyacrylamide gel under denaturing and reducing conditions. Protein bands were visualized by staining with Coomassie Brilliant Blue R.

The crystal structure of BA3943 reveals a unique *N*-terminal domain

The crystal structure of BA3943 was determined at 1.14 Å resolution by A. Molfetas (Prof. M. Kokkinidis lab, Biology Department, University of Crete) (Fig. 34). The *N*-terminus of BA3943, contains 11 Lys residues (13.5% frequency) among a total of 82.

BA3943 structure confirmed the absence of the features of active PDAs which were observed in the sequence alignment (Fig. 32). The metal cation binding site of BA3943 is disrupted since the well-conserved Asp of characterized PGDAs is mutated to Val^{95}, which points away from the active site, as already observed in MurNAc PG deacetylases (138, 139). The presence of Ala instead of the Arg residue of motif MT3 in the vicinity of the catalytic Asp, creates a cavity which potentially destabilizes the active site. The Pro residue of motif MT3 that was hydroxylated on BC1960 and other PDAs, lacks the α-carbon hydroxyl group, consistent with the absence of deacetylase activity. The determination of the crystal structure at a high resolution revealed important information for the restoration of enzyme activity.

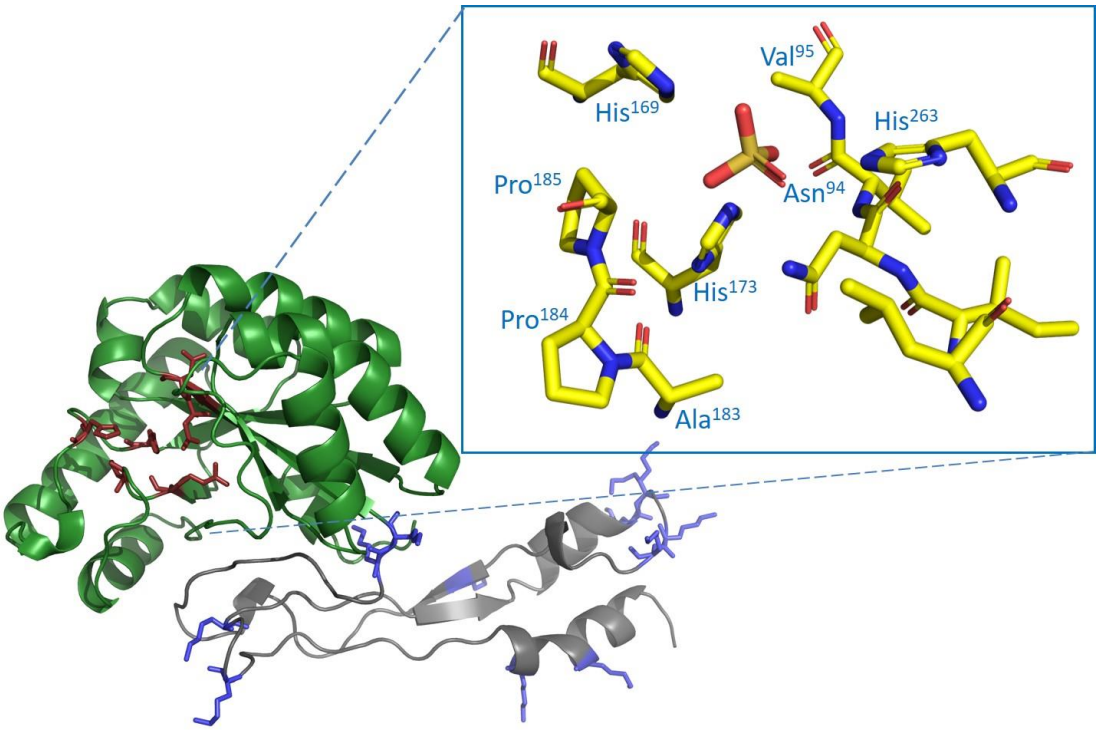

Figure 34. Crystal structure and active site of BA3943. The *N*-terminal lysine-rich domain in grey color, lysines in blue, NodB domainin green and the active site residues in red. BA3943 structure was determined by A. Molfetas (Prof. M. Kokkinidis lab, Biology Department, University of Crete).

Restoration of deacetylase activity and levels of hydroxylation and the effect of mutations on active-site residues on deacetylase activity

Since BA3943 is a pseudoPDA, we decided to restore the deacetylase activity and the levels of hydroxylation employing site-directed mutagenesis of specific, essential for catalysis residues of the active site. Asn^{94} and Val^{95} of motif MT1 and Ala^{183} of motif MT3 were mutated sequentially to the conserved Asp, Asp and Arg respectively, thus resulting in three mutant proteins: BA3943 N94D (*ba3943mut1*), BA3943 N94D V95D (*ba3943mut2*) and BA3943 N94D V95D A183R (*ba3943mut3*).

The *ba3943*mut1, *ba3943mut2* and *ba3943mut3* were expressed in *E.coli* and when feasible, the recombinant BA3943 mutants were purified to homogeneity (data not shown) in order to measure deacetylase activity and levels of hydroxylation.

BA3943 N94D was inactive against H^3-glycol chitin and Pro^{185} hydroxylation was not detected (Table 5). BA3943 N94D V95D could not be purified because it was

insoluble and remained in the cell pellet (data not shown). As a result, its activity could not be estimated (Table 5).

BA3943 N94D V95D A183R however, was active against H^3-glycol chitin (Table 5) with optimum reaction conditions: 1 mM $CoCl_2$, 25 mM Tris-HCl pH= 7.0, overnight incubation at 37^{o}C. Except from the deacetylase activity, Pro^{185} hydroxylation was also detected (Table 5). Unlike the characterized PGDAs, BC1974 and BC1960 from *B. cereus,* homologues of BA1977 and BA1961 respectively from *B. anthracis*, BA3943 N94D V95D A183R was inactive when $CoCl_2$ was not added in the enzyme assay.

Table 5. Deacetylase activity against H^3-glycol chitin and mass spectrometric quantitation of 2-Hyp level in BA3943 and BA3943 mutant proteins. The resurrected enzyme is highlighted in red color. cpm, counts per minute; NE, not estimated

Protein	Activity (cpm)	% 2-Hyp
Control	53	-
BA3943	50	8,67±1,697
BA3943 N94D	55	4,05±1,923
BA3943 N94D V95D	NE	6,39±2,960
BA3943 N94D V95D A183R	558	25±6,397
BA3943 N94D V95D A183K	48	NE
BA3943 N94D V95D A183R P185G	58	NE
BA3943 N94D V95N A183R	45	NE
BA3943 N94D A183R	140	NE

BA3943 N94D V95D A183R was also incubated with $GlcNAc_6$ and $GlcNAc_7$ and reaction products were separated by HPLC revealing two peaks (Fig. 35A, 35B). The two peaks resulting from the incubation of BA3943 N94D V95D A183R with $GlcNAc_7$ were collected and subsequently subjected to electrospray ionization (ESI-MS) analysis. The first peak corresponded to $GlcNAc_7$ while the second peak corresponded to $GlcNAc_7$ lacking an acetyl group from the 3rd and/or the 4th position indicating that BA3943 N94D V95D A183R is able to perform a deacetylation reaction on the 3rd and/or the 4th GlcNAc residue (Fig. 36). In contrast, BA3943 N94D V95D A183R was inactive against PG isolated from *E. coli* and *B. subtilis* (Fig. 37A, 37B).

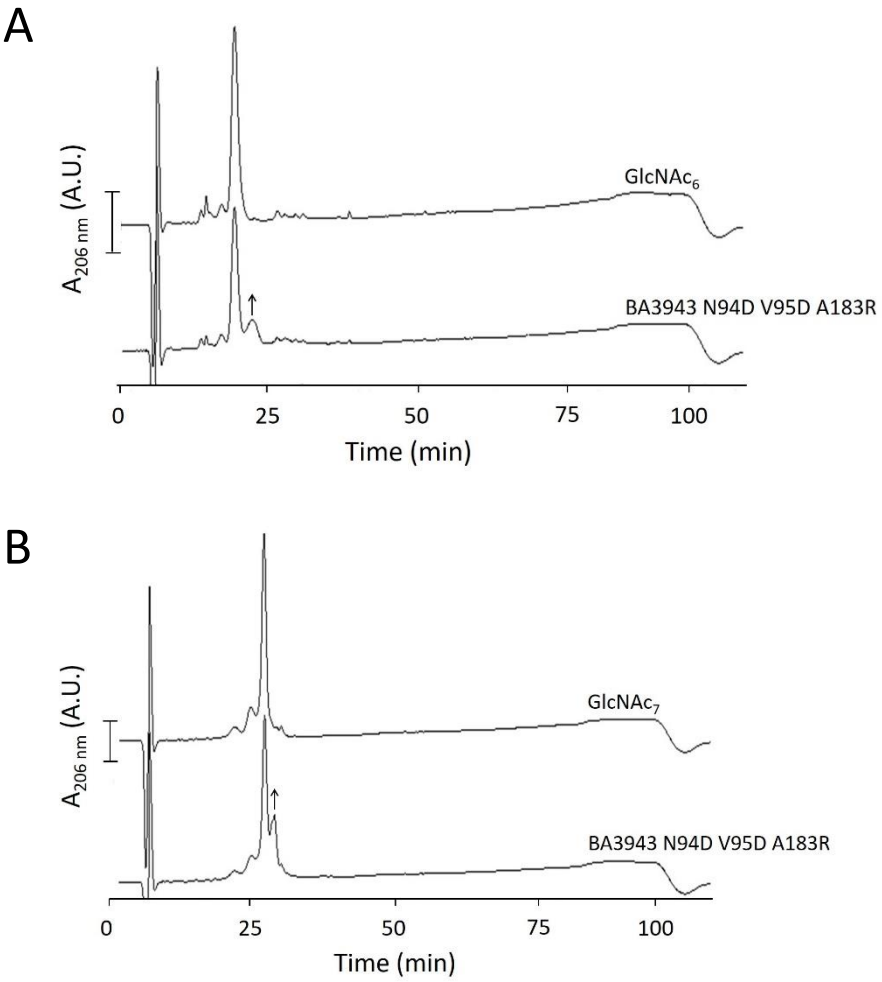

Figure 35. HPLC analysis of (A) $GlcNAc_6$ and (B) $GlcNAc_7$ following incubation with BA3943 N94D V95D A183R. The arrow indicates the appearance of an extra peak in the analysis. Bar, 50 mAU.

A

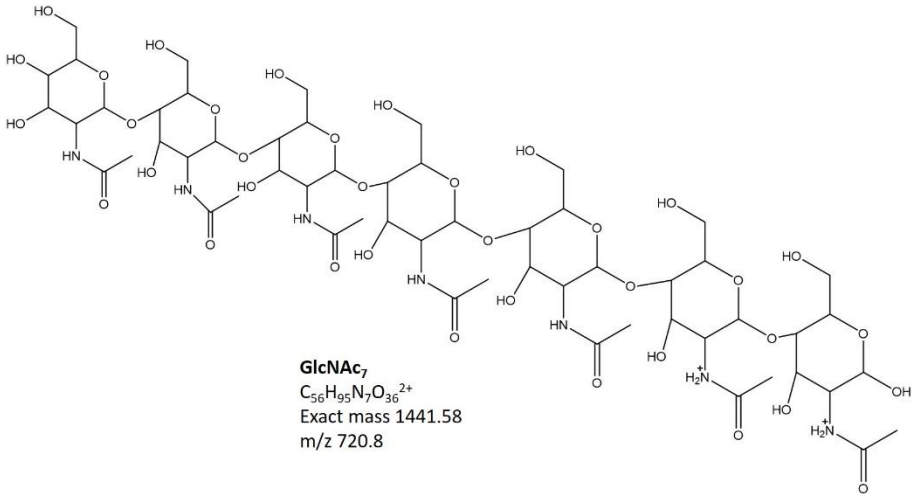

GlcNAc$_7$
$C_{56}H_{95}N_7O_{36}^{2+}$
Exact mass 1441.58
m/z 720.8

B

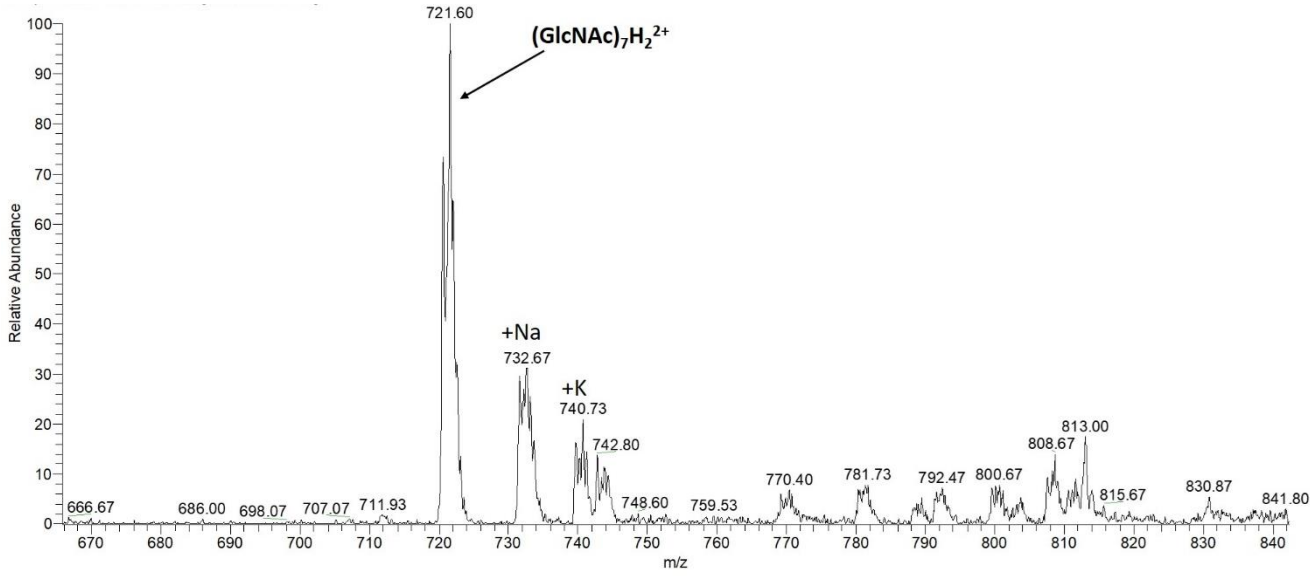

C

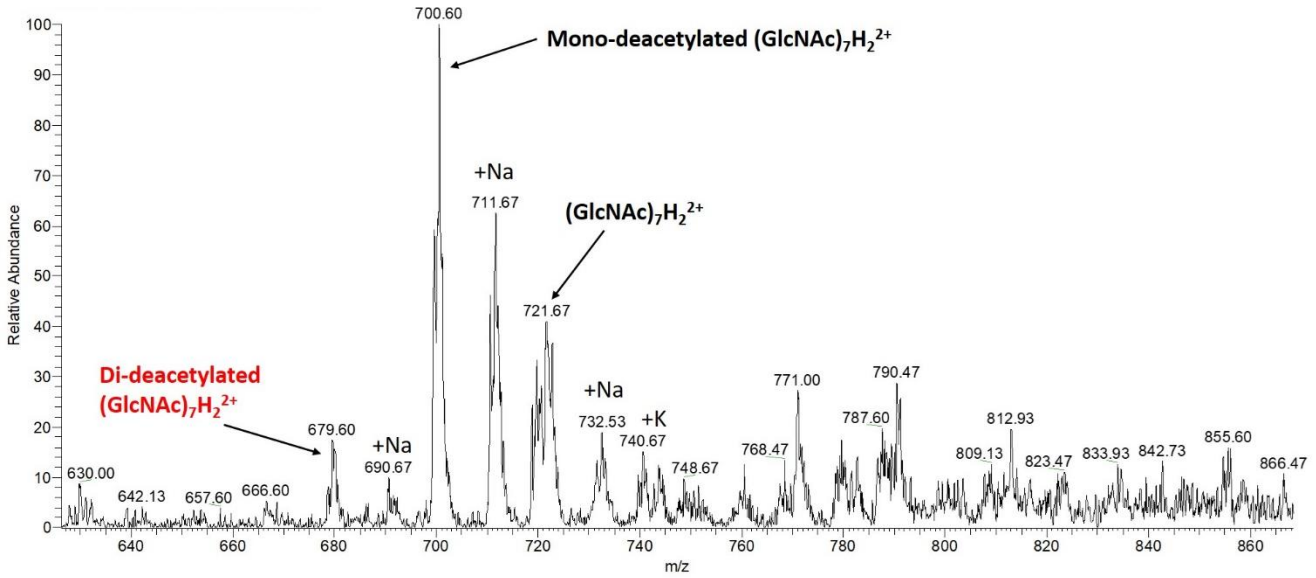

D

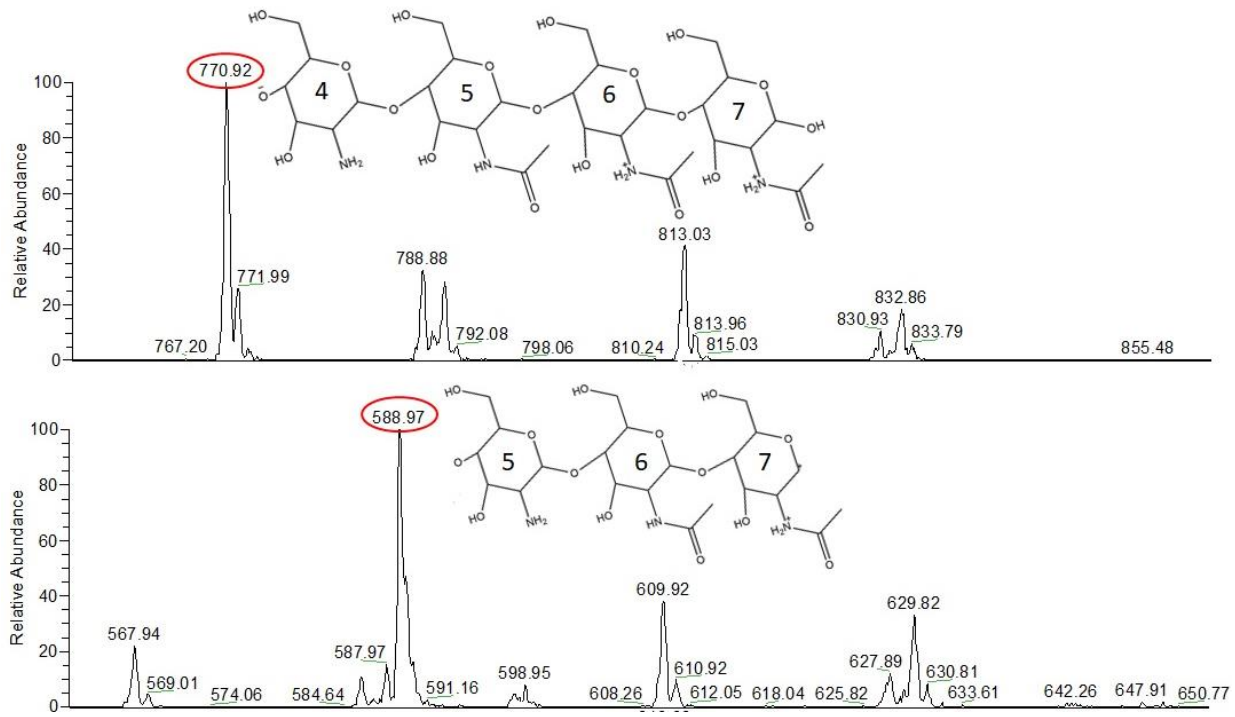

Figure 36. ESI-MS analysis of reaction products resulting from incubation of $GlcNAc_7$ with BA3943 N94D V95D A183R. (A) Chemical structure, mass and m/z ratio of $GlcNAc_7$. (B) ESI-MS analysis of the first peak collected after HPLC analysis of $GlcNAc_7$ reaction products (Fig. 31B). (C) ESI-MS analysis of the second peak collected after HPLC analysis of $GlcNAc_7$ reaction products (Fig. 31B). (D) Deacetylation of $GlcNAc_7$ is performed on the third and/or the fourth unit since fragments of 770.92 and 588.97 mass respectively, are observed in the second peak spectra. The ESI-MS analysis was performed by L. Mavroudakis (Prof. S. Pergantis Lab, Chemistry Department, University of Crete).

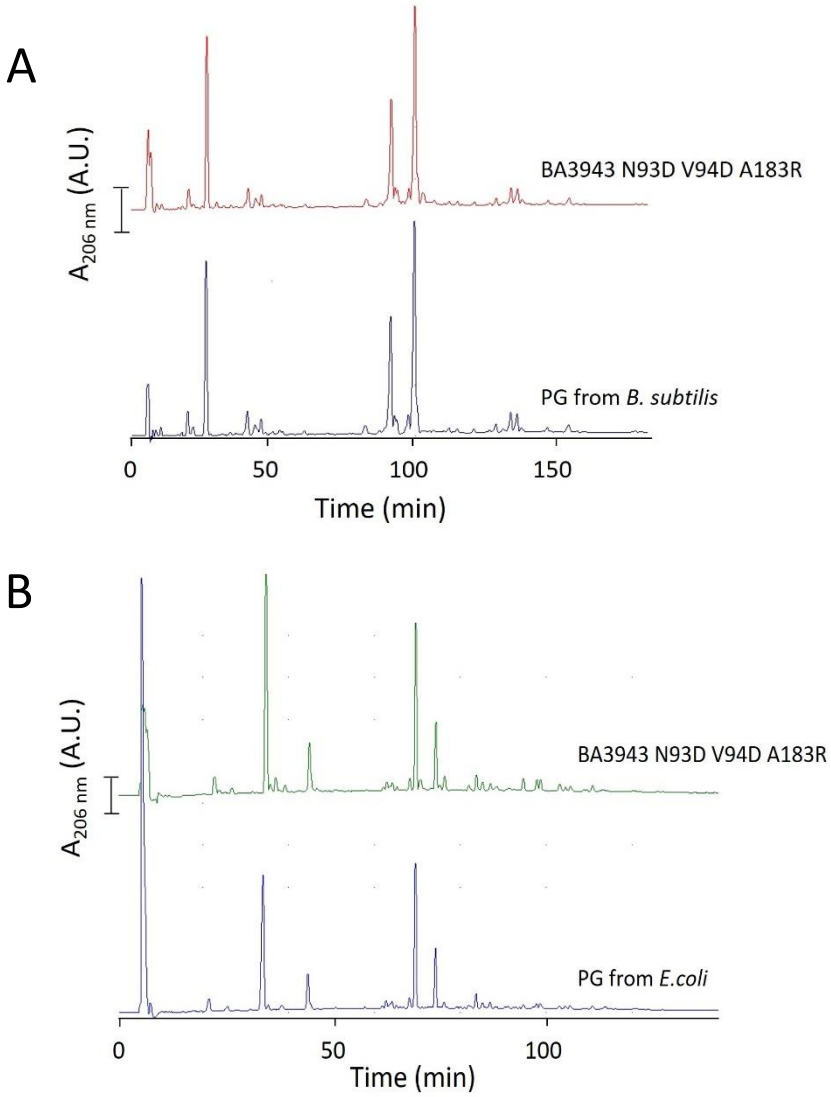

Figure 37. HPLC analysis of PG isolated from (A) *B. subtilis* and (B) *E. coli* following incubation with BA3943 N94D V95D A183R. Bar, (A) 200 mAU, (B) 100 mAU.

The crystal structure of BA3943 N94D V95D A183R was determined at 1.71 Å resolution by A. Molfetas (Prof. M. Kokkinidis lab, Biology Department, University of Crete). The overall structure is identical to that of the wild-type protein except from the active site (Fig. 38A). The active site of BA3943 N94D V95D A183R is similar to that of the characterized PGDA BC1960, with the exception of Asp^{95} of the metal cation binding triad, which points away from the active site (Fig. 38B). In addition, no metal is detected in the electron density map. This finding was confirmed by ICP-MS analysis (data not shown).

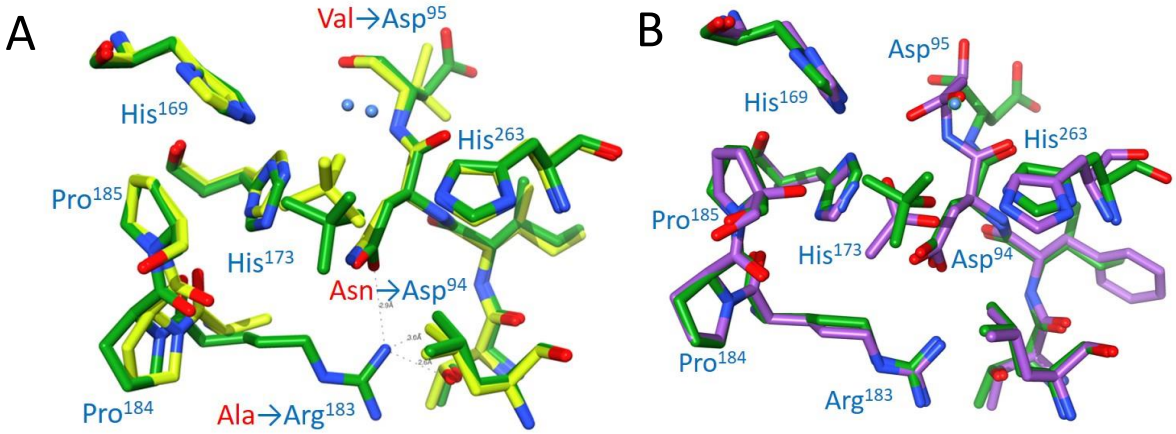

Figure 38. (A) Superposition of the active sites of BA3943 N94D V95D A183R (green) and BA3943 (yellow). The residues of BA3943 active site which were mutated are shown in red. (B) Superposition of the active sites of BA3943 N94D V95D A183R (green) and the PGDA BC1960 (purple). The numbers indicate the position of the residues in the sequence of BA3943. The determination of the crystal structure of BA3943 N94D V95D A183R was performed by A. Molfetas (Prof. M. Kokkinidis lab, Biology Department, University of Crete).

BA3943 N94D V95D was unstable and remained in the insoluble cell fraction. Enzyme stability as well as deacetylase activity and levels of hydroxylation were restored when the third point mutation of Ala^{183} to Arg was performed, suggesting a critical role for Arg in folding and catalysis. In order to examine this hypothesis, Arg^{183} was mutated to Lys, which has similar chemical structure and physicochemical properties (pKa) to Arg and thus similar behavior was expected. However, most of the overexpressed BA3943 N94D V95D A183K was insoluble and remained in the cell pellet (data not shown). The soluble protein fraction was purified and H^3-glycol chitin was examined as substrate at the optimum reaction conditions of the resurrected enzyme. BA3943 N94D V95D A183K was inactive against H^3-glycol chitin (Table 5), confirming the importance of Arg in the active site and its involvement in the deacetylation/hydroxylation reaction, in a way which remains to be unraveled.

We next decided to mutate the hydroxylated Pro^{185} constructing the quadruple mutant BA3943 N94D V95D A183R P185G protein. Pro^{185} was mutated to Gly since Gly of certain neuropeptides and prohormones has also been identified to be hydroxylated in the Cα (192-194). BA3943 N94D V95D A183R P185G was incubated with H^3-glycol chitin at optimum reaction conditions but it was inactive. The levels of 2-hydroxyglycine have not been determined yet (Table 5).

As shown in Fig. 32, the Asp of the metal-binding triad is not highly conserved. The MurNAc PGDAs BA0424 and PdaA contain Asn instead of Asp at this position and it has been proposed that Asp can also be replaced by other hydrophobic residues like Ala and Val (139). In order to test whether the specificity of BA3943 N94D V95D A183R could possibly be altered from GlcNAc to MurNAc, Asp^{95} was mutated to either Asn, resulting in BA3943 N94D D95N A183R (*ba3943mut7*), or Val (as it initially was in wild-type BA3943), resulting in BA3943 N94D D95V A183R (*ba3943mut8*).

The *ba3943mut7* and *ba3943mut8* were expressed in *E.coli* and the recombinant BA3943 mutant proteins were purified to homogeneity (data not shown). Subsequently, their activity against common deacetylase substrates was examined. BA3943 N94D D95V A183R was slightly active against H^3-glycol chitin while BA3943 N94D D95N A183R was inactive (Table 5).

BA3943 N94D D95V A183R was also incubated with $GlcNAc_7$ and the reaction products were separated by HPLC revealing three peaks (Fig. 39). The peaks were collected and subsequently subjected to ESI-MS but $GlcNAc_7$ was fully acetylated (data not shown). Next, both BA3943 mutant proteins were incubated with *N*-acetylmuramyl-L-alanyl-D-isoglutamine hydrate (MDP) in order to test whether they were able to deacetylate MurNAc residues. The reaction products were separated by HPLC (Fig. 40) and the resulting peaks were collected and further analyzed by ESI-MS but MurNAc residues were acetylated (data not shown). Conclusively, BA3943 N94D D95V A183R and BA3943 N94D D95N A183R have neither GlcNAc nor MurNAc deacetylase activity against the tested substrates.

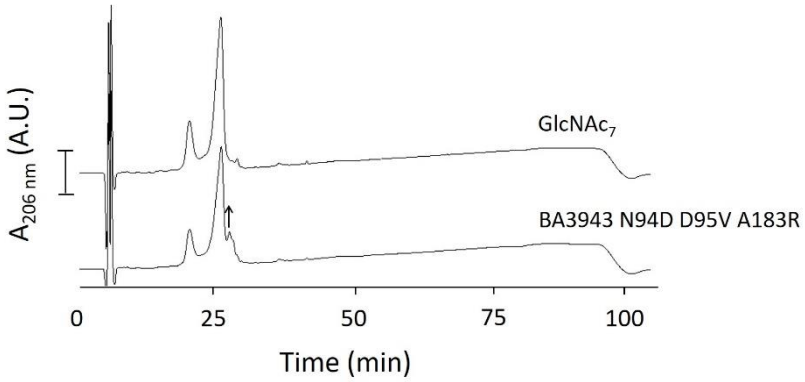

Figure 39. HPLC analysis of $GlcNAc_7$ following incubation with BA3943 N94D D95V A183R. The arrow indicates the appearance of an extra peak in the analysis. Bar, 50 mAU.

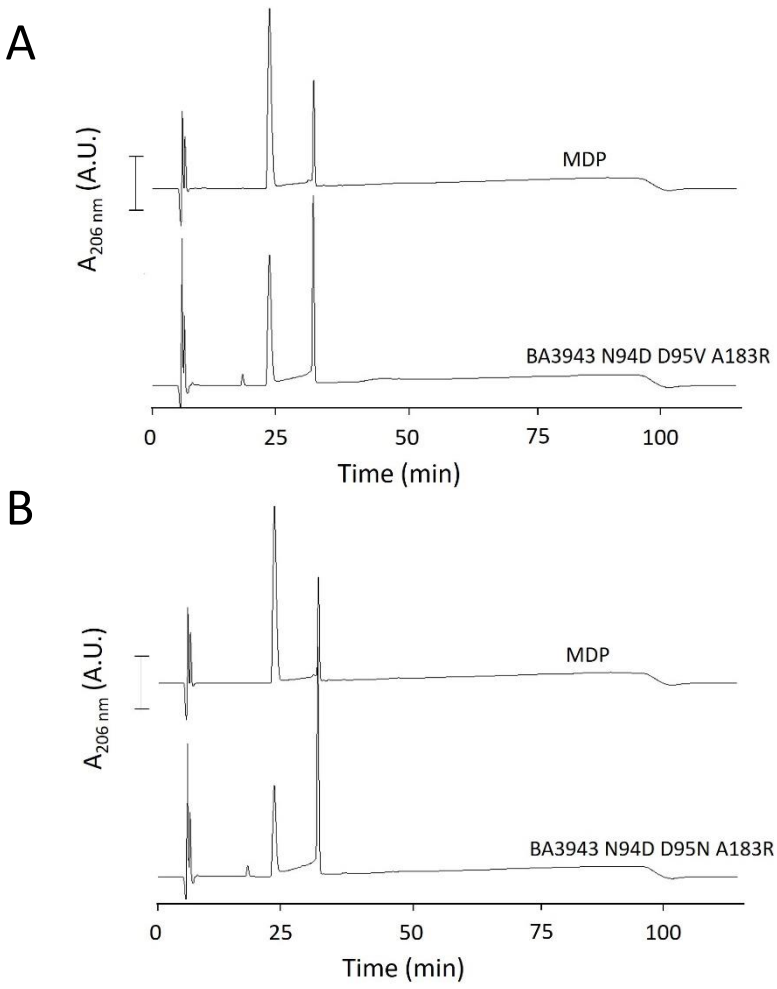

Figure 40. HPLC analysis of MDP following incubation with (A) BA3943 N94D D95V A183R and (B) BA3943 N94D D95N A183R. Bar, 250 mAU.

ba3943 is expressed at the engulfment stage of sporulation

In order to monitor the expression of the *ba3943* we constructed a transcriptional reporter by fusing an upstream fragment of *ba3943* (containing the promoter region) with the start codon of the *E. coli lacZ* gene.

We resuspended exponential phase 7702 *B. anthracis* cells carrying this construct into sporulation-inducing medium and collected samples at various time points during sporulation. As we observed by optical microscopy, most cells were in stage II of sporulation (asymmetric division) about 8-12 h after transfer into sporulation medium, in stage III (engulfment) after 12-16 hours, in stage IV-V (coat and cortex assembly) after 16-20 hours and in stage VI-VII (spore maturation and

mother cell lysis) after 20-24 hours. As shown in Fig. 41A, *ba3943* promoter driven lacZ expression was rapidly induced to high level shortly after cells entered into the engulfment of the forespore from the mother cell. In contrast, *ba3943* promoter remained silent during vegetative (exponential and stationary) growth (Fig. 41B).

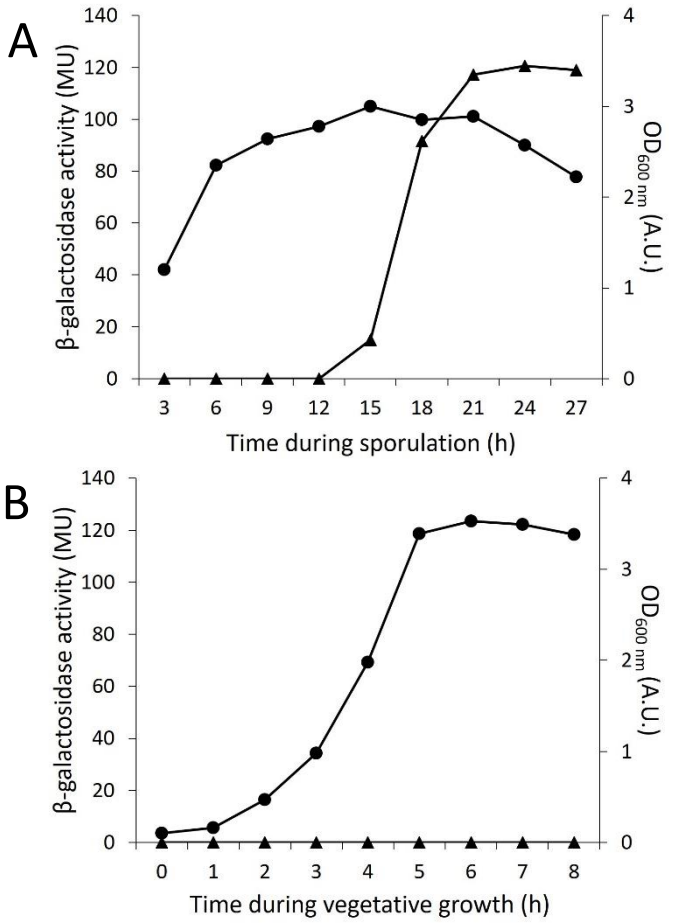

Figure 41. Expression of *ba3943* gene. (A) Induction of sporulation of exponential phase *B. anthracis* 7702 cells, carrying the *lacZ* transcriptional reporter for *ba3943* gene. Samples taken at the indicated time points were assayed for β-galactosidase activity. (B) *B. anthracis* 7702 strain grown in BHI. *ba3943* is expressed after cells entered the engulfment stage of sporulation. (●) $OD_{600\ nm}$ (A.U.) (▲) β-galactosidase activity in Miller Units (MU).

BA3943-GFP localizes to the forespore membrane

The amino acid sequence of BA3943 is predicted to include an *N*-terminal membrane spanning region that is not removed by a signal peptidase. In order to determine the subcellular localization of BA3943, a C-terminal *gfp* fusion of the *ba3943* was constructed and was introduced into *B. anthracis* 7702. We induced the expression of BA3943-GFP in *B. anthracis* sporulating cells that entered the engulfment, i.e., when *ba3943* is normally expressed. Expression of the GFP-fused BA3943 was confirmed by Western blot analysis (Fig. 42B). BA3943-GFP localized at the forespore membrane, during its engulfment by the mother cells, with lower fluorescence at the septa of the mother cell (Fig. 42A). Δ*ba3943* transformed with GFP-fused BA3943 protein could not restore the phenotypes discussed in the sections "Cells lacking ba3943 suffer reduced sporulation fitness" and "BA3943 affects autolysis of vegetative cells". In order to examine the effect of the lysine rich domain on BA3943 localization, a C-terminal *gfp* fusion of the *ba3943* lacking the lysine-rich domain was constructed and was introduced into *B. anthracis* 7702. Expression of the GFP-fused BA3943^{-}K was confirmed by Western blot analysis (Fig. 42B). The BA3943^{-}K-GFP localized at the same cellular sites as the wild type protein (data not shown).

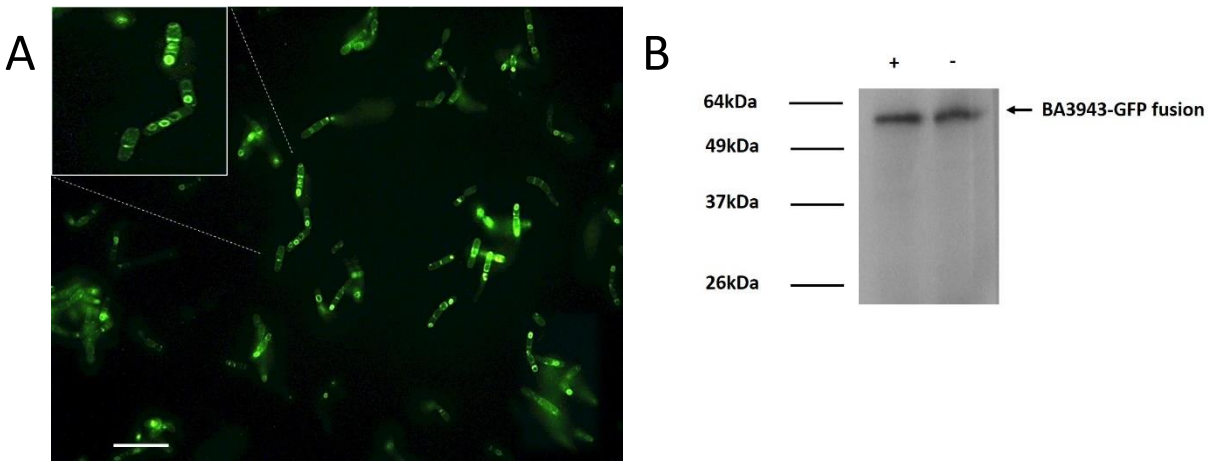

Figure 42. (A) Localization of BA3943-GFP. BA3943-GFP localizes at the forespore membrane and the mother-cell septa. Scale bar 10 μm. (B) Western blot analysis of lysates of 7702 cells expressing BA3943-GFP, with (+) and without (-) the lysine-rich domain, during sporulation using a polyclonal anti-GFP antibody.

Cells lacking *ba3943* suffer reduced sporulation fitness

To investigate the physiological role of BA3943, Δ*ba3943* mutant was constructed in *B. anthracis* 7702 strain (172). Since *ba3943* gene is expressed during sporulation, a series of experiments with Δ*ba3943* spores were performed. Δ*ba3943* mature spores, observed by SEM and TEM, showed no abnormalities (Fig. 43A). The efficiency of Δ*ba3943* spore formation, spore viability and rate of germination were similar to those of the parental strain (Fig. 43B, 43C). The PG composition of Δ*ba3943* mature spores was similar to that of the parental strain (Fig. 43D).

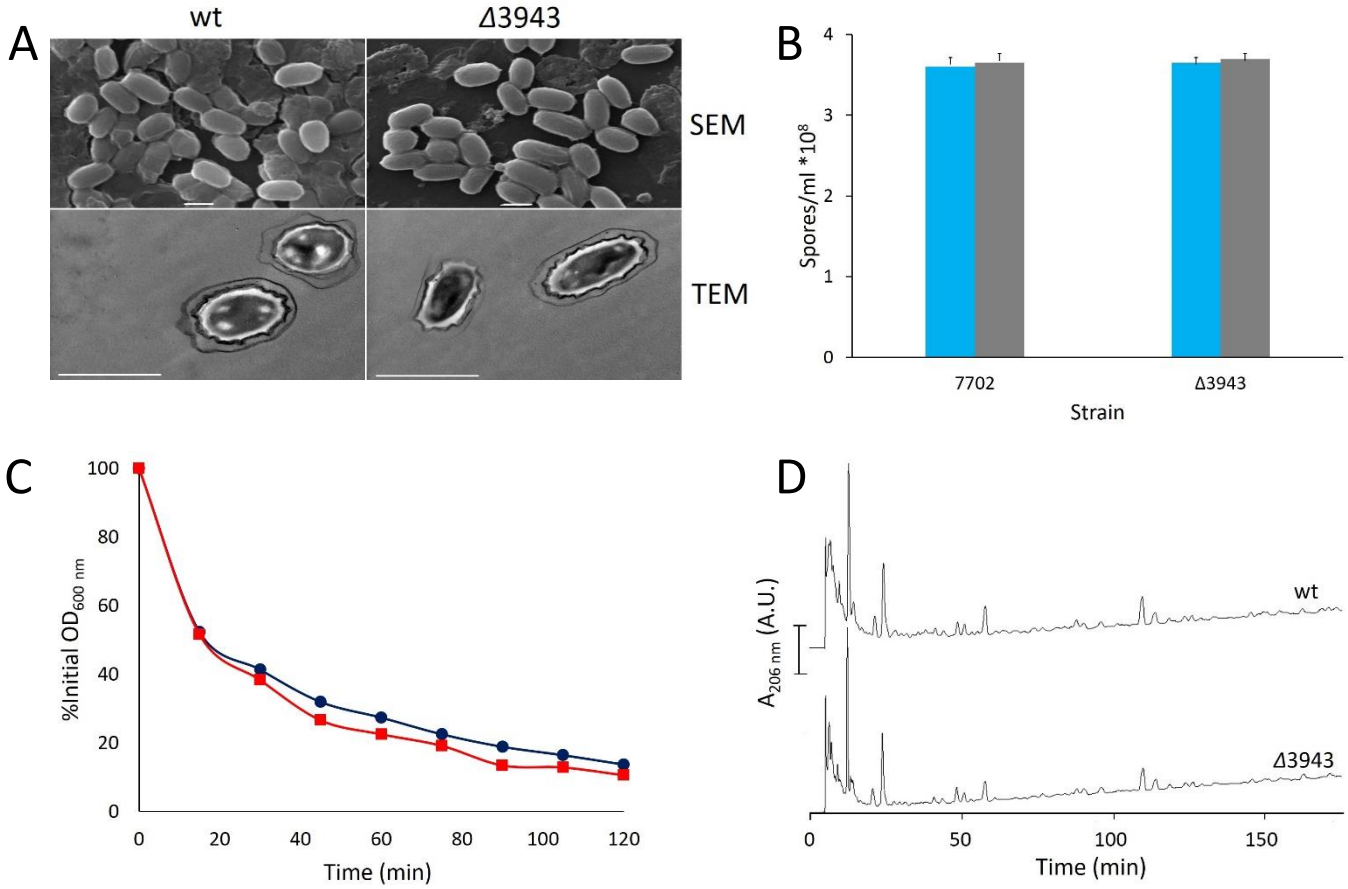

Figure 43. (A) Examination of morphology and structure of parental 7702 and mutant Δ*ba3943* mature spores using SEM and TEM. Scale bar 1 µm. (B) Spore viability of 7702 and Δ*ba3943* spores. Spore viability is defined as the number of phase bright spore particles plated (■) CFU/ml (■) spores/ml. (C) Germination of parental and mutant spores in response to L-ala and inosine. Spores of 7702 (●) and Δ*ba3943* (■) were induced to germinate by the addition of L-ala and inosine. Germination was monitored by loss of absorbance at 600 nm. (D) HPLC analysis of muropeptide composition of peptidoglycan isolated from 7702 and Δ*ba3943* mature spores. Bar, 200 mAU.

In order to examine for a subtle role of *ba3943* in spore formation, competition experiments were conducted in which Δ*ba3943* mutant strain competed against 7702 wild type strain for several rounds of sporulation. In 7702 wild type strain, *lacZ* is under the transcriptional control of the *eag* promoter. The competition experiment was initially performed with a ratio of 1:1 (wild type to mutant cells) (Fig. 44A) but because Δ*ba3943* cells showed a severe competition deficit the mutant cells were added in threefold excess (Fig. 44B). Δ*ba3943* mutant strain had a significant competition deficit under sporulation-inducing conditions. Over the course of seven days of co-culturing the percentage of the mutant strain decreased from 75% to 3% of the population (Fig. 44B). On the contrary, the Δ*ba3943* mutant strain had no fitness defect under vegetative growth conditions (Fig. 44C). Genetic complementation by reintroducing a copy of *ba3943* gene restored competiveness to the mutant strain. These results suggest that BA3943 is involved in sporulation process.

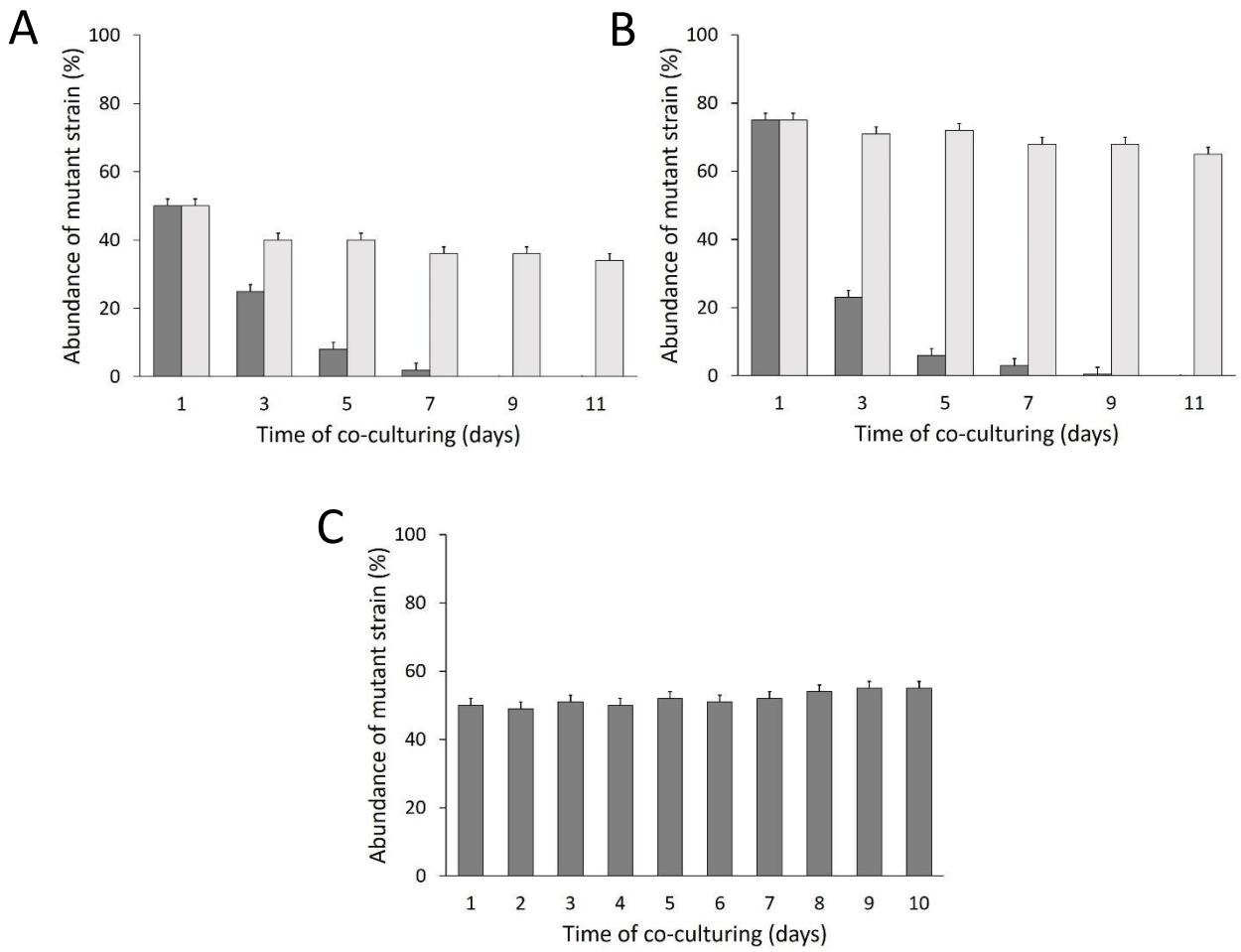

Figure 44. Competition experiment. Δ*ba3943* mutant strain exhibits reduced sporulation fitness. A wild-type reference strain carrying a *Peag-lacZ* transcriptional reporter was competed against Δ*ba3943* mutant in sporulation-inducing medium, starting with (A) 1:1 and (B) 1:3 ratio 7702 to Δ*ba3943*. Mutant strain complemented with BA3943 recovered the phenotype. (C) Δ*ba3943* mutant strain has no fitness defect under growth conditions.

BA3943 affects autolysis of vegetative cells

Even though BA3943 is expressed during sporulation and plays a subtle role in sporulation process, we decided to examine any possible effect of *ba3943* deletion in vegetative cells. Δ*ba3943* mutant cells were able to grow normally in both BHI and SPY medium indicating that BA3943 was not required for *B. anthracis* viability and growth (data not shown). Growth of Δ*ba3943* mutant cells was also monitored in the presence of lysozyme since many bacterial PG deacetylases described so far contribute to lysozyme resistance. However, Δ*ba3943* mutant strain did not display any sensitivity to lysozyme compared to the parental strain in the exponential or stationary growth phase (Fig. 45A). We then tested the autolytic activity of 7702 and Δ*ba3943* strains by addition of NaN_3, a known inducer of autolysis in growing cultures. Δ*ba3943* mutant strain showed decreased autolysis under these conditions compared to that of the parental strain. Genetic complementation by reintroducing a copy of *ba3943* gene restored autolysis of the mutant strain (Fig. 45B). In order to examine and visualize the morphological phenotype of Δ*ba3943* mutant, we collected cell samples during exponential and stationary growth phase in SPY medium and observed them using SEM. Δ*ba3943* mutant cells exhibited longer chains of septated daughter cells compared to the parental strain which were able to separate (Fig. 45C). The presence of long daughter cell chains of Δ*ba3943* mutant cells correlated with the reduced autolysis. Lastly, the PG and PS composition from stationary phase cells of Δ*ba3943* mutant was also examined and it was found similar to that of the parental strain (Fig. 46A, 46B).

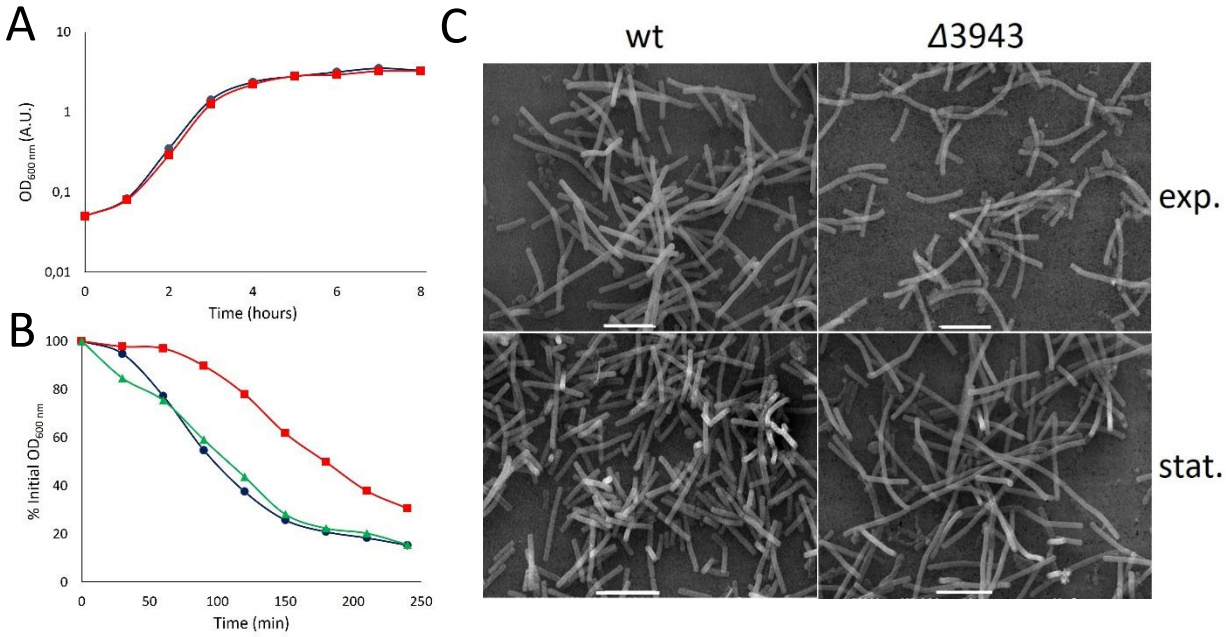

Figure 45. Lysozyme sensitivity, autolysis rate and morphology of parental and mutant strains. (A) Effect of lysozyme on 7702 (●) and Δ*ba3943* mutant (■) strains. Strains were grown in SPY liquid broth at 37°C. Δ*ba3943* mutant is not affected by the addition of lysozyme. (B) Autolysis rate of 7702 (●) and Δ*ba3943* (■) cells. Cell lysis was monitored by loss of absorbance at 600 nm. Mutant strain complemented with BA3943 recovered the phenotype (▲). (C) SEM of wild type 7702 and Δ*ba3943* cells during exponential (exp.) and stationary (stat.) phase of growth. Δ*ba3943* cells exhibit longer chains of daughter cells compared to the wild type only during stationary phase of growth. Scale bar 10 µm.

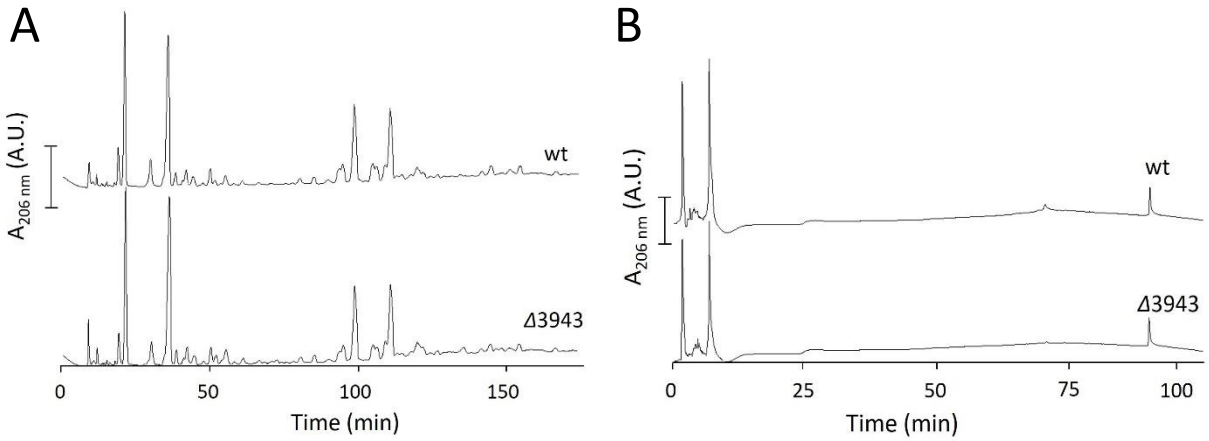

Figure 46. HPLC analysis of (A) muropeptide composition of PG and (B) PS isolated from 7702 and Δ*ba3943* cells during stationary phase of growth. Bar, 200 mAU for PG and 500 mAU for PS.

Discussion

In this study we employed gene knock-out, protein localization, expression profile analysis as well as sporulation and germination assays to elucidate the physiological role of the putative PDAs BA1836 and BA3943 from *B. anthracis*. Biochemical characterization and structure determination was additionally performed for BA3943.

ba1836 gene expression was triggered upon entrance in the stationary phase of growth and was enhanced during the early stages of sporulation (Fig. 20A and 20B). Sporulation conditions alone were not sufficient to induce *ba1836* expression (Fig. 21). Presently characterized PDAs from *B. anthracis* are expressed during vegetative growth, in either exponential (BA0330, BA0331) (144) or stationary phase (BA1977, BA1961, BA2944, BA3679, BA5436) (130) and they have not been reported to be further induced in sporulation.

BA1836-GFP localized at the cell membrane and septa in stationary phase cells (Fig. 22A). Membrane localization is consistent with the presence of a transmembrane domain at the *N*-terminus of the protein. Two other PDAs from *B. anthracis* namely, BA0330, a putative PDA, and BA3679, a characterized PGDA, have been demonstrated to exhibit similar localization patterns (130, 144).

Δ*ba1836* showed a defect in cell separation and a lower rate of autolysis compared to the wild type strain suggesting a mechanism of impaired substrate recognition by PG hydrolases that are crucial for autolysis and cell division (Fig. 24B and 24C). Reduced lysis has been similarly observed with all PDA mutants of *B. anthracis* examined so far, except Δ*ba1977* (130).

Deletion of *ba1836* resulted in a significant competition deficit specific to sporulation–inducing conditions (Fig. 27A and 27B). Δ*ba1836* cells displayed a severe delay from the onset of sporulation compared to the wild type strain (Fig. 28), although mutant spores are morphologically and structurally normal and fully functional since they are able to germinate (Fig. 26A and 26B). We therefore conclude that the loss of BA1836 function results only in a delay in spore development and not to a complete block.

Deletion of other genes from *B. anthracis* has been similarly reported to result in noticeable delay in spore development which has been attributed to different reasons. Inactivation of each of the sensor histidine kinase genes in *B. anthracis* resulted in a delay in sporulation of the resulting mutant strains, especially with the Δ*ba2291* strain (195). Similarly to *ba1836*, *ba2291* is expressed during stationary phase of growth and was inferred to be involved in sporulation by its strong inhibition of sporulation when inactivated in *B. anthracis* and also when expressed in *B. subtilis*. The inhibitory activity of BA2291 has been proposed to be due to either dephosphorylation of the phosphotransferase Spo0F or the transcription factor Spo0A or sequestering one or both of these proteins preventing access by sporulation kinases (195). Similarly one of the three sortase mutant strains of *B. anthracis,* namely the *Srtc* mutant, did not readily form spores in guinea pig tissue or sheep blood unless their vegetative forms were expressed in the presence of oxygen (196). It is currently unclear if BA1836 is functionally linked to BA2291 or SrtC.

In repeated muramidase digests of spore PG from Δ*ba1836* we obtained a lower amount of similar muropeptides compared to digests of spore PG from wild-type (Fig. 29). This could be due to a reduced amount of PG in the mutant, less efficient digestions, or both (Fig. 26). The wild-type spore PG profile was partially complemented when the mutant strain was transformed with BA1836-GFP. A similar phenotype has been reported for the sporulation proteins SpoVM and SpoVS of *B. subtilis* (197). The reduced PG amount of *spoVM* deficient spores has been attributed to incomplete cortex synthesis which was suggested to result either from its interaction with the spore coat morphogenesis protein SpoIVA (198) or the protease FtsH (199, 200). Additionally to the reduced amount of spore PG, *spoVS*-deficient spores showed a delay in the initiation of sporulation. Similarly to SpoVM and SpoVS, BA1836 might have a regulatory role via its interaction with other protein(s).

Δ*ba1836* exhibited a reduced rate of germination which was partially complemented by *ba1836-gfp* expression (Fig. 30). The decreased rate of germination of *B. anthracis* spores has been so far attributed to the absence or non-functionality of GRs and/or CLEs (184, 201). It could also be caused by inefficient recruitment of CLEs. To determine whether this phenotype is due to the putative de-*N*-acetylase activity, a protein version lacking the catalytic aspartic acid residue, BA1836 (D53A)

was expressed in Δ*ba1836*. Remarkably, the putative inactive BA1836 version partially complemented this phenotype indicating that it is not caused by the lack of enzymatic activity. This result suggests that BA1836 might participate in the organization of other enzymes or proteins involved in the germination process.

We were unable to test *in vitro* whether BA1836 is active on known deacetylase substrates due to immediate proteolysis of the *E. coli* produced protein (Fig. 19B). This observation might indicate that interaction of BA1836 with other protein(s) is necessary for its stabilization against proteolysis. In addition, the effect of BA1836 on spore development and germination might be the result of possible interactions as previously described for SpoVM and SpoVS.

Sporulation proteins appear to have mainly regulatory functions participating in protein-DNA, protein-protein and/or protein/PG interactions and only a small number of them have enzymatic activity. Many of these proteins have lost their enzymatic activity and retained only substrate binding ability while some might have preserved the initial activity which is probably not directly relevant to their role in sporulation (202).

BA1836 has the characteristic zinc binding (His^{103}, His^{107} and Asp^{54}) and catalytic (Asp^{53} and His^{196}) motifs of active PDAs as well as Arg^{143}, which coordinates the catalytic Asp^{53}, and the conserved Pro^{145} which has been recently demonstrated to be modified at the Ca atom to produce 2-Hyp thus enhancing significantly deacetylase activity (149) (Fig. 18).

However, we cannot exclude the possibility that mutations resulting in altering BA1836 conformation had occurred, and led to steric blocking of the active site or disruption of substrate-binding site (158).

Absence of BA1836 did not change the muropeptide profile of muramidase digested PG either from stationary phase of growth or spores (Fig. 25A, 29). Furthermore, the putative inactive deacetylase version BA1836 (D53A), partially complemented the reduced rate of germination suggesting that the putative enzyme activity is not related to the observed phenotype (Fig. 30).These results support the hypothesis that BA1836 is an inactive deacetylase version.

However, we cannot exclude that BA1836 might have an enzymatic activity that is limited to a restricted cell surface area and is not detectable by our techniques.

Alternatively, it might have an as-yet-unidentified substrate not directly relevant to its role in sporulation, distinct from the neutral polysaccharide of *B. anthracis* or the deacetylase-specific GlcNAc residues for subsequent anchoring of cell wall polymers as demonstrated previously for BA1961 and BA3679 (109).

Pseudoenzymes are present in almost every enzyme family and have been identified in organisms as heterogeneous as bacteria (153). However, the best studied dead enzymes belong to the kinase, phosphatase and protease families of eukaryotic organisms (156). Different roles of pseudoenzymes have been reported including regulation of their active homologues, interaction with the substrates of their enzyme homologues, binding and targeting of other proteins to specific cellular locations, modulation of protein ubiquitination and signal transduction (161).

Biochemical characterization showed that BA3943 is a pseudoenzyme that lacks both deacetylation on PGDA substrates and hydroxylation of the conserved Pro^{185} (Table 5). This is the first report of a doubly dead enzyme. The sequence alignment of BA3943 with its active homologues revealed several key characteristics (Fig. 32) which were confirmed by the crystal structure. BA3943 adopts the conserved $(\alpha/\beta)_8$ barrel motif, typical of the NodB fold (Fig. 34). The catalytic Asp of motif MT1 is replaced by Asn^{94} while the conserved Pro^{185} is not hydroxylated, suggesting the absence of maturation of the active site. The metal-binding triad is disrupted and the Val^{95} residue of BA3943 points away from the active site in contrast to the well-conserved Asp of characterized PGDAs (149, 150) and in consistence with the Asn of characterized MurNAc PG deacetylases (139, 146). Moreover, the crystal structure revealed the absence of a metal ion. The well-conserved Arg in the vicinity of the catalytic Asp is replaced by an Ala^{183} creating a cavity potentially destabilizing the active site. In addition to the NodB domain, there is an *N*-terminal lysine-rich domain, consisting of two alpha helices, connected to the NodB domain through an intrinsically disordered domain (Fig. 34). Lys is a positively charged aliphatic amino acid, and its ε-amino group is often engaged in hydrogen bonding. Therefore, it is possible that the lysine-rich domain aids BA3943 to participate in interactions with macromolecules (nucleic acids, proteins, polysaccharides). This is the first member of the CE4 family with a lysine-rich domain.

B. anthracis has another pseudoPDA named BA0150. Sequence alignment indicates that BA0150 does not retain the conserved Asp-His-His metal-binding triad, present in the majority of the enzymes of the CE4 family, but instead it contains Ile, Met and Tyr residues respectively, none of which have a strong affinity for metal ions (Fig. 32). The recently determined crystal structure of BA0150 is consistent with a non-functional PDA which maintains the conserved $(\alpha/\beta)_8$ homology domain, characteristic of this family of enzymes, and its overall structure aligns well with other known PDA structures from Gram-positive bacteria. However, the crystal structure does not contain a catalytic metal ion (usually zinc) which is required for enzyme activity. BA0150 was not active on H^3-glycol chitin (unpublished data) while 2-Hyp quantification by MS has not been estimated yet. BA0150 shares 55% identity with PdaB from *B. subtilis*. The absence of PdaB, results in empty or cortex-less spores implying its importance in cortex formation and further maintenance of spores after the late stage of sporulation (140).

There is a small number of bacterial enzymes which have been characterized as dead based on a disrupted metal-binding site or the lack of residues essential for catalysis rather than *in vitro* testing of the enzymatic activity. For example, in the sequence of the *E. coli* enolase, which shows 26% identity with Chitinase A from *S. mercescents*, the general catalytic acid Glu is mutated to Gln, suggesting that it is inactive (203).

The results of the present study demonstrate that the loss of enzymatic activity of BA3943 is attributed, in part, to substitutions in motif MT1 (TFDD) and motif MT3 (RpPxG) since restoration of these two motifs by site-directed mutagenesis, at just three positions, resulted in recovery of the deacetylase activity and levels of hydroxylation. BA3943 N94D V95D A183R was active against H^3-glycol chitin and chitooligomers but not against PG isolated from either *B. subtilis* or *E. coli*. This can be attributed to the fact that the metal-binding site of BA3943 N94D V95D A183R remains disrupted since the Asp^{95} residue continues to point away from the active site, exactly like Val^{95} of BA3943 (Fig. 38A). Additionally, no metal was detected either from crystal structure determination or ICP-MS analysis. However, when a divalent cation, preferably Co^{+2}, was added in the enzymatic reaction, BA3943 N94D V95D

A183R was active, suggesting that metal coordination can still be achieved possibly by water molecules as previously observed in other PDAs (204).

The importance of Arg^{183} of motif MT3 in the deacetylation/hydroxylation mechanism was also highlighted. It was already proposed that Arg coordinates the catalytic base (Asp) of the deacetylation mechanism (145). Here we showed that its chemical structure and physicochemical properties are essential in order for deacetylation/hydroxylation reaction to occur since when Arg^{183} was mutated to Lys, the deacetylase activity of BA3943 N94D V95D A183K was lost. The way in which Arg contributes to the deacetylation/hydroxylation mechanism remains to be elucidated.

As far as we know, there are two studies related to pseudoenzymes from eukaryotes, where restoration of the enzymatic activity, via site-directed mutagenesis, was achieved.

Dual-specificity phosphatases (ds-PTPases) hydrolyze phosphoserine/ threonine/ tyrosine-containing substrates *in vitro* and exhibit a substrate preference *in vitro* and *in vivo* for diphosphorylated (Thr(P)/Tyr(P)) mitogen-activated protein kinase (MAPK) homologues. All ds-PTPases contain the sequence HCxxGxxR(S/T), which has been shown to correspond to their active site. The essential Cys forms a thiophosphate intermediate during ds-PTPases-catalyzed dephosphorylation and it is not essential for substrate binding. The sequence of phosphoserine/ threonine/ tyrosine-binding proteins (STYX) is similar to that of ds-PTPases, but contains a Gly residue in place of the active site, catalytic Cys. Residues that have been shown to be important for phosphorylated substrate-binding by ds-PTPases are present in STYX. STYX are unable to hydrolyze Tyr(P)-containing substrates, however, a single mutation of Gly^{120} to Cys restored phosphatase activity. STYX G120C had binding and kinetic parameters similar to that of human ds-PTPases (205).

The human genome possesses two genes encoding for active chitinases, the chitotriosidase (hCHT) and the acidic mammalian chitinase (hAMCase), both belonging to the CAZy Glycoside Hydrolase 18 (GH18) family. Along with active chitinases, a number of closely related proteins without detectable chitinase activity have been identified in mammalian genomes. One of these is chitinase 3-like-2 (YKL-39) which has been suggested as a diagnostic marker for diagnosis and management of osteoarthritis based on increased expression levels in osteoarthritic cartilage. Despite

a relatively high sequence identity and predicted structural similarity to the GH18 family, such as hCHT, YKL-39 lacks glycosyl hydrolase activity. The loss of enzymatic activity is attributed to the substitution of the catalytic residues of the DxxDxDxE motif, which is characteristic of the GH18 family. YKL-39 showed micromolar binding affinity for chitooligosaccharides but no chitinase activity. The crystal structure revealed the molecular basis for this affinity as well as for the lack of hydrolytic activity. The last Asp residue in the DxxDxDxE motif positions the acetamido group for nucleophilic attack, whereas the Glu residue performs general acid/base catalysis. In YKL-39 these catalytic residues are substituted to a Ser^{143} and an Ile^{145} residue respectively. The hydrolytic activity of YKL-39 was restored by reconstructing the active site motif. The YKL-39 S143D I145E showed significant chitinase activity. The active YKL-39 mutant showed similar affinity for 4MU-($GlcNAc_3$) to hCHT but significantly lower substrate turnover (206).

ba3943 gene expression was triggered upon entrance in Stage III of sporulation which corresponds to the engulfment of the forespore from the mother cell (Fig. 41A). None of the presently characterized PDA genes from *B. anthracis* has been reported to be expressed during sporulation except from *ba1836* whose expression was further induced in the first stages of sporulation (Fig. 20A). As already mentioned, BA3943 shares 56% sequence identity to the sporulation protein YlxY from *B. subtilis* (Fig. 31). *ylxY* gene expression is under σ^E control and is induced between hours 1 and 2 of sporulation of *B. subtilis* (181). σ^E is a mother-cell specific sigma factor which is synthesized during Stage II of sporulation but is held in inactive state until the septum forms (207, 208). It is possible that the expression of *ba3943* gene is also σ^E-dependent. Even though *ba3943* gene encodes for a pseudoenzyme, it is expressed, suggesting that its presence in the chromosome it is not a burden for the cell and it is involved in *B. anthracis* physiology.

BA3943-GFP, with or without the lysine-rich domain, was enhanced at the forespore cell membrane but fluorescent signal was also observed at the mother cell septa (Fig. 42A). Membrane localization is consistent with the presence of a transmembrane domain at the *N*-terminus of the protein. BA3943-GFP fusion could not restore the observed phenotypes when overexpressed in Δ*ba3943* mutant cells. This observation does not necessarily mean that the GFP fusion is not an accurate

reporter of BA3943 localization. There are studies which have shown that GFP-fused proteins were non-functional, however, they were accurate reporters of protein localization (209).

Deletion of *ba3943* resulted in a significant competition deficit specific to sporulation–inducing conditions (Fig. 44A, 44B), which was complemented after reintroduction of the *ba3943* gene into Δ*ba3943* mutant strain. However, mutant spores were morphologically and structurally normal and fully functional since they were able to sporulate and germinate (Fig. 43A, 43B). As a result, the precise step of sporulation in which BA3943 is involved is currently unknown. Similarly, the *ylxY* mutant had no conspicuous phenotype as judged by colony morphology or spore formation but had a clear competition deficit under sporulation-inducing conditions and not under growth conditions (181).

Δ*ba3943* showed a defect in cell separation and a lower rate of autolysis compared to the wild type strain, which was complemented after reintroduction of the *ba3943* gene (Fig. 45B). This phenotype suggests a mechanism of impaired substrate recognition by PG hydrolases that are crucial for autolysis and cell division. Reduced lysis has been similarly observed with all PDA mutants of *B. anthracis* examined so far, including Δ*ba1836*, except Δ*ba1977* (130).

BA3943 is a pseudoPDA and therefore its role in sporulation is related to a non-enzymatic function. The functions of pseudoenzymes include major regulatory roles in the cellular processes of prokaryotic and eukaryotic organisms. Their regulatory function mainly involves protein-protein or protein-substrate interactions. Although the role of its lysine-rich domain located at the *N*-terminus has not been elucidated, might be important for BA3943 function.

Pseudoenzymes have been demonstrated to have different biological roles including regulation of their active homologues. For this reason, the activity of the characterized PGDAs BC1960 and BC1974 from *B. cereus*, highly homologous enzymes to BA1961 and BA1977 from *B. anthracis* respectively, against H^3-glycol chitin, was tested in the presence of BA3943. However, the pseudoPDA neither enhanced nor inhibited their activity (data not shown). It is possible that BA3943 might regulate the activity of another putative or known PDA from *B. anthracis*.

Dead enzymes can also interact with the substrates of their active homologues directly, sequestering them and preventing their processing by other enzymes or anchoring them in a particular subcellular space. BA3943 was incubated with purified vegetative and spore PG from *B. anthracis* (since spores have two PGs) but no binding was observed (data not shown). BA3943 might bind to another polysaccharide like the recently identified one pZX (125) or even an un-identified one.

We also attempted to complement the observed phenotypes with the introduction of the *ba3943* without containing the lysine rich domain but the construction of the complemented strain was unsuccessful.

Presently studied putative and characterized PDAs from *B. anthracis* have been demonstrated to be involved in resistance to host lysozyme, stabilization of the cell wall, biogenesis of PG, for neutral polysaccharide modification and attachment to PG.

To our knowledge BA1836 has a unique, sporulation/germination-specific role among the functions of other PDAs, while BA3943 is the first characterized pseudoPDA which affects the sporulation process in *B. anthracis*.

References

1. Bourgeois SL, Doherty MJ. 2005. Bioterrorism and biologic warfare. Oral Maxillofac Surg Clin North Am 17:299-330.
2. Derzelle S, Thierry S. 2013. Genetic diversity of Bacillus anthracis in Europe: genotyping methods in forensic and epidemiologic investigations. Biosecur Bioterror 11 Suppl 1:S166-76.
3. Koch R. 1876. Die Ätiologie der Milzbrand-Krankheit, begründet auf die Entwicklungsgeschichte des Bacillus Anthracis d. Robert Koch-Institut.
4. Pasteur L. 1881. Compte-rendu, sommaire des expériences faites à Pouillly-le-Fort, près Melun, sur la vaccination charbonneuse. Comptes-rendus des séances de l'Académie des Sciences.
5. Cohn F. 1872. Untersuchungen uber Bacterien. Beiträge zur Biologie der Pflanzen 127-244.
6. Turnbull PC. 1999. Definitive identification of Bacillus anthracis-a review. J Appl Microbiol 87:237-40.
7. Eitzen EM, Takafuji ET. 1997. Historical overview of biological welfare. Med Asp Chem Biol Welfare 415-423
8. Inglesby TV, O'Toole T, Henderson DA, Bartlett JG, Ascher MS, Eitzen E, Friedlander AM, Gerberding J, Hauer J, Hughes J, McDade J, Osterholm MT, Parker G, Perl TM, Russell PK, Tonat K. 2002. Anthrax as a biological weapon, 2002: updated recommendations for management. JAMA 287:2236-52.
9. Jernigan JA, Stephens DS, Ashford DA, Omenaca C, Topiel MS, Galbraith M, Tapper M, Fisk TL, Zaki S, Popovic T, Meyer RF, Quinn CP, Harper SA, Fridkin SK, Sejvar JJ, Shepard CW, McConnell M, Guarner J, Shieh WJ, Malecki JM, Gerberding JL, Hughes JM, Perkins BA. 2001. Bioterrorism-related inhalational anthrax: the first 10 cases reported in the United States. Emerg Infect Dis 7:933-44.
10. Soufiane B, Cote JC. 2009. Discrimination among Bacillus thuringiensis H serotypes, serovars and strains based on 16S rRNA, gyrB and aroE gene sequence analyses. Anton Leeuw Int J G 95:33-45.
11. Pilo P, Frey J. 2011. Bacillus anthracis: molecular taxonomy, population genetics, phylogeny and patho-evolution. Infect Genet Evol 11:1218-24.
12. Dragon DC, Rennie RP. 1995. The ecology of anthrax spores: tough but not invincible. Can Vet J 36:295-301.
13. Dixon TC, Meselson M, Guillemin J, Hanna PC. 1999. Anthrax. N Engl J Med 341:815-26.
14. Guidi-Rontani C, Weber-Levy M, Labruyere E, Mock M. 1999. Germination of Bacillus anthracis spores within alveolar macrophages. Mol Microbiol 31:9-17.
15. Fouet A, Namy O, Lambert G. 2000. Characterization of the operon encoding the alternative sigma(B) factor from Bacillus anthracis and its role in virulence. J Bacteriol 182:5036-45.
16. Mock M, Fouet A. 2001. Anthrax. Annu Rev Microbiol 55:647-71.
17. Goel AK. 2015. Anthrax: A disease of biowarfare and public health importance. World J Clin Cases 3:20-33.
18. Ganz HH, Turner WC, Brodie EL, Kusters M, Shi Y, Sibanda H, Torok T, Getz WM. 2014. Interactions between Bacillus anthracis and plants may promote anthrax transmission. PLoS Negl Trop Dis 8:e2903.
19. Leppla SH. 1982. Anthrax toxin edema factor: a bacterial adenylate cyclase that increases cyclic AMP concentrations of eukaryotic cells. Proc Natl Acad Sci U S A 79:3162-6.

20. Collier RJ. 2009. Membrane translocation by anthrax toxin. Mol Aspects Med 30:413-22.
21. Sweeney DA, Hicks CW, Cui X, Li Y, Eichacker PQ. 2011. Anthrax infection. Am J Respir Crit Care Med 184:1333-41.
22. Collier RJ, Young JA. 2003. Anthrax toxin. Annu Rev Cell Dev Biol 19:45-70.
23. Kintzer AF, Thoren KL, Sterling HJ, Dong KC, Feld GK, Tang, II, Zhang TT, Williams ER, Berger JM, Krantz BA. 2009. The protective antigen component of anthrax toxin forms functional octameric complexes. J Mol Biol 392:614-29.
24. Abrami L, Reig N, van der Goot FG. 2005. Anthrax toxin: the long and winding road that leads to the kill. Trends Microbiol 13:72-8.
25. Duesbery NS, Webb CP, Leppla SH, Gordon VM, Klimpel KR, Copeland TD, Ahn NG, Oskarsson MK, Fukasawa K, Paull KD, Vande Woude GF. 1998. Proteolytic inactivation of MAP-kinase-kinase by anthrax lethal factor. Science 280:734-7.
26. Vitale G, Pellizzari R, Recchi C, Napolitani G, Mock M, Montecucco C. 1999. Anthrax lethal factor cleaves the N-terminus of MAPKKS and induces tyrosine/threonine phosphorylation of MAPKS in cultured macrophages. J Appl Microbiol 87:288.
27. Park JM, Greten FR, Li ZW, Karin M. 2002. Macrophage apoptosis by anthrax lethal factor through p38 MAP kinase inhibition. Science 297:2048-51.
28. Anthrax Toxin. https://en.wikipedia.org/wiki/Anthrax_toxin.
29. Goossens PL. 2009. Animal models of human anthrax: the quest for the Holy Grail. Mol Aspects Med 30:467-80.
30. Hicks CW, Sweeney DA, Cui X, Li Y, Eichacker PQ. 2012. An overview of anthrax infection including the recently identified form of disease in injection drug users. Intens Care Med 38:1092-104.
31. Price EP, Seymour ML, Sarovich DS, Latham J, Wolken SR, Mason J, Vincent G, Drees KP, Beckstrom-Sternberg SM, Phillippy AM, Koren S, Okinaka RT, Chung WK, Schupp JM, Wagner DM, Vipond R, Foster JT, Bergman NH, Burans J, Pearson T, Brooks T, Keim P. 2012. Molecular epidemiologic investigation of an anthrax outbreak among heroin users, Europe. Emerg Infect Dis 18:1307-13.
32. Centers for Disease Control and Prevention CDC. https://www.cdc.gov/anthrax/index.html.
33. Stroud C. 2011. Antibiotics for Anthrax Postexposure Prophylaxis, Prepositioning Antibiotics for Anthrax. National Academy Press (US), Washington (DC).
34. Beierlein JM, Anderson AC. 2011. New developments in vaccines, inhibitors of anthrax toxins, and antibiotic therapeutics for Bacillus anthracis. Curr Med Chem 18:5083-94.
35. Greig SL. 2016. Obiltoxaximab: first global approval. Drugs 76:823-30.
36. Spencer RC. 2003. Bacillus anthracis. J Clin Pathol 56:182-7.
37. Errington J, Wu LJ. 2017. Cell Cycle Machinery in Bacillus subtilis. In Löwe J, Amos LA eds, Prokaryotic Cytoskeletons: Filamentous Protein Polymers Active in the Cytoplasm of Bacterial and Archaeal Cells, Springer International Publishing 67-101.
38. Tan IS, Ramamurthi KS. 2014. Spore formation in Bacillus subtilis. Environ Microbiol Rep 6:212-25.
39. Higgins D, Dworkin J. 2012. Recent progress in Bacillus subtilis sporulation. FEMS Microbiol Rev 36:131-48.
40. Burbulys D, Trach KA, Hoch JA. 1991. Initiation of sporulation in B. subtilis is controlled by a multicomponent phosphorelay. Cell 64:545-52.
41. Molle V, Fujita M, Jensen ST, Eichenberger P, Gonzalez-Pastor JE, Liu JS, Losick R. 2003. The Spo0A regulon of Bacillus subtilis. Mol Microbiol 50:1683-701.
42. Fujita M, Losick R. 2005. Evidence that entry into sporulation in Bacillus subtilis is governed by a gradual increase in the level and activity of the master regulator Spo0A. Genes Dev 19:2236-44.

43. Eswaramoorthy P, Dinh J, Duan D, Igoshin OA, Fujita M. 2010. Single-cell measurement of the levels and distributions of the phosphorelay components in a population of sporulating Bacillus subtilis cells. Microbiology 156:2294-304.
44. Eswaramoorthy P, Duan D, Dinh J, Dravis A, Devi SN, Fujita M. 2010. The threshold level of the sensor histidine kinase KinA governs entry into sporulation in Bacillus subtilis. J Bacteriol 192:3870-82.
45. Levine JH, Fontes ME, Dworkin J, Elowitz MB. 2012. Pulsed feedback defers cellular differentiation. PLoS Biol 10:e1001252.
46. Dworkin J, Losick R. 2005. Developmental commitment in a bacterium. Cell 121:401-9.
47. Ben-Yehuda S, Fujita M, Liu XS, Gorbatyuk B, Skoko D, Yan J, Marko JF, Liu JS, Eichenberger P, Rudner DZ, Losick R. 2005. Defining a centromere-like element in Bacillus subtilis by identifying the binding sites for the chromosome-anchoring protein RacA. Mol Cell 17:773-782.
48. Rahn-Lee L, Merrikh H, Grossman AD, Losick R. 2011. The sporulation protein SirA inhibits the binding of DnaA to the origin of replication by contacting a patch of clustered amino acids. J Bacteriol 193:1302-7.
49. Cunningham KA, Burkholder WF. 2009. The histidine kinase inhibitor Sda binds near the site of autophosphorylation and may sterically hinder autophosphorylation and phosphotransfer to Spo0F. Mol Microbiol 71:659-77.
50. Errington J. 2003. Regulation of endospore formation in Bacillus subtilis. Nat Rev Microbiol 1:117-26.
51. Hilbert DW, Piggot PJ. 2004. Compartmentalization of gene expression during Bacillus subtilis spore formation. Microbiol Mol Biol Rev 68:234-62.
52. Abanes-De Mello A, Sun YL, Aung S, Pogliano K. 2002. A cytoskeleton-like role for the bacterial cell wall during engulfment of the Bacillus subtilis forespore. Genes Dev 16:3253-64.
53. Tocheva EI, Lopez-Garrido J, Hughes HV, Fredlund J, Kuru E, Vannieuwenhze MS, Brun YV, Pogliano K, Jensen GJ. 2013. Peptidoglycan transformations during Bacillus subtilis sporulation. Mol Microbiol 88:673-86.
54. Blaylock B, Jiang X, Rubio A, Moran CP, Jr., Pogliano K. 2004. Zipper-like interaction between proteins in adjacent daughter cells mediates protein localization. Genes Dev 18:2916-28.
55. Doan T, Marquis KA, Rudner DZ. 2005. Subcellular localization of a sporulation membrane protein is achieved through a network of interactions along and across the septum. Mol Microbiol 55:1767-81.
56. Meisner J, Wang X, Serrano M, Henriques AO, Moran CP, Jr. 2008. A channel connecting the mother cell and forespore during bacterial endospore formation. Proc Natl Acad Sci U S A 105:15100-5.
57. Camp AH, Losick R. 2009. A feeding tube model for activation of a cell-specific transcription factor during sporulation in Bacillus subtilis. Genes Dev 23:1014-24.
58. McKenney PT, Driks A, Eskandarian HA, Grabowski P, Guberman J, Wang KH, Gitai Z, Eichenberger P. 2010. A distance-weighted interaction map reveals a previously uncharacterized layer of the Bacillus subtilis spore coat. Curr Biol 20:934-8.
59. McKenney PT, Eichenberger P. 2012. Dynamics of spore coat morphogenesis in Bacillus subtilis. Mol Microbiol 83:245-60.
60. Levin PA, Fan N, Ricca E, Driks A, Losick R, Cutting S. 1993. An unusually small gene required for sporulation by Bacillus subtilis. Mol Microbiol 9:761-71.
61. Driks A. 1999. Bacillus subtilis spore coat. Microbiol Mol Biol Rev 63:1-20.

62. Tipper DJ, Linnett PE. 1976. Distribution of peptidoglycan synthetase activities between sporangia and forespores in sporulating cells of Bacillus sphaericus. J Bacteriol 126:213-21.
63. Popham DL. 2013. Visualizing the production and arrangement of peptidoglycan in Gram-positive cells. Mol Microbiol 88:645-649.
64. Warth AD, Ohye DF, Murrell WG. 1963. The composition and structure of bacterial spores. J Cell Biol 16:579-592.
65. Popham DL, Setlow P. 1993. The cortical peptidoglycan from spores of Bacillus megaterium and Bacillus subtilis is not highly cross-linked. J Bacteriol 175:2767-9.
66. Meador-Parton J, Popham DL. 2000. Structural analysis of Bacillus subtilis spore peptidoglycan during sporulation. J Bacteriol 182:4491-9.
67. Popham DL, Gilmore ME, Setlow P. 1999. Roles of low-molecular-weight penicillin-binding proteins in Bacillus subtilis spore peptidoglycan synthesis and spore properties. J Bacteriol 181:126-32.
68. Popham DL, Bernhards CB. 2015. Spore peptidoglycan. Microbiol Spectr 3.
69. Sowell MO, Buchanan CE. 1983. Changes in penicillin-binding proteins during sporulation of Bacillus subtilis. J Bacteriol 153:1331-7.
70. Gilmore ME, Bandyopadhyay D, Dean AM, Linnstaedt SD, Popham DL. 2004. Production of muramic delta-lactam in Bacillus subtilis spore peptidoglycan. J Bacteriol 186:80-9.
71. Setlow P. 2013. Summer meeting 2013-when the sleepers wake: the germination of spores of Bacillus species. J Appl Microbiol 115:1251-68.
72. Setlow P. 2014. Germination of spores of Bacillus species: what we know and do not know. J Bacteriol 196:1297-305.
73. Zhang P, Liang J, Yi X, Setlow P, Li YQ. 2014. Monitoring of commitment, blocking, and continuation of nutrient germination of individual Bacillus subtilis spores. J Bacteriol 196:2443-54.
74. Popham DL, Helin J, Costello CE, Setlow P. 1996. Muramic lactam in peptidoglycan of Bacillus subtilis spores is required for spore outgrowth but not for spore dehydration or heat resistance. Proc Natl Acad Sci U S A 93:15405-10.
75. Tovar-Rojo F, Chander M, Setlow B, Setlow P. 2002. The products of the spoVA operon are involved in dipicolinic acid uptake into developing spores of Bacillus subtilis. J Bacteriol 184:584-7.
76. Li Y, Davis A, Korza G, Zhang P, Li YQ, Setlow B, Setlow P, Hao B. 2012. Role of a SpoVA protein in dipicolinic acid uptake into developing spores of Bacillus subtilis. J Bacteriol 194:1875-84.
77. Moir A, Cooper G. 2015. Spore germination. Microbiol Spectr 3.
78. Li Y, Butzin XY, Davis A, Setlow B, Korza G, Üstok FI, Christie G, Setlow P, Hao B. 2013. Activity and regulation of various forms of CwlJ, SleB, and YpeB proteins in degrading cortex peptidoglycan of spores of Bacillus species in vitro and during spore germination. J Bacteriol 195:2530-2540.
79. Boland FM, Atrih A, Chirakkal H, Foster SJ, Moir A. 2000. Complete spore-cortex hydrolysis during germination of Bacillus subtilis 168 requires SleB and YpeB. Microbiology 146:57-64.
80. Chirakkal H, O'Rourke M, Atrih A, Foster SJ, Moir A. 2002. Analysis of spore cortex lytic enzymes and related proteins in Bacillus subtilis endospore germination. Microbiology 148:2383-92.
81. Nicholson WL, Munakata N, Horneck G, Melosh HJ, Setlow P. 2000. Resistance of Bacillus endospores to extreme terrestrial and extraterrestrial environments. Microbiol Mol Biol Rev 64:548-572.

82. Sanchez-Salas JL, Santiago-Lara ML, Setlow B, Sussman MD, Setlow P. 1992. Properties of Bacillus megaterium and Bacillus subtilis mutants which lack the protease that degrades small, acid-soluble proteins during spore germination. J Bacteriol 174:807-14.
83. Mesnage S, Tosi-Couture E, Gounon P, Mock M, Fouet A. 1998. The capsule and S-layer: two independent and yet compatible macromolecular structures in Bacillus anthracis. J Bacteriol 180:52-8.
84. Fouet A. 2009. The surface of Bacillus anthracis. Mol Aspects Med 30:374-85.
85. Boneca IG. 2005. The role of peptidoglycan in pathogenesis. Curr Opin Microbiol 8:46-53.
86. Microbiology. http://trishul.sci.gu.edu.au/courses/2008BPS/2016_structure_function/2008BPS_final2_structure_function_2016.html.
87. Barreteau H, Kovac A, Boniface A, Sova M, Gobec S, Blanot D. 2008. Cytoplasmic steps of peptidoglycan biosynthesis. FEMS Microbiol Rev 32:168-207.
88. van Heijenoort J. 2007. Lipid intermediates in the biosynthesis of bacterial peptidoglycan. Microbiol Mol Biol Rev 71:620-35.
89. Mohammadi T, van Dam V, Sijbrandi R, Vernet T, Zapun A, Bouhss A, Diepeveen-de Bruin M, Nguyen-Disteche M, de Kruijff B, Breukink E. 2011. Identification of FtsW as a transporter of lipid-linked cell wall precursors across the membrane. EMBO J 30:1425-32.
90. Lovering AL, Gretes M, Strynadka NC. 2008. Structural details of the glycosyltransferase step of peptidoglycan assembly. Curr Opin Struct Biol 18:534-43.
91. Bugg TD, Braddick D, Dowson CG, Roper DI. 2011. Bacterial cell wall assembly: still an attractive antibacterial target. Trends Biotechnol 29:167-73.
92. Read TD, Peterson SN, Tourasse N, Baillie LW, Paulsen IT, Nelson KE, Tettelin H, Fouts DE, Eisen JA, Gill SR, Holtzapple EK, Okstad OA, Helgason E, Rilstone J, Wu M, Kolonay JF, Beanan MJ, Dodson RJ, Brinkac LM, Gwinn M, DeBoy RT, Madpu R, Daugherty SC, Durkin AS, Haft DH, Nelson WC, Peterson JD, Pop M, Khouri HM, Radune D, Benton JL, Mahamoud Y, Jiang L, Hance IR, Weidman JF, Berry KJ, Plaut RD, Wolf AM, Watkins KL, Nierman WC, Hazen A, Cline R, Redmond C, Thwaite JE, White O, Salzberg SL, Thomason B, Friedlander AM, Koehler TM, Hanna PC, et al. 2003. The genome sequence of Bacillus anthracis Ames and comparison to closely related bacteria. Nature 423:81-6.
93. Navarre WW, Schneewind O. 1999. Surface proteins of gram-positive bacteria and mechanisms of their targeting to the cell wall envelope. Microbiol Mol Biol Rev 63:174-229.
94. Ekwunife FS, Singh J, Taylor KG, Doyle RJ. 1991. Isolation and purification of cell wall polysaccharide of Bacillus anthracis (delta Sterne). FEMS Microbiol Lett 66:257-62.
95. Fox A, Black GE, Fox K, Rostovtseva S. 1993. Determination of carbohydrate profiles of Bacillus anthracis and Bacillus cereus including identification of O-methyl methylpentoses by using gas chromatography-mass spectrometry. J Clin Microbiol 31:887-94.
96. Choudhury B, Leoff C, Saile E, Wilkins P, Quinn CP, Kannenberg EL, Carlson RW. 2006. The structure of the major cell wall polysaccharide of Bacillus anthracis is species-specific. J Biol Chem 281:27932-41.
97. Schneewind O, Missiakas DM. 2012. Protein secretion and surface display in Gram-positive bacteria. Philos Trans R Soc Lond B Biol Sci 367:1123-39.
98. Leoff C, Saile E, Rauvolfova J, Quinn CP, Hoffmaster AR, Zhong W, Mehta AS, Boons GJ, Carlson RW, Kannenberg EL. 2009. Secondary cell wall polysaccharides of Bacillus anthracis are antigens that contain specific epitopes which cross-react with three

pathogenic Bacillus cereus strains that caused severe disease, and other epitopes common to all the Bacillus cereus strains tested. Glycobiology 19:665-73.
99. Mesnage S, Fontaine T, Mignot T, Delepierre M, Mock M, Fouet A. 2000. Bacterial SLH domain proteins are non-covalently anchored to the cell surface via a conserved mechanism involving wall polysaccharide pyruvylation. EMBO J 19:4473-84.
100. Forsberg LS, Choudhury B, Leoff C, Marston CK, Hoffmaster AR, Saile E, Quinn CP, Kannenberg EL, Carlson RW. 2011. Secondary cell wall polysaccharides from Bacillus cereus strains G9241, 03BB87 and 03BB102 causing fatal pneumonia share similar glycosyl structures with the polysaccharides from Bacillus anthracis. Glycobiology 21:934-48.
101. Kern J, Ryan C, Faull K, Schneewind O. 2010. Bacillus anthracis surface-layer proteins assemble by binding to the secondary cell wall polysaccharide in a manner that requires csaB and tagO. J Mol Biol 401:757-75.
102. Couture-Tosi E, Delacroix H, Mignot T, Mesnage S, Chami M, Fouet A, Mosser G. 2002. Structural analysis and evidence for dynamic emergence of Bacillus anthracis S-layer networks. J Bacteriol 184:6448-56.
103. Mesnage S, Tosi-Couture E, Mock M, Gounon P, Fouet A. 1997. Molecular characterization of the Bacillus anthracis main S-layer component: evidence that it is the major cell-associated antigen. Mol Microbiol 23:1147-55.
104. Kern J, Wilton R, Zhang R, Binkowski TA, Joachimiak A, Schneewind O. 2011. Structure of surface layer homology (SLH) domains from Bacillus anthracis surface array protein. J Biol Chem 286:26042-9.
105. Green BD, Battisti L, Koehler TM, Thorne CB, Ivins BE. 1985. Demonstration of a capsule plasmid in Bacillus anthracis. Infect Immun 49:291-7.
106. Candela T, Fouet A. 2006. Poly-gamma-glutamate in bacteria. Mol Microbiol 60:1091-8.
107. Candela T, Fouet A. 2005. Bacillus anthracis CapD, belonging to the gamma-glutamyltranspeptidase family, is required for the covalent anchoring of capsule to peptidoglycan. Mol Microbiol 57:717-26.
108. Richter S, Anderson VJ, Garufi G, Lu L, Budzik JM, Joachimiak A, He C, Schneewind O, Missiakas D. 2009. Capsule anchoring in Bacillus anthracis occurs by a transpeptidation reaction that is inhibited by capsidin. Mol Microbiol 71:404-20.
109. Candela T, Balomenou S, Aucher W, Bouriotis V, Simore JP, Fouet A, Boneca IG. 2014. N-acetylglucosamine deacetylases modulate the anchoring of the gamma-glutamyl capsule to the cell wall of Bacillus anthracis. Microb Drug Resist 20:222-30.
110. Roelants GE, Senyk G, Goodman JW. 1969. Immunochemical studies on the poly-gamma-D-glutamyl capsule of Bacillus anthracis. V. The in vivo fate and distribution in rabbits of the polypeptide in immunogenic and nonimmunogenic forms. Isr J Med Sci 5:196-208.
111. Makino S, Uchida I, Terakado N, Sasakawa C, Yoshikawa M. 1989. Molecular characterization and protein analysis of the cap region, which is essential for encapsulation in Bacillus anthracis. J Bacteriol 171:722-30.
112. Driks A. 2009. The Bacillus anthracis spore. Mol Aspects Med 30:368-73.
113. Setlow B, Atluri S, Kitchel R, Koziol-Dube K, Setlow P. 2006. Role of dipicolinic acid in resistance and stability of spores of Bacillus subtilis with or without DNA-protective alpha/beta-type small acid-soluble proteins. J Bacteriol 188:3740-7.
114. Atrih A, Foster SJ. 2001. Analysis of the role of bacterial endospore cortex structure in resistance properties and demonstration of its conservation amongst species. J Appl Microbiol 91:364-72.
115. Popham DL. 2002. Specialized peptidoglycan of the bacterial endospore: the inner wall of the lockbox. Cell Mol Life Sci 59:426-33.

116. Dowd MM, Orsburn B, Popham DL. 2008. Cortex peptidoglycan lytic activity in germinating Bacillus anthracis spores. J Bacteriol 190:4541-8.
117. Driks A. 2002. Maximum shields: the assembly and function of the bacterial spore coat. Trends Microbiol 10:251-4.
118. Driks A, Eichenberger P. 2016. The spore coat. Microbiol Spectr 4.
119. Setlow P. 2014. Spore resistance properties. Microbiol Spectr 2.
120. Bozue JA, Welkos S, Cote CK. 2015. The Bacillus anthracis exosporium: what's the big "hairy" deal? Microbiol Spectr 3.
121. Sylvestre P, Couture-Tosi E, Mock M. 2002. A collagen-like surface glycoprotein is a structural component of the Bacillus anthracis exosporium. Mol Microbiol 45:169-178.
122. Waller LN, Stump MJ, Fox KF, Harley WM, Fox A, Stewart GC, Shahgholi M. 2005. Identification of a second collagen-like glycoprotein produced by Bacillus anthracis and demonstration of associated spore-specific sugars. J Bacteriol 187:4592-4597.
123. Steichen C, Chen P, Kearney JF, Turnbough CL. 2003. Identification of the immunodominant protein and other proteins of the Bacillus anthracis exosporium. J Bacteriol 185:1903-1910.
124. Steichen CT, Kearney JF, Turnbough CL, Jr. 2005. Characterization of the exosporium basal layer protein BxpB of Bacillus anthracis. J Bacteriol 187:5868-5876.
125. Li Z, Hwang S, Bar-Peled M. 2016. Discovery of a unique extracellular polysaccharide in members of the pathogenic Bacillus that can co-form with spores. J Biol Chem 291:19051-67.
126. Caufrier F, Martinou A, Dupont C, Bouriotis V. 2003. Carbohydrate esterase family 4 enzymes: substrate specificity. Carbohydr Res 338:687-92.
127. Balomenou S, Arnaouteli S, Koutsioulis D, Fadouloglou VE, Bouriotis V. 2015. Polysaccharide Deacetylases: New Antibacterial Drug Targets. In Atta-ur-Rahman, Choudhary MI eds, Frontiers in Anti-Infective Drug Discovery, Bentham eBooks 4:68-130
128. Vollmer W. 2008. Structural variation in the glycan strands of bacterial peptidoglycan. FEMS Microbiol Rev 32:287-306.
129. Vollmer W, Tomasz A. 2000. The pgdA gene encodes for a peptidoglycan N-acetylglucosamine deacetylase in Streptococcus pneumoniae. J Biol Chem 275:20496-501.
130. Balomenou S, Fouet A, Tzanodaskalaki M, Couture-Tosi E, Bouriotis V, Boneca IG. 2013. Distinct functions of polysaccharide deacetylases in cell shape, neutral polysaccharide synthesis and virulence of Bacillus anthracis. Mol Microbiol 87:867-83.
131. Boneca IG, Dussurget O, Cabanes D, Nahori MA, Sousa S, Lecuit M, Psylinakis E, Bouriotis V, Hugot JP, Giovannini M, Coyle A, Bertin J, Namane A, Rousselle JC, Cayet N, Prevost MC, Balloy V, Chignard M, Philpott DJ, Cossart P, Girardin SE. 2007. A critical role for peptidoglycan N-deacetylation in Listeria evasion from the host innate immune system. Proc Natl Acad Sci U S A 104:997-1002.
132. Meyrand M, Boughammoura A, Courtin P, Mezange C, Guillot A, Chapot-Chartier MP. 2007. Peptidoglycan N-acetylglucosamine deacetylation decreases autolysis in Lactococcus lactis. Microbiology 153:3275-85.
133. Fittipaldi N, Sekizaki T, Takamatsu D, de la Cruz Dominguez-Punaro M, Harel J, Bui NK, Vollmer W, Gottschalk M. 2008. Significant contribution of the pgdA gene to the virulence of Streptococcus suis. Mol Microbiol 70:1120-35.
134. Kaoukab-Raji A, Biskri L, Bernardini ML, Allaoui A. 2012. Characterization of SfPgdA, a Shigella flexneri peptidoglycan deacetylase required for bacterial persistence within polymorphonuclear neutrophils. Microbes Infect 14:619-27.

135. Benachour A, Ladjouzi R, Le Jeune A, Hebert L, Thorpe S, Courtin P, Chapot-Chartier MP, Prajsnar TK, Foster SJ, Mesnage S. 2012. The lysozyme-induced peptidoglycan N-acetylglucosamine deacetylase PgdA (EF1843) is required for Enterococcus faecalis virulence. J Bacteriol 194:6066-73.
136. Moynihan PJ, Sychantha D, Clarke AJ. 2014. Chemical biology of peptidoglycan acetylation and deacetylation. Bioorg Chem 54:44-50.
137. Smith TJ, Blackman SA, Foster SJ. 2000. Autolysins of Bacillus subtilis: multiple enzymes with multiple functions. Microbiology 146 (Pt 2):249-62.
138. Fukushima T, Yamamoto H, Atrih A, Foster SJ, Sekiguchi J. 2002. A polysaccharide deacetylase gene (pdaA) is required for germination and for production of muramic delta-lactam residues in the spore cortex of Bacillus subtilis. J Bacteriol 184:6007-15.
139. Oberbarnscheidt L, Taylor EJ, Davies GJ, Gloster TM. 2007. Structure of a carbohydrate esterase from Bacillus anthracis. Proteins 66:250-2.
140. Fukushima T, Tanabe T, Yamamoto H, Hosoya S, Sato T, Yoshikawa H, Sekiguchi J. 2004. Characterization of a polysaccharide deacetylase gene homologue (pdaB) on sporulation of Bacillus subtilis. J Biochem 136:283-91.
141. Colvin KM, Alnabelseya N, Baker P, Whitney JC, Howell PL, Parsek MR. 2013. PelA deacetylase activity is required for Pel polysaccharide synthesis in Pseudomonas aeruginosa. J Bacteriol 195:2329-39.
142. Vuong C, Kocianova S, Voyich JM, Yao Y, Fischer ER, DeLeo FR, Otto M. 2004. A crucial role for exopolysaccharide modification in bacterial biofilm formation, immune evasion, and virulence. J Biol Chem 279:54881-6.
143. Little DJ, Poloczek J, Whitney JC, Robinson H, Nitz M, Howell PL. 2012. The structure- and metal-dependent activity of Escherichia coli PgaB provides insight into the partial de-N-acetylation of poly-beta-1,6-N-acetyl-D-glucosamine. J Biol Chem 287:31126-37.
144. Arnaouteli S, Giastas P, Andreou A, Tzanodaskalaki M, Aldridge C, Tzartos SJ, Vollmer W, Eliopoulos E, Bouriotis V. 2015. Two putative polysaccharide deacetylases are required for osmotic stability and cell shape maintenance in Bacillus anthracis. J Biol Chem 290:13465-78.
145. Blair DE, Schuttelkopf AW, MacRae JI, van Aalten DM. 2005. Structure and metal-dependent mechanism of peptidoglycan deacetylase, a streptococcal virulence factor. Proc Natl Acad Sci U S A 102:15429-34.
146. Blair DE, van Aalten DM. 2004. Structures of Bacillus subtilis PdaA, a family 4 carbohydrate esterase, and a complex with N-acetyl-glucosamine. FEBS Lett 570:13-9.
147. Robert X, Gouet P. 2014. Deciphering key features in protein structures with the new ENDscript server. Nucleic Acids Res 42:W320-4.
148. Psylinakis E, Boneca IG, Mavromatis K, Deli A, Hayhurst E, Foster SJ, Varum KM, Bouriotis V. 2005. Peptidoglycan N-acetylglucosamine deacetylases from Bacillus cereus, highly conserved proteins in Bacillus anthracis. J Biol Chem 280:30856-63.
149. Fadouloglou VE, Balomenou S, Aivaliotis M, Kotsifaki D, Arnaouteli S, Tomatsidou A, Efstathiou G, Kountourakis N, Miliara S, Griniezaki M, Tsalafouta A, Pergantis SA, Boneca IG, Glykos NM, Bouriotis V, Kokkinidis M. 2017. Unusual α-carbon hydroxylation of proline promotes active-site maturation. J Am Chem Soc 139:5330-5337.
150. Giastas P, Andreou A, Papakyriakou A, Koutsioulis D, Balomenou S, Tzartos SJ, Bouriotis V, Eliopoulos EE. 2018. Structures of the peptidoglycan N-Acetylglucosamine deacetylase Bc1974 and its complexes with zinc metalloenzyme inhibitors. Biochemistry 57:753-763.

151. Strunk RJ, Piemonte KM, Petersen NM, Koutsioulis D, Bouriotis V, Perry K, Cole KE. 2014. Structure determination of BA0150, a putative polysaccharide deacetylase from Bacillus anthracis. Acta Crystallogr F Struct Biol Commun 70:156-9.
152. Fadouloglou VE, Kapanidou M, Agiomirgianaki A, Arnaouteli S, Bouriotis V, Glykos NM, Kokkinidis M. 2013. Structure determination through homology modelling and torsion-angle simulated annealing: application to a polysaccharide deacetylase from Bacillus cereus. Acta Crystallogr D Biol Crystallogr 69:276-83.
153. Leslie M. 2013. Molecular biology. 'Dead' enzymes show signs of life. Science 340:25-7.
154. Jackson BC, Thompson DC, Charkoftaki G, Vasiliou V. 2015. Dead enzymes in the aldehyde dehydrogenase gene family: role in drug metabolism and toxicology. Expert Opin Drug Metab Toxicol 11:1839-47.
155. Manning G, Whyte DB, Martinez R, Hunter T, Sudarsanam S. 2002. The protein kinase complement of the human genome. Science 298:1912-34.
156. Pils B, Schultz J. 2004. Inactive enzyme-homologues find new function in regulatory processes. J Mol Biol 340:399-404.
157. Brew K, Vanaman TC, Hill RL. 1967. Comparison of the amino acid sequence of bovine alpha-lactalbumin and hens egg white lysozyme. J Biol Chem 242:3747-9.
158. Adrain C, Freeman M. 2012. New lives for old: evolution of pseudoenzyme function illustrated by iRhoms. Nat Rev Mol Cell Biol 13:489-98.
159. Kurosky A, Barnett DR, Rasco MA, Lee TH, Bowman BH. 1974. Evidence of homology between the beta-chain of human haptoglobin and the chymotrypsin family of serine proteases. Biochem Genet 11:279-93.
160. Kurosky A, Barnett DR, Lee TH, Touchstone B, Hay RE, Arnott MS, Bowman BH, Fitch WM. 1980. Covalent structure of human haptoglobin: a serine protease homolog. Proc Natl Acad Sci U S A 77:3388-92.
161. Eyers PA, Murphy JM. 2016. The evolving world of pseudoenzymes: proteins, prejudice and zombies. BMC Biol 14:98.
162. Reiterer V, Eyers PA, Farhan H. 2014. Day of the dead: pseudokinases and pseudophosphatases in physiology and disease. Trends Cell Biol 24:489-505.
163. Tonks NK. 2009. Pseudophosphatases: grab and hold on. Cell 139:464-5.
164. Murphy JM, Czabotar PE, Hildebrand JM, Lucet IS, Zhang JG, Alvarez-Diaz S, Lewis R, Lalaoui N, Metcalf D, Webb AI, Young SN, Varghese LN, Tannahill GM, Hatchell EC, Majewski IJ, Okamoto T, Dobson RC, Hilton DJ, Babon JJ, Nicola NA, Strasser A, Silke J, Alexander WS. 2013. The pseudokinase MLKL mediates necroptosis via a molecular switch mechanism. Immunity 39:443-53.
165. Murphy JM, Lucet IS, Hildebrand JM, Tanzer MC, Young SN, Sharma P, Lessene G, Alexander WS, Babon JJ, Silke J, Czabotar PE. 2014. Insights into the evolution of divergent nucleotide-binding mechanisms among pseudokinases revealed by crystal structures of human and mouse MLKL. Biochem J 457:369-77.
166. Zou J, Zhang C, Marjanovic J, Kisseleva MV, Majerus PW, Wilson MP. 2012. Myotubularin-related protein (MTMR) 9 determines the enzymatic activity, substrate specificity, and role in autophagy of MTMR8. Proc Natl Acad Sci U S A 109:9539-44.
167. Fukuda K, Gupta S, Chen K, Wu C, Qin J. 2009. The pseudoactive site of ILK is essential for its binding to α-parvin and localization to focal adhesions. Mol Cell 36:819-830.
168. Trieu-Cuot P, Carlier C, Martin P, Courvalin P. 1987. Plasmid transfer by conjugation from Escherichia coli to Gram-positive bacteria. FEMS Microbiol Let 48:289-294.
169. Pezard C, Berche P, Mock M. 1991. Contribution of individual toxin components to virulence of Bacillus anthracis. Infect Immun 59:3472-7.

170. Fortinea N, Trieu-Cuot P, Gaillot O, Pellegrini E, Berche P, Gaillard JL. 2000. Optimization of green fluorescent protein expression vectors for in vitro and in vivo detection of Listeria monocytogenes. Res Microbiol 151:353-60.
171. Agaisse H, Lereclus D. 1994. Structural and functional analysis of the promoter region involved in full expression of the cryIIIA toxin gene of Bacillus thuringiensis. Mol Microbiol 13:97-107.
172. Janes BK, Stibitz S. 2006. Routine markerless gene replacement in Bacillus anthracis. Infect Immun 74:1949-53.
173. Horton RM, Cai ZL, Ho SN, Pease LR. 1990. Gene splicing by overlap extension: tailor-made genes using the polymerase chain reaction. Biotechniques 8:528-35.
174. Araki Y, Oba S, Araki S, Ito E. 1980. Enzymatic deacetylation of N-acetylglucosamine residues in cell wall peptidoglycan. J Biochem 88:469-79.
175. Bui NK, Eberhardt A, Vollmer D, Kern T, Bougault C, Tomasz A, Simorre JP, Vollmer W. 2012. Isolation and analysis of cell wall components from Streptococcus pneumoniae. Anal Biochem 421:657-66.
176. Flouret B, Mengin-Lecreulx D, van Heijenoort J. 1981. Reverse-phase high-pressure liquid chromatography of uridine diphosphate N-acetylmuramyl peptide precursors of bacterial cell wall peptidoglycan. Anal Biochem 114:59-63.
177. Rygus T, Hillen W. 1991. Inducible high-level expression of heterologous genes in Bacillus megaterium using the regulatory elements of the xylose-utilization operon. Appl Microbiol Biotechnol 35:594-9.
178. Kim HU, Goepfert JM. 1974. A sporulation medium for Bacillus anthracis. J Appl Bacteriol 37:265-7.
179. Miller J. 1972. Experiments in Molecular Genetics. Cold Spring Harbor Laboratory Press, Cold Spring Harbor, NY.
180. Mignot T, Mesnage S, Couture-Tosi E, Mock M, Fouet A. 2002. Developmental switch of S-layer protein synthesis in Bacillus anthracis. Mol Microbiol 43:1615-27.
181. Traag BA, Pugliese A, Eisen JA, Losick R. 2013. Gene conservation among endospore-forming bacteria reveals additional sporulation genes in Bacillus subtilis. J Bacteriol 195:253-60.
182. Popham DL, Helin J, Costello CE, Setlow P. 1996. Analysis of the peptidoglycan structure of Bacillus subtilis endospores. J Bacteriol 178:6451-8.
183. Mesnage S, Tosi-Couture E, Fouet A. 1999. Production and cell surface anchoring of functional fusions between the SLH motifs of the Bacillus anthracis S-layer proteins and the Bacillus subtilis levansucrase. Mol Microbiol 31:927-36.
184. Carr KA, Lybarger SR, Anderson EC, Janes BK, Hanna PC. 2010. The role of Bacillus anthracis germinant receptors in germination and virulence. Mol Microbiol 75:365-75.
185. Fazzini MM, Schuch R, Fischetti VA. 2010. A novel spore protein, ExsM, regulates formation of the exosporium in Bacillus cereus and Bacillus anthracis and affects spore size and shape. J Bacteriol 192:4012-21.
186. Krogh A, Larsson B, von Heijne G, Sonnhammer EL. 2001. Predicting transmembrane protein topology with a hidden Markov model: application to complete genomes. J Mol Biol 305:567-80.
187. Bendtsen JD, Nielsen H, Widdick D, Palmer T, Brunak S. 2005. Prediction of twin-arginine signal peptides. BMC Bioinform 6:167.
188. Nielsen H. 2017. Predicting secretory proteins with SignalP. Methods Mol Biol 1611:59-73.
189. Taylor EJ, Gloster TM, Turkenburg JP, Vincent F, Brzozowski AM, Dupont C, Shareck F, Centeno MS, Prates JA, Puchart V, Ferreira LM, Fontes CM, Biely P, Davies GJ. 2006. Structure and activity of two metal ion-dependent acetylxylan esterases involved in

plant cell wall degradation reveals a close similarity to peptidoglycan deacetylases. J Biol Chem 281:10968-75.
190. Blair DE, Hekmat O, Schuttelkopf AW, Shrestha B, Tokuyasu K, Withers SG, van Aalten DM. 2006. Structure and mechanism of chitin deacetylase from the fungal pathogen Colletotrichum lindemuthianum. Biochemistry 45:9416-26.
191. Deng DM, Urch JE, ten Cate JM, Rao VA, van Aalten DM, Crielaard W. 2009. Streptococcus mutans SMU.623c codes for a functional, metal-dependent polysaccharide deacetylase that modulates interactions with salivary agglutinin. J Bacteriol 191:394-402.
192. Tajima M, Iida T, Yoshida S, Komatsu K, Namba R, Yanagi M, Noguchi M, Okamoto H. 1990. The reaction product of peptidylglycine alpha-amidating enzyme is a hydroxyl derivative at alpha-carbon of the carboxyl-terminal glycine. J Biol Chem 265:9602-5.
193. Bolkenius FN, Ganzhorn AJ. 1998. Peptidylglycine alpha-amidating mono-oxygenase: neuropeptide amidation as a target for drug design. Gen Pharmacol 31:655-9.
194. Takahashi K, Satani M, Gao Y, Noguchi M. 2002. The reaction of mechanism of peptidylglycine α-hydroxylating monooxygenase. Intern Congr Ser 1233:235-240.
195. Brunsing RL, La Clair C, Tang S, Chiang C, Hancock LE, Perego M, Hoch JA. 2005. Characterization of sporulation histidine kinases of Bacillus anthracis. J Bacteriol 187:6972-81.
196. Marraffini LA, Schneewind O. 2006. Targeting proteins to the cell wall of sporulating Bacillus anthracis. Mol Microbiol 62:1402-17.
197. Vasudevan P, Weaver A, Reichert ED, Linnstaedt SD, Popham DL. 2007. Spore cortex formation in Bacillus subtilis is regulated by accumulation of peptidoglycan precursors under the control of sigma K. Mol Microbiol 65:1582-94.
198. Ramamurthi KS, Clapham KR, Losick R. 2006. Peptide anchoring spore coat assembly to the outer forespore membrane in Bacillus subtilis. Mol Microbiol 62:1547-57.
199. Cutting S, Anderson M, Lysenko E, Page A, Tomoyasu T, Tatematsu K, Tatsuta T, Kroos L, Ogura T. 1997. SpoVM, a small protein essential to development in Bacillus subtilis, interacts with the ATP-dependent protease FtsH. J Bacteriol 179:5534-42.
200. Prajapati RS, Ogura T, Cutting SM. 2000. Structural and functional studies on an FtsH inhibitor from Bacillus subtilis. Biochim Biophys Acta 1475:353-9.
201. Bernhards CB, Popham DL. 2014. Role of YpeB in cortex hydrolysis during germination of Bacillus anthracis spores. J Bacteriol 196:3399-409.
202. Galperin MY, Mekhedov SL, Puigbo P, Smirnov S, Wolf YI, Rigden DJ. 2012. Genomic determinants of sporulation in Bacilli and Clostridia: towards the minimal set of sporulation-specific genes. Environ Microbiol 14:2870-90.
203. Todd AE, Orengo CA, Thornton JM. 2002. Sequence and structural differences between enzyme and nonenzyme homologs. Structure 10:1435-51.
204. Hernick M, Fierke CA. 2005. Zinc hydrolases: the mechanisms of zinc-dependent deacetylases. Arch Biochem Biophys 433:71-84.
205. Wishart MJ, Denu JM, Williams JA, Dixon JE. 1995. A single mutation converts a novel phosphotyrosine binding domain into a dual-specificity phosphatase. J Biol Chem 270:26782-5.
206. Schimpl M, Rush CL, Betou M, Eggleston IM, Recklies AD, van Aalten DM. 2012. Human YKL-39 is a pseudo-chitinase with retained chitooligosaccharide-binding properties. Biochem J 446:149-57.
207. Ju J, Luo T, Haldenwang WG. 1998. Forespore expression and processing of the SigE transcription factor in wild-type and mutant Bacillus subtilis. J Bacteriol 180:1673-81.
208. Hofmeister A. 1998. Activation of the proprotein transcription factor pro-sigmaE is associated with its progression through three patterns of subcellular localization during sporulation in Bacillus subtilis. J Bacteriol 180:2426-33.

209. Ingerson-Mahar M, Briegel A, Werner JN, Jensen GJ, Gitai Z. 2010. The metabolic enzyme CTP synthase forms cytoskeletal filaments. Nat Cell Biol 12:739-46.

Curriculum Vitae

Education

03/2013-present **PhD Candidate in Biology, University of Crete (UOC), Heraklion, Crete, GR**

02/2011-02/2013 **Master Degree in Biomedical Sciences, Utrecht University (UU), Utrecht, NL**

2 year-diploma in Drug Innovation (GPA 3.96)

10/2006-07/2010 **Bachelor Degree in Biochemistry and Biotechnology, University of Thessaly (UTH), Larisa, GR**

4 year-diploma in Biochemistry and Biotechnology (Grade 7.91/10)

Publications

- "Role of the putative polysaccharide deacetylase BA1836 from *B. anthracis* in spore development and germination". **Tomatsidou A**., Koutsioulis D., Tzamarias D., Kokkinidis M., Vollmer W., Bouriotis V., **2019** (*Microbiology* under review)
- "Polysaccharide deacetylases serve as new targets for the design of inhibitors against *Bacillus anthracis* and *Bacillus cereus*". Balomenou S., Koutsioulis D., **Tomatsidou A**., Tzanodaskalaki M., Petratos K., Bouriotis V., *Bioorg. Med. Chem.* **2018**; 26; 3845-3851
- "An unusual α-Carbon hydroxylation of proline promotes active-site maturation". Fadouloglou VE., Balomenou S., Aivaliotis M., Kotsifaki D., Arnaouteli S., Efstathiou G., Kountourakis N., Tsalafouta A., Miliara S., **Tomatsidou A.**, Griniezaki M., Pergantis SA., Boneca IG., Glykos NM., Bouriotis V., Kokkinidis M., *J. Am. Chem. Soc.,* **2017**; 139; 5330-5337
- "AtHESPERIN: a novel regulator of circadian rhythms with poly(A)-degrading activity in plants". **Tomatsidou A**., Delis C., Krokida A., Tsikou D., Beta RA., Tsioumpekou M., Moustaka J., Stravodimos G., Leonidas DD., Balatsos NA., Papadopoulou KK., *RNA Biol.,* **2016**; 13 (1): 68-82

Honors

- Doctorate Fellowship of Excellence – Siemens

IKY Fellowships of Excellence for Postgraduate Studies in Greece – Siemens Program – 2013

Conference Attendance

- EMBO/FEBS Summer School for Proteins and Organized Complexity. Spetsai, Greece, September 24- October 1 2017.

"A doubly dead enzyme" Molfetas-Lygkiaris A., Tomatsidou A., Kotsifaki D., Bouriotis V. and Kokkinidis M. (Poster Presentation)

- Pseudoenzymes 2016: from Signaling Mechanisms to Disease. Liverpool, United Kingdom, September 11-14 **2016**.

"A doubly dead enzyme" Molfetas-Lygkiaris A., Tomatsidou A., Kotsifaki D., Bouriotis V. and Kokkinidis M. (Poster Presentation)

- 7th European Spores Conference. Egham, Surrey, United Kingdom, April 18-20 **2016**.

"Two putative polysaccharide deacetylases from *B.anthracis*" Tomatsidou A., Balomenou S., Tzanodaskalaki M., Koutsioulis D. and Bouriotis V. (Poster presentation)

- 32nd Scientific Conference of Hellenic Association for Biological Sciences. Karpenisi, Greece, May 20-22 **2010.**

"AtNOC is a circadian-regulated deadenylase in *A.thaliana*" Tomatsidou A., Delis C., Papadopoulou KK. and Balatsos NA. (Oral and Poster presentation)